United States
Department of
Agriculture

Agricultural
Research
Service

ARS-98

July1992

Opus: An Integrated Simulation Model for Transport of Nonpoint-Source Pollutants at the Field Scale

Volume I, Documentation

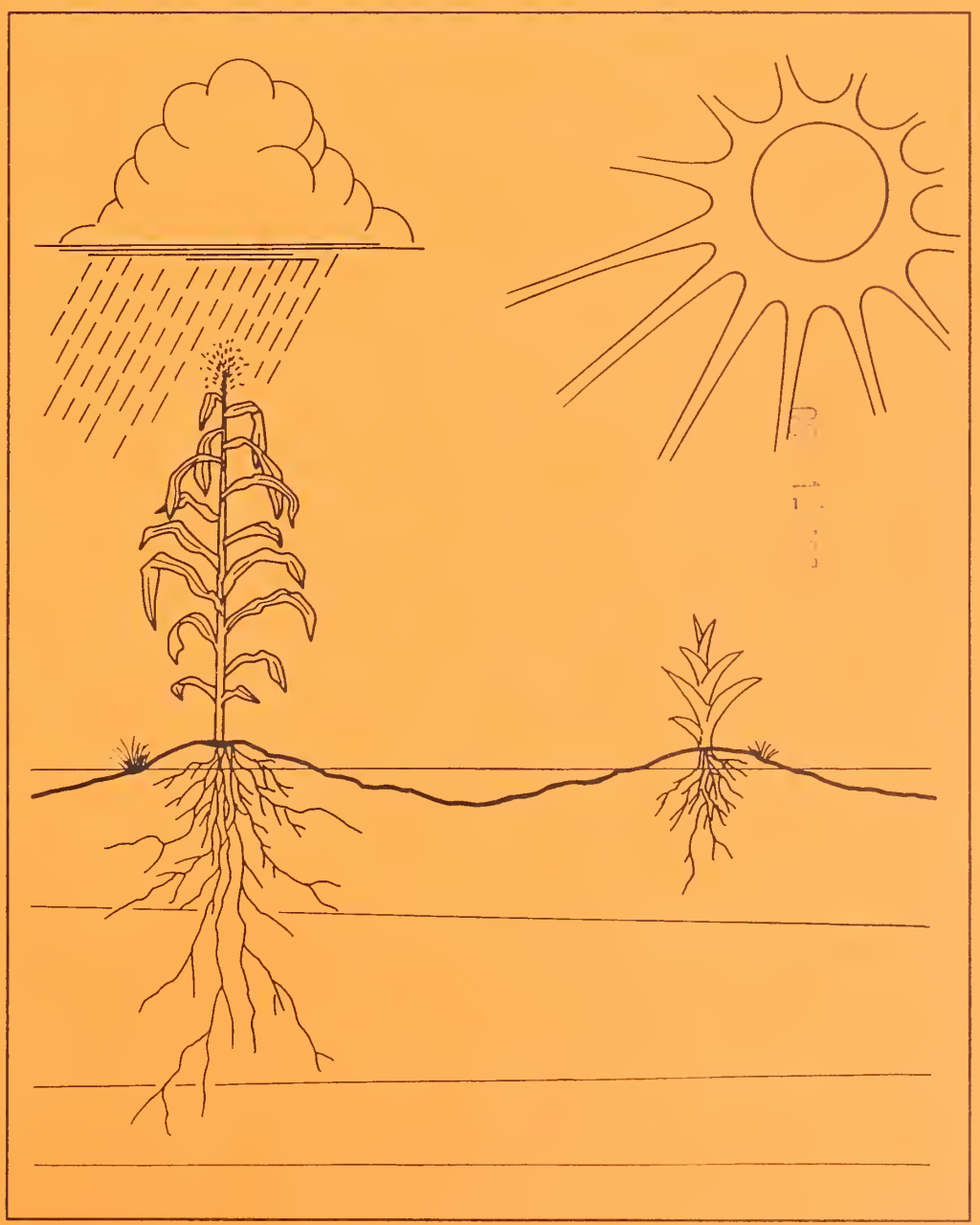

ABSTRACT

Smith, R.E. 1992. Opus, An Integrated Simulation Model for Transport of Nonpoint-Source Pollutants at the Field Scale: Volume I, Documentation. U.S. Department of Agriculture, Agricultural Research Service, ARS-98, 120 pp.

Opus (not an acronym) is a computer model for the transport of material in soil and surface water. The model is a simulation tool for studying the potential pollution from various agricultural management practices. It simulates water movement that results from rainfall and other weather inputs and that is affected by soil, crop, topography, and many types of management actions and water use influencing the surface condition. Opus includes models for the growth of plants; development of cover; water use; uptake of nutrients; cycling of soil nitrogen, phosphorus, and carbon; transport of adsorbed pesticides and nutrients; interaction of surface water and soil water; runoff; and erosion. This tool allows the user to choose between (a) detailed simulation involving data on the time-intensity pattern of rainfall and (b) a more lumped approach using either recorded daily rainfall or stochastically generated rainfall. To illustrate its use, Opus is applied to a set of rather comprehensive data from a watershed study in Watkinsville, GA.

KEYWORDS: runoff, erosion, infiltration, simulation, pollution, hydrology, soil water, transport

While supplies last, single copies of this publication may be obtained, at no cost, on request from USDA-ARS-NPA, Water Management Research Unit, AERC, CSU, Fort Collins, CO 80523.

Copies of this publication may also be purchased from the National Technical Information Service, 5285 Port Royal Road, Springfield, VA 22161.

ACKNOWLEDGMENTS

Methodology in this model borrows some material (as acknowledged herein) from earlier work in the EPIC model by Jimmy Williams, Agricultural Research Service, Temple, TX; from published research on various aspects of erosion relationships by George Foster; and from the Century soil-nutrient model of Bill Parton, NREL, Colorado State University, Fort Collins, CO. We are grateful for Dr. Parton's help in the inclusion of a revision of his model (ch. 6). Opus also owes part of its origin to ideas not included in CREAMS due to time and other limitations. Much of the methodology for surface runoff benefited from the concurrent development of KINEROS (ARS-77), involving the help of David Woolhiser and David Goodrich, ARS, Tucson, AZ. Much of the testing was done over several years with major assistance by Virginia Ferreira, ARS, and help from CSU students Walter Nicolli, Robert Flynn, and especially Fernando Pons.

CONTENTS

LIST OF SYMBOLS

This list contains the most significant or the most used symbols but is not exhaustive. Locally defined symbols may not be included but do not conflict with this list. A few of the symbols, to retain accepted usage, have different meanings (as indicated here) in different contexts. These symbols are used only when the meanings differ sufficiently to avoid ambiguity and when usages do not overlap. In addition, common abbreviations, such as N for nitrogen and C for carbon, are used in the text. Units throughout the text are abbreviated as follows:

m = meter
mm = millimeter
l = liter
gm = gram
kg = kilogram
ha = hectare
min = minute

Symbol	Definition	Unit
a	cross-sectional area	m^2
A	surface area	m^2
A_p	pond area at h = 0	m^2
A_u	surface area contributing at the upstream point of a channel	m2
b	parameter used with local definitions	
B	parameter used with local definitions	
c	General, locally defined parameter used with subscripts	
c_h	conversion coefficient	ha-mm/l
C	concentration by weight	
C_a	concentration of solute adsorbed to soil particles	kg/kg
C_p	concentration of phosphorus	kg/l
C_w	concentration of solute in liquid soil water	kg/l

Symbol	Definition	Unit
C_s	concentration of sediment in surface water	
C_{smx}	equilibrium concentration of sediment in surface water at current conditions	
C_z	concentration of solute at time 0	kg/l
d	rate of transfer of suspended particles between surface water and soil surface	$kg/m^2/min$
d_{pr}	potential rill detachment rate	$kg/m^2/min$
d_r	actual rill detachment rate	$kg/m^2/min$
d_e	net rate of loss or entrainment	$kg/m^2/min$
D	diffusivity of soil water	mm^2/min
D_T	soil thermal diffusivity	mm^2/min
e_c	efficiency of cultivation mixing	
e_r	parameter for efficiency of plant respiration	
E_p	daily potential plant-transpirable water	mm
E_{ps}	daily potential soil evaporation	mm
E_s	daily soil evaporation	mm
E_t	daily potential evapotranspiration	mm
E_t'	daily potential evapotranspiration less intercepted water	mm
f	rate of infiltration	mm/min
f_b	content of soil carbon by weight	
f_c	fraction of clay in surface soil	
f_{NH}	NH_4 factor in decay of residue	
f_{pw}	fraction of pesticide on plant surface that is subject to washoff	
f_{rs}	content of soil residue by weight	
f_{rm}	fraction of plant residue that is metabolic	
f_{rs}	fraction of plant residue that is structural	

Symbol	Definition	Unit
f_s	fraction of sand in surface soil	
f_T	temperature factor in decay of residue	
f_W	water-content factor in decay of residue	
F( )	objective function for numerical minimization	
F_p	maximum fraction of surface area shaded by plants	
F_L	leaf area index: leaf area divided by shaded area	
F_{LM}	index of potential maximum leaf area	
F_{LT}	total leaf area, considering all plants	
F_m	fraction of soil-surface area shaded by mulch	
F_s	fraction of total shaded soil surface area	
g	gravitational acceleration	m/sec/sec
g_c	capacity for transport of sediment	$kg/m^2/min$
g_s	actual sediment transport rate	$kg/m^2/min$
G	parameter of capillary and water deficit for infiltration model	mm
G_1	value of G for surface, uncrusted soil	mm
G_e	value of G for wetting front, including crust effect	mm
h	depth or height of water	m
h_o	Chapter 5: normal flow depth for surface waterflow	m
	Chapter 4: initial value of h_m at $t = t_o$	

Symbol	Definition	Unit
$\bar{h}$	average depth of superelevation of water table above draintiles	mm
h_m	maximum height of superelevation of water table above draintiles	mm
H	total soil water potential, ψ - z	mm
H_c	integral capillary drive infiltration parameter	mm
H_o	daily net effective radiant energy in terms of equivalent evaporated water	mm
i	index subscript: represents spatial step in Chapters 4 and 5	
I	depth of infiltrated water	mm
I_a	initial abstraction in SCS Curve Number formula	mm
I_p	I at ponding during rainfall	mm
j	index of time increment in numerical expressions	
J	jacobian tri-diagonal matrix	
k_x	decay coefficient of carbon pool x in equations of residue decay	day^{-1}
k_o	dimensionless kinematic flow number: $= S_o L/h_o$	
K	local hydraulic conductivity of soil	mm/min
K_d	adsorption ratio	l/kg
K_{oc}	base adsorption ratio (multiplied by carbon content of soil to get K_d)	
K_g	K for gravitational flow of soil water	
K_s	effective saturated hydraulic conductivity, K at $\psi = 0$	mm/min
K_u	K for diffusive flow in soil water	mm/min

Symbol	Definition	Unit
L_p	length of flow path of surface water	m
L_c	length of flow path through channel	m
L_u	length factor in USLE equation	
m_p	content of pesticide in soil	kg/ha
m_{rL}	content of lignin in soil residue	g/m^2
m_{rN}	content of nitrogen in soil residue	g/m^2
m_{rC}	content of carbon in soil residue	g/m^2
m_{rP}	content of phosphorus in soil residue	g/m^2
M	number of identical surfaces feeding into sides of a channel (1 or 2)	
M_{lv}	plant dry matter in leaves and stems	kg/ha
M_m	density of mulch cover	kg/ha
M_p	total plant dry matter	kg/ha
M_{pm}	total potential maximum plant dry matter	kg/ha
M_s	mass of soil layer	kg/ha
n	Chapter 5: Manning roughness coefficient	
	Chapter 7: content of plant nitrogen	kg/kg
N	number of elementary units of runoff making up the catchment area	
p	probability function of a continuous random variable	
p_i	probability of a discrete random variable	
P	total depth of daily or storm rainfall	mm
P_u	factor for cropping practice in USLE equation	

Symbol	Definition	Unit
q	flux of local surface water, per unit width	m^2/min
q_e	flux of sink or source in soil column	mm/min
q_g	flux of soil water due to gravity	mm/min
q_i	inflow to computational layer	mm/min
q_m	flux of soil water into saturated zone that feeds draintiles	mm/min
q_o	outflow from computational layer	mm/min
q_p	peak rate of runoff	mm/min
q_s	flux of suspended sediment, by volume	m^3/min
q_u	flux of soil water due to capillary gradient	mm/min
Q	surface discharge	m^3/min
Q_{in}	inflow to pond	m^3/min
Q_o	outflow from pond	m^3/min
Q_s	outflow of sediment from watershed	kg/m^2
r	rate of rainfall	mm/min
R	hydraulic radius, a/ρ	m
$\underline{R}$	vector of R values at nodes along flow path	m
R_i	daily incoming solar radiation	langley
R_u	energy factor in USLE equation	ha-mm/N/hr
s_w	parameter of soil-water storage, used in SCS Curve Number method for runoff	mm
s_c	slope of soil-water characteristic, $d\theta/d\psi$	mm^{-1}
S	slope of flowing water surface	
S_o	slope of soil surface along flow path	
S_u	slope factor in USLE equation	
t	time (units vary with process)	
T	temperature	^oC

Symbol	Definition	Unit
T_K	Kelvin temperature	^oK
T_{min}	minimum daily temperature	^oC
T_{max}	maximum daily temperature	^oC
u	velocity of water	m/min
u_*	shear velocity	m/min
U_i	size-3 vector representing cross correlations in weather-generation model	
v	local variable of integration or local coefficient	
v_s	velocity of settling of particles	m/min
V	volume of water	m^3
w	width of section of surface flow (Ch. 5)	m
w_s	water equivalence of a snowpack unit	mm
W	width of distributed-flow unit (Ch. 2)	m
x	distance along path of surface flow	m
y_d	size of particle	mm
y_s	spacing of subsurface parallel drains	m
Y	random variate, value 0 to 1	
z	depth from surface	mm
z_c	side slope (ratio of h to v) of furrow or channel	
Z_t	total depth of soil profile modeled	mm
Z_r	depth of rooting	mm
α	Chapter 2: curvature parameter in soil-water characteristic function Chapter 3: shape parameter for gamma probability distribution function	
β	Chapter 3: scale parameter for gamma probability distribution function; elsewhere: relaxation fraction in numerical computations	

Symbol	Definition	Unit
γ	specific weight of water	
γ_s	heat capacity of a soil particle	$cal/cm^3/deg$
γ_w	volumetric heat capacity of water	$cal/cm^3/deg$
$\delta( )$	iterative correction term for equation of surface runoff	
Δ	slope of curve for saturation vapor pressure at mean air temperature	
ϵ	exponent in relation of K to Θ: $= (2 + 3\lambda)/\lambda$	
θ	content of volumetric soil water	
θ_r	content of residual soil water, a parameter in the soil characteristic function	
θ_s	content of natural saturated water, θ at $\psi = 0$	
Θ	normalized water content: $= (\theta-\theta_r)/(\theta_s-\theta_r)$	
κ_s	thermal conductivity of surface soil	mcal/cm
λ	pore-size distribution parameter, log slope of soil hydraulic characteristic	
ν	rate coefficient for kinetic model of adsorption partitioning exchange	min^{-1}
ξ	albedo	
ρ	wetted perimeter	m
ρ_b	wetted perimeter along the bottom of a furrow or channel	m
ρ_s	specific gravity of a particle	
ρ_z	wetted perimeter of the sides of a furrow or channel	m
σ	standard deviation of a random variable	
τ_c	critical shear at bed on which erosion is assumed to occur	N/m^2

Symbol	Definition	Unit
τ_N	stress factor for crop growth due to N deficiency in soil	
τ_s	shear at bed of surface flow	N/m^2
τ_T	stress factor for crop growth due to suboptimum temperature	
τ_W	stress factor for crop growth due to inadequate soil water	
ϕ	modifying coefficient for crop effects, used in various formulas to estimate erosion detachment	
χ_i	residual vector in generation model for daily weather	
ψ	capillary potential of soil water	mm
ψ_b	air-entry parameter for soil capillary characteristic function	mm
ω	relative time weighting in numerical method (0.5 to 1.0) (0.7 used in Opus)	

OPUS, AN INTEGRATED SIMULATION MODEL FOR TRANSPORT OF NONPOINT-SOURCE POLLUTANTS AT THE FIELD SCALE: VOLUME I, DOCUMENTATION

Roger E. Smith

1. INTRODUCTION

Models allow scientists to mathematically state what they have learned about nature and natural processes. The familiar equations $F = ma$ and $e = mc^2$ are models. The advent of computers has given scientists the ability to represent knowledge of the interactions of several related processes. To the extent that the resulting model duplicates nature, the model allows the study of "what if" questions and the completion of certain limited experiments that may require years or centuries by physical experiment.

Several models have recently been produced that deal with the many interactive processes occurring in the water-based ecosystem of an agricultural field (SPAW, NTRM, CREAMS, and EPIC, to name a few). All such models are imperfect in some sense because of the limited knowledge of the various processes and their interactions. Although good theories may exist for parts of this ecosystem, at least under laboratory conditions, natural heterogeneities always confound the application of these theories to field conditions. Other processes may be described only imperfectly, and empiricisms or conceptual approximations may be required to represent some parts of the system.

Nevertheless, the need to study the movement of potential pollutants from today's chemically intensive agriculture has stimulated the building of and the use of models for agricultural hydrology and transport. In all cases, published models are a compromise between scientific rigor and the practical limits as to the kinds of data that can reasonably be expected to be obtained for any model applications.

Opus (not an acronym) is offered herein as a potential improvement over currently available models for the processes of agricultural hydrology. It too is imperfect and has the same limitations as described above. However, Opus does overcome many of the weaknesses identified in several existing models (Smith and Ferreira 1989), and it has relatively advanced approaches to the simulation of water movement and chemical transport.

R.E. Smith, U.S. Department of Agriculture, Agricultural Research Service, Water Management Research Unit, Fort Collins, CO.

The purpose of Opus is to allow the study of the effects of management and weather inputs on the movement of water and potential pollutants within and from a small catchment. Using the available physical and chemical information and the guidelines in the User Manual (vol. II), one can describe the plant profile, soil profile, and topography of a small catchment; subject that information to either historical or statistically generated inputs related to weather and to management; and select from a variety of output types and details to summarize the results of interest.

This volume I describes the theory and methodology used in the various processes simulated by the model, to provide the user a background for understanding the capabilities and limits of the model. A second volume, the User Manual, describes the required input data and the output options, and gives (where possible) a guideline for the selection of appropriate parameters for a given condition.

In addition to and in conjunction with water movement, Opus simulates the processes of sediment transport and chemical transport, and also the cycles of carbon, nitrogen and phosphorus involved in microbiological decay in soil, flow of heat in soil, and growth of crops. The model shows the changes in these responses due to a wide variety of simulated management practices. Simulations of runoff, plant growth, and movement of soil water are always included; at the user's option, any or all of the other processes may be simulated concurrently.

The components of Opus were designed or selected to be of generally comparable precision. In other words, it was intended that one component not be treated with a level of detail incongruent with another component of equal importance to the simulation outcome. Nevertheless, the model components involve various degrees of development across the scientific disciplines represented. For example, the modeling of plant growth and response to stress has received less overall attention than has the modeling of surface runoff. There are necessarily some empiricisms in parts of the model; no model is entirely physically based, in the pure sense of the term.

Some parts or processes in Opus have been intentionally limited, as a choice between the complexity and the significance to most envisioned applications. For example, much of the thermodynamics of the soil-freezing and snowmelt processes involves latent heat of the ice/water system, which is not considered in Opus except in the case of snowmelt. The use of degree-day methods for estimating snowmelt is understood to be very approximate for a small area such as that treated by Opus. Also, diurnal variations in the surface-soil temperature are not treated: the average daily surface soil temperature is

considered acceptable for study of long-term variations in profiles of soil temperature. This eliminates detail that may make a limited improvement in long-term simulation and also eliminates the need for great detail in input data.

The scope of Opus is limited to runoff areas that are characterized by a single soil profile, have hydrologic complexity limited to first-order or second-order channel networks, and contain a single cropping system or plant-cover regime. This does not mean that only one crop per year is considered but rather that any given crop combination must represent the entire field area of interest. The model is not limited to annual crops, and it can treat perennials such as grassed and grazed pasture. Opus can simulate periods of a few days (with an intensive look at one or two hydrographs) to many decades.

The model allows several choices for simulation of the hydrologic process. The choice will generally reflect the amount of detail of data that a user is expected to have. The hydrologic options are diagrammed in figure 1. Implied in the variety of choices here is that the model is intended to have potential uses ranging from management to research. The available data should be appropriate for the intended use of the model. Stochastically generated weather may be adequate for long-term simulations to observe alternate management schemes, but to look at details of hydrologic processes such as peak runoff and sensitivity of erosion to microtopographic changes, one should have data on the pattern of rainfall intensity. The physically based simulation of infiltration from rainfall is impossible without such rainfall data. Because these data are often recorded by noting the times and depths when the rate of accumulation changes, or the graph slope "breaks," these data are commonly and herein referred to as breakpoint rainfall data.

Much of the model is original, but parts have taken advantage of process models developed by others. Included is a daily weather generation model, which was taken with minor adaptation from the WGEN model of Richardson (1981). The evaporation and evapotranspiration potential is based on the model of Ritchie (1972), which is also used in the CREAMS and EPIC models. The daily runoff model is basically a modified SCS Curve Number approach that was developed by Williams (Smith and Williams 1980) and is similar to that in the EPIC and SWWRB models (Williams et al. 1984). The soil erosion model accompanying the daily model is from MUSLE (Williams and Berndt 1977).

The soil microbial system, including cycles of carbon, nitrogen, and phosphorus, is a daily time step version of the Century model (Parton et al. 1988a,b). That model was modified by Parton for Opus to operate on daily time scales and to include the addition of fertilizers and plant residue from the plowing under of surface material.

Opus operates on a basic daily cycle of simulations (illustrated in fig. 2), with an accounting cycle of 1 year for purposes of summaries. In the more intensive hydrology option based on rainfall intensities, a smaller interstorm cycle is used for the redistribution of soil water between storms when more than one storm occurs in a day. The processes of management changes, plant growth, snowmelt, and nutrient cycling are implemented on a daily time step.

The remaining chapters in this volume (2 through 9) detail the methodology used in the simulated processes and indicate how the processes interact. Volume II, the User's Manual, further describes the structure and various options of the program and gives information on specific data requirements. References cited in volume I are listed after chapter 9.

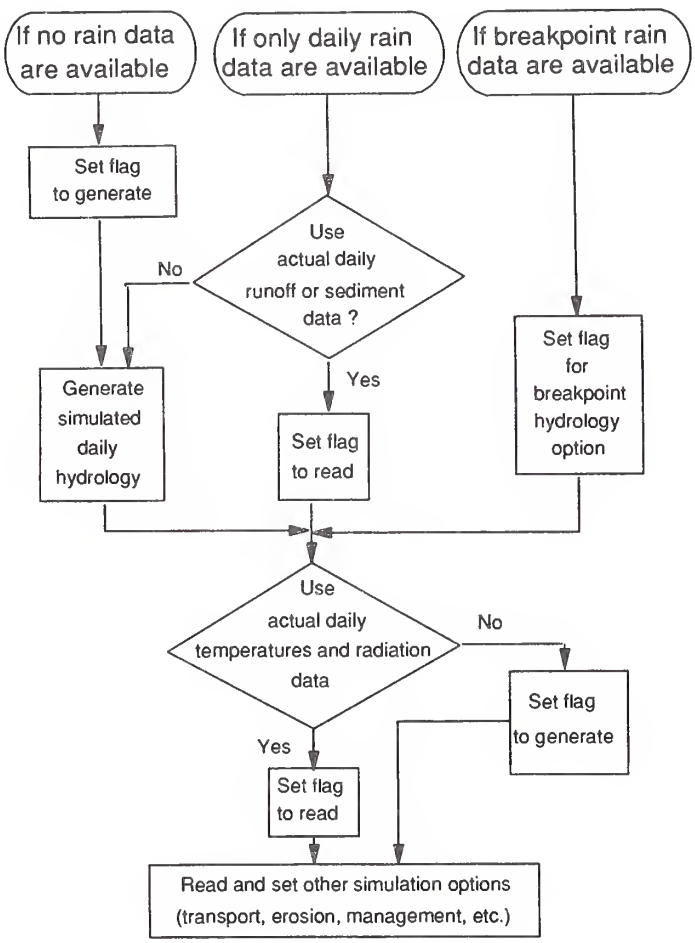

Figure 1.
Options for method of hydrologic simulation available within the Opus program.

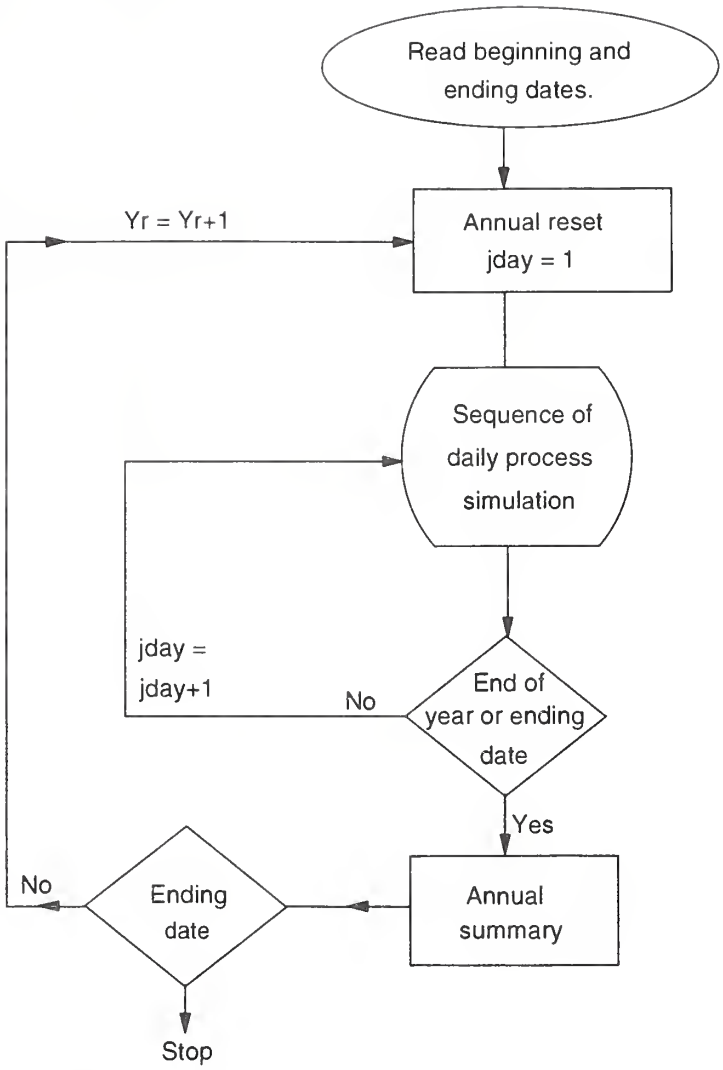

Figure 2.
Basic daily and annual cycles of continuous simulation for Opus.

Opus deals with the space over and within small catchments, from above the plant to below the root zone in the soil. This is almost never a simple system, and any computer simulation begins with abstractions to describe the system in terms that allow satisfactory simulation of the processes. Two of the most important geophysical features of a catchment are the surface topology (slopes and flow paths of surface water) and the soil profile (soil hydraulic properties and how they may vary with depth from the surface). This chapter indicates how these two key hydrologic components are described for Opus.

Specifying the Catchment Topography

Topography is a key factor in the transport of potential pollutants within and from a catchment. Topography controls the paths of surface waterflows and influences the velocity of those that occur from rainfall runoff or from irrigation. Finally, topography can enhance or inhibit the erosion of surface material.

Actual catchments are almost always complex in shape at any level of detail. To simulate the surface hydrology without requiring excessive amounts of input and/or computational detail, it is necessary to describe the catchment in geometrically simple terms while retaining the most important features in the hydraulics of the surface flow.

The daily hydrology option is a lumped-time approximation and is necessarily also a spatially lumped method. Topographic information is useful in that method only in general measures, such as mean flow lengths and slopes. Some of the following discussion will therefore not apply because of the lumping involved. On the other hand, the infiltration-based hydrology option is relatively sensitive to topography, and the runoff is routed over the space of the simulated areas according to the specified geometry (described below).

The method used in Opus to interpret the actual topography of a catchment is illustrated in figure 3. From our present understanding of surface-water hydrology, we recognize the following features that should be preserved in the geometrically simplified description: Catchment area; mean path length for shallow distributed flows; mean path length for channelized flows, where applicable; and net slope of the mean flow path.

As shown in figure 3, the properties of each part of the flow path are conserved separately. In addition, the mean-slope profiles may be preserved and treated in the distributed hydrology option. As explained in the User Manual, the profile is described by specifying the slope at each point along the profile where there is a change in the rate of change of slope (illustrated in fig. 4). Convergence of the surface (distributed) flow, as when water flows toward one point at the catchment boundary, may also be simulated. As illustrated in figure 3, this convergence is simulated by preserving the width at the catchment divide in the transformed geometry.

Abstracting the Real Catchment

The basic topology of the catchment in the model is limited to (a) a single distributed flow surface contributing uniformly along one side of a first-order channel, (b) a matched pair of such surfaces contributing to both sides of a first-order channel, or (c) item b plus a small area contributing to the uppermost point of the channel. The total simulated area may be made up of N units of such topology, integrated by a second channel. The second channel does not directly receive input of surface water from a runoff surface, but takes the outflow from the N catchments uniformly along its length. Such a channel receiving multiple inputs would simulate, for example, the function of a terrace outlet channel.

The structure described above can be used in varying forms and degrees of approximation to represent most topologies found in small catchments. Asymmetrical cases (where a first-order channel receives contributions from different-sized areas on its two sides, or where the slope profiles on each side may be significantly different) can be treated in Opus only by taking mean properties (forcing symmetry) in each case. Inclusion of detail of simulation and necessary data to treat asymmetrical cases explicitly is believed to be uneconomic for the purpose of the model, because of the additional computation time required. When the area on one side of a channel is quite small compared with the other, the small side can (for most purposes) be added to the large side without significant error.

An important feature to be considered in describing the flow-path topology for hydrologic simulation is the role of agricultural row furrows in controlling the path of water across a given field. This path seldom corresponds to the path that would be taken by surface water in the absence of furrows. In the case of contour or near-contour plowing with or without terraces, the flow path may be entirely different. In some cases where management changes sufficiently during a rotation period, the flow-path topology may change from year to year, or may change at the end of a season if the rows are obliterated. For this reason, the Opus model provides for alternate descriptions (sets of descriptive variables) of the flow topology within the same field area. Case 1 describes the flow topology for flow unaffected by furrows, as on a meadow. Case 2 describes flow-path geometry when the flow path is affected by a furrow direction superimposed on the natural contours. If the model is used for natural catchments (for example, untilled pasture), only the case-1 topology needs to be described.

Figures 5 and 6 show topology of two possible cases of flow path for one hypothetical field. Subscript 1 is for natural flow (case 1), and subscript 2 is for furrow-directed flow (case 2). In figure 5, flow follows the natural shape, flowing

across the contours and thus converging toward the outlet (here pictured as a small pond). In the methodology of Opus, the width of the flow surface at the upper end of the flow path is calculated from the user's estimate of the mean length of the flow path, the field area, and the width of the flow path at the bottom. If the same field is tilled as in figure 6, case-2 hydrologic topography is produced, and the furrows cause runoff to flow from left to right along the furrow "microchannels." Convergence of flow cannot occur as in case 1 (unless the furrows are overtopped and/or eroded away). In the furrowed case, the total flow path is lengthened and the path-slope profiles are correspondingly changed. The total change in elevation from top to bottom is the same, and the topological parameters should preserve it. This may be stated mathematically, using subscripts for the respective cases, as follows:

$$\int_0^{L_1} S_1(x)dx = \int_0^{L_2} S_2(x)dx \qquad [1]$$

where L_1 and L_2 are total path length for cases 1 and 2, respectively, S_1 and S_2 are case-1 and -2 slopes, and x is distance along flow path.

Figure 7 gives two other examples in which simplified hydrologic geometry is obtained from natural topography. In the upper example, because natural flow occurs normally with the contours, the field's actual shape should be distorted somewhat to preserve the actual flow-path length in the simplification. This is because the flow, as shown, is at some angle to the (constructed) field border and is thus somewhat longer. Thus the simplified width is made slightly less than the topographic width to preserve the total area and mean path length. Another way to describe this is to say that the area is represented by a parallelogram of the given area.

In the lower case in figure 7, flow diverges as it moves from the hilltop toward the channels. This case could be simplified into two planes, each contributing to the side of a different channel, with the two channels then joining. To preserve the area ABC and a selected mean flow length (L_{p1}), the width of each abstracted plane is calculated as $W_1 = \text{area}/L_{p1}$. The mean width in this case would be less than L_{c1}. Opus accounts for this situation by apportionment of surface flow along the receiving channel length. On the other hand, if the width so calculated is greater than L_{c1}, then converging flow is indicated, which is explicitly modeled in the equations for surface routing (see ch. 5).

Terrace systems are common; figure 8 is a representation of a terrace system. The Opus topological approximation requires that the individual areas of terrace drainage be represented as equal. Usually this is more or less true. Further, it is assumed that terrace spacings are identical. This is even more commonly the case. Note the two sequential channels labeled L_{c1} and L_{c2}.

This case illustrates another important aspect of hydrologic topology. If the rows are plowed closely parallel to the contours and to the terraces, the major direction of runoff will be across the furrows and will occur only after a certain amount of surface water has accumulated. Opus recognizes this case by investigating the furrow slopes. When slopes are negligible and runoff exceeds an estimated furrow storage based on furrow depth and width, Opus simulates furrow overtopping.

Implementing Topography in the Model

Once the subject topology has been conceptually simplified, it must be described to the computer program. The minimum requirement for input to Opus is description of case-1 (unfurrowed) topology. This is sufficient for natural catchments or unplowed pastures and meadows. Case-2 topology is also described whenever (a) the initial furrow depth is significant or (b) management operations creating significant furrow depths are included in the operations menu (described below). Undisturbed fields where no management operations are used need to have only the case-1 topology described.

As noted above, from one to three elements make up the topological network, through which water is routed in order. The first element is a flow surface across which flow is assumed to be uniformly distributed, but the surface is not necessarily a plane surface. This element may represent one of two relative scales. At the smallest scale, where furrows or ridges are a significant part of the surface area (such as large furrow terraces used on severely sloping land), the first element may represent the sides of the ridges and may be only a few meters long. In this case, the furrow or swale between ridges becomes the channel element 2. Where ridges are close as in ordinary furrows, it is not recommended to represent fields in this detail, because it is unnecessary to route water over a flow path 1 meter or less long.

For ordinary use, it is preferable to use a larger scale approach and consider all the furrows on a slope together as the first element. The input data for Opus allow the user to describe the flow geometry of the furrows without needing to treat each one as the second (channel) element in the routing sequence.

The elementary catchment unit of an Opus field is made up of either one or two (M = 2) distributed flow elements contributing to a channel (element 2). The topology of Opus, for simplicity alone, is characterized by symmetry. Thus there can be a number (N) of elementary catchments, but they must be equal. An additional upstream area (A_u) that contributes to the head of the channel (element 2) may also be designated. Figure 9 is a scheme of an example system for a case where M = 2, there are three elements in the field (one surface and two channels, not counting the A_u areas), and four units make up the field (N = 4).

If specified, the third element (the second channel) receives uniformly distributed input from elements 2 along its length. It can also have an upstream area (A_u) contributing separately from the N basic catchment units. At the third element level, however, no multiples (N) make up the total field; there can be only one channel element 3. Figure 10 shows the third element acting as a terrace channel outlet, such as in figure 8. In figure 10, all A_u values are 0 and M = 1.

Within the program, the flow length of each element is divided into computational increments. There can be from 3 to 20 such increments for any element flow path, depending on length of the flow path. The number of segments is generally taken as $\sqrt{2L}$, with L in meters.

Convergence of flow along element 1 is found from the geometry parameters. As discussed above, the mean flow length (L_p) and the area of distributed flow surface are preferentially preserved, and the mean width is found by division: $W = A_p/L_p$. If the channel (element 2) length is greater than W, then P_p flow is assumed parallel in element 1. But if the channel length is shorter, a convergence rate is calculated and used in the surface-water routing. Convergence is not allowed when parallel flow along furrows of case 2 has been otherwise indicated.

More details and examples of how to specify various conditions within this system are given in the User Manual.

Characterizing the Soil Profile

The soil profile is assumed to consist of one or more soil horizons, with each horizon differing from its neighbor in some significant manner. Such differentiation may consist of (a) differences in texture and thus hydraulic characteristics or (b) significant differences in nutrient or other organic characteristics.

An Opus user may describe a soil profile made up of as many as 10 horizons. For computational purposes, the specified profile is subdivided systematically (by the program) into smaller layers, as illustrated in figure 11. Smaller divisions are main-

tained at shallower depths, where the most rapid soil-water changes occur. Opus also internally subdivides the soil profile into three sectors for the dynamics of residue and nutrients: a litter layer at the surface, a microbiologically active soil layer, and the deepest layer. Presumably, these divisions separate microbiologically dissimilar environments. The active layer is assumed to extend from the soil surface to the horizon interface nearest a depth of 200 mm (Parton et al. 1988b), or to that depth if only one horizon exists.

The soil profile is an important hydrologic element because it is a porous medium through which water flows and is also a medium in which plants grow and extract water. Thus the soil horizons must be described in quantitative terms that relate to the soil's hydraulic characteristics. The statement that a certain horizon is a "B1" horizon, for example, does not give information that can be used in simulating its water-holding and water-movement characteristics. The same is true to a certain extent for a soil's taxonomic name or color; that is, those labels do not indicate a soil's hydraulic characteristics.

Whenever the soil is partially saturated, liquid soil water occurs in intergranular interfaces. Because of the strong surface tension of water, a significant negative pressure, which is locally continuous through the soil, is characteristic of the soil water at a particular water content. The lower the water content, the smaller the effective radii of the water surface at the granular interfaces, and the higher the negative pressure. This pressure is usually measured in terms of effective potential or head of water. It is the gradient of this potential that causes water to move in the soil. Most management models today, by contrast, treat soil-water movement using concepts of storage filling and draining.

The function used in Opus to describe the relation of water content to matric potential is illustrated in figure 12. The general expression, which can describe the characteristic relation, may be stated as

$$\Theta = [1 + (\psi/\psi_b)^{\alpha}]^{-\lambda/\alpha} \qquad [2]$$

in which Θ is normalized volumetric water content, defined as

$$\Theta = (\theta - \theta_r)/(\theta_s - \theta_r) \qquad [3]$$

and ψ is matric soil-water potential (mm),

ψ_b is a parameter representing air-entry potential (mm),

α is a curvature coefficient affecting the shape of the curve near ψ_b,

λ is a pore-size distribution parameter,

θ is volumetric water content,

θ_r is residual water, theoretically the water unextractable by capillary forces, and

θ_s is water content at 0 matric tension.

This expression is similar to that of van Genuchten (1980) but relates directly to the Brooks and Corey relation (1964), which contains parameters that represent physical concepts.

The companion relationship describing the unsaturated hydraulic properties of soils is the relation of hydraulic conductivity (K) to water content. One robust expression for this relation is

$$K = K_s \theta^{\epsilon} \qquad [4]$$

in which K_s is effective saturated ($\psi = 0$) hydraulic conductivity (L/T),

and according to Brooks and Corey (1964), ϵ may be approximated as

$$\epsilon = (2 + 3\lambda)/\lambda \qquad [5]$$

In general, ψ_b is smaller for soils with large particle sizes and is larger for soils with fine particle sizes. Similarly, λ is small for soils with a well-distributed range of particle sizes and is large for soils with a very uniform particle size, such as sand. The value of K_s varies widely but follows a trend similar to that of λ.

To describe a soil horizon, therefore, Opus requires five major parameters: λ, θ_s, θ_r, ψ_b, and K_s. In Opus, α is fixed for simplicity at 5.0. The selection of reasonable values for the hydraulic characteristics of a particular soil horizon is an important task for the user of a physically based model. Opus takes advantage of the extensive data assembly and analysis by Rawls et al. (1982) to give the user a survey of the expected values of these critical parameters. This use of regression provides a way to estimate reasonable parameters in most cases from the user's knowledge of the soil texture (Brakensiek et al. 1984). The accuracy of Opus in simulation depends in large measure on the accuracy of the parameters chosen. Experimentally determined soil data are, of course, most preferable. Other sources of such soil hydraulic data exist (e.g., Holtan et al. 1968). The importance of characteristic relations in the simulation of soil-water movement is discussed in chapter 4.

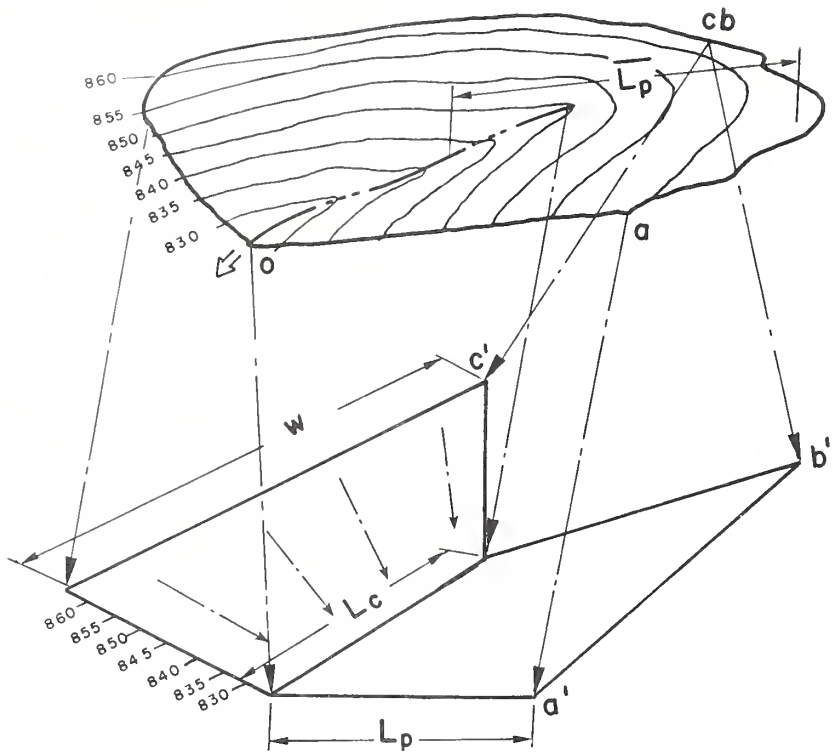

Figure 3.
The geometric variables used to describe topography of a catchment. The descriptive variables represent a geometric simplification of the real catchment, which retains the major hydrologically sensitive measures of the catchment. These include area, mean flow path of surface water (L_p), channel length (L_c), and convergence.

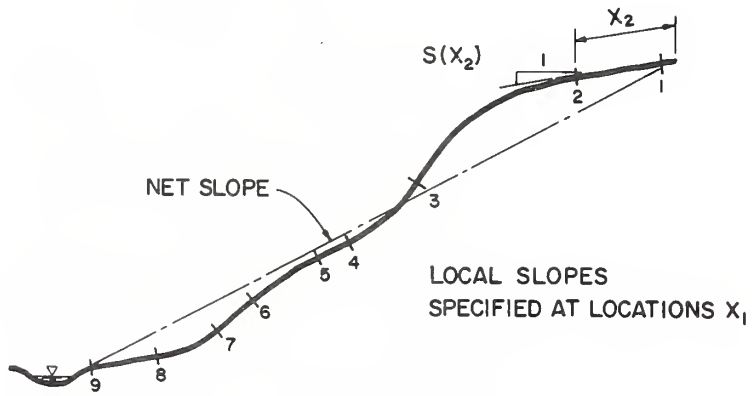

Figure 4.
Varying slope profile of a catchment described by specifying each point at which slope trend changes, assuming each slope segment to be an arc. For example, the slope between x_2 and x_3 changes smoothly and needs no intermediate specification points.

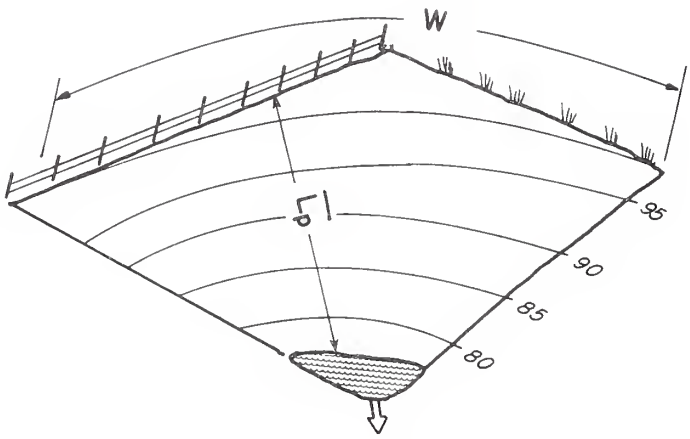

Figure 5.
Example geometry of a convergent field with flow not controlled by furrows. A mean length is estimated as shown. The upper catchment width would be very large compared to the width at bottom, to represent convergence of flow lines toward the pond.

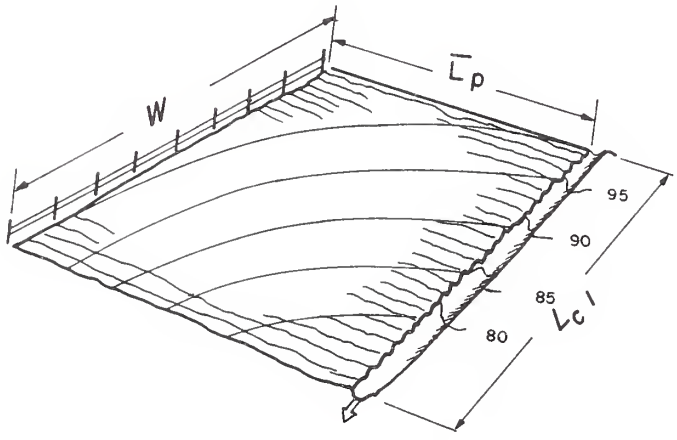

Figure 6.
The same field as in figure 5, plowed to produce very different flow path. The width and length are both changed, but the area remains the same. Now a channel of length L_{cl} receives water from the furrows.

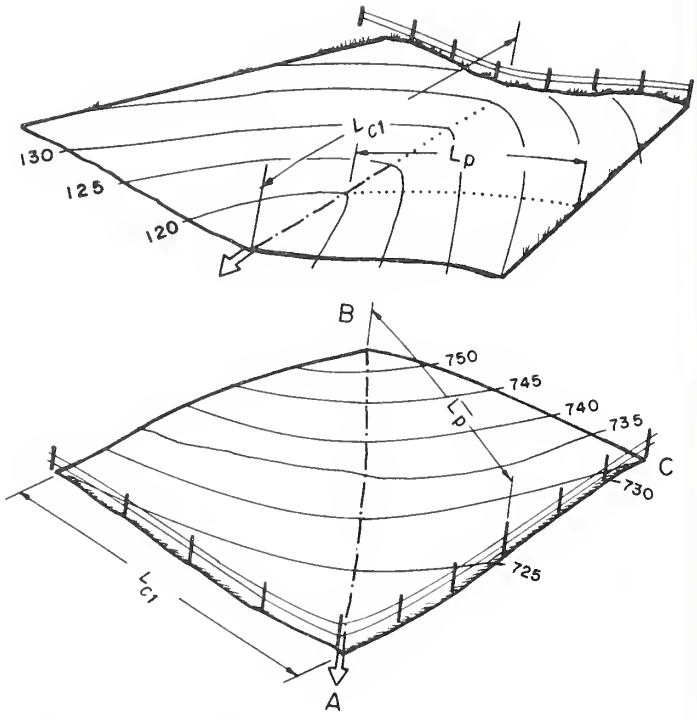

Figure 7.
Two more examples of how surface flow is specified for fields of different topological characteristics. Divergent flow from the lower field is simulated by two different approximate planes. L_p is average flow length.

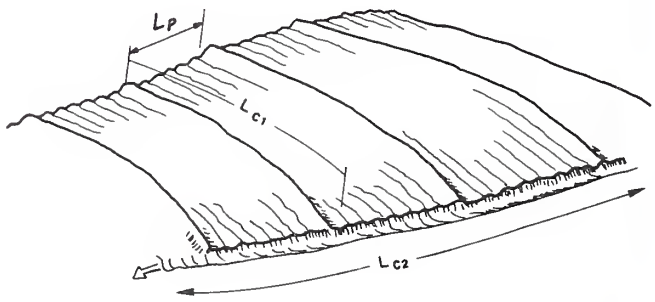

Figure 8.
Representation of a typical terrace system. Terrace systems are common. Opus provides for a second-order channel (length L_{c2}) to collect flow from the terrace intercept channels (length L_{cl}).

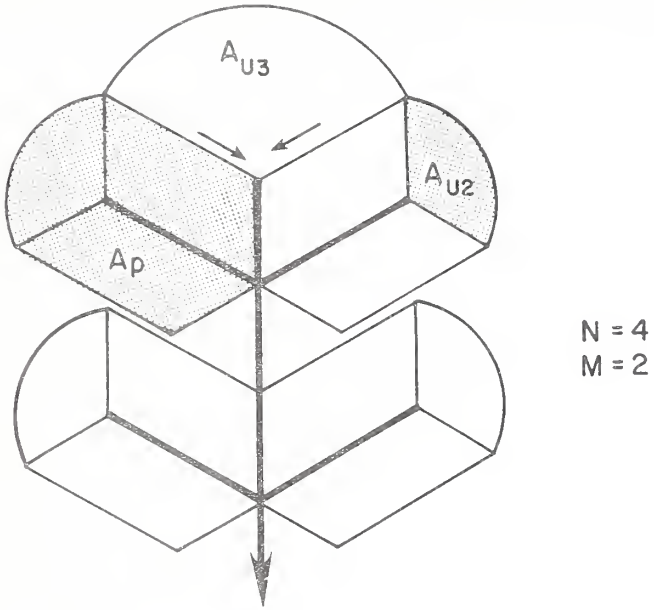

Figure 9.
Example scheme of field topography. Opus limits complex geometries to symmetrical patterns, as shown here. Opus allows upslope areas that feed into the upper end of channels, here labeled A_{u2} for first-order channels and A_{u3} for second-order channels. The overall area is divided into four units, and each unit feeds from both sides of the channel (M = 2).

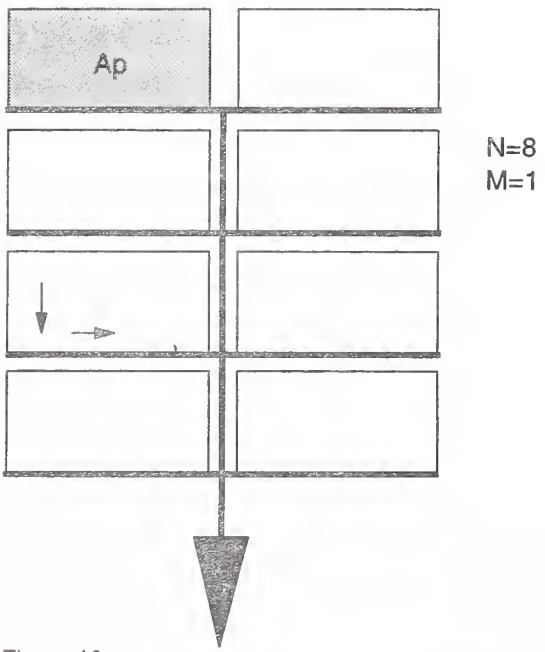

Figure 10.
The terrace channel system as described for Opus, in simple geometry. Each of the eight units feeds to one side of its receiving channel (M = 1).

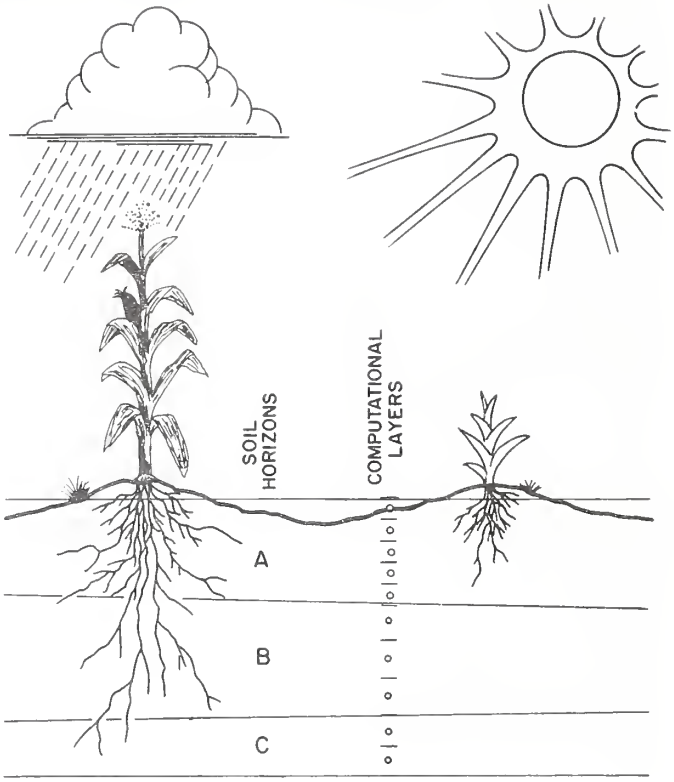

Figure 11.
Soil horizons (e.g.,A, B, C) are specified by the user and further divided into computational increments within the program.

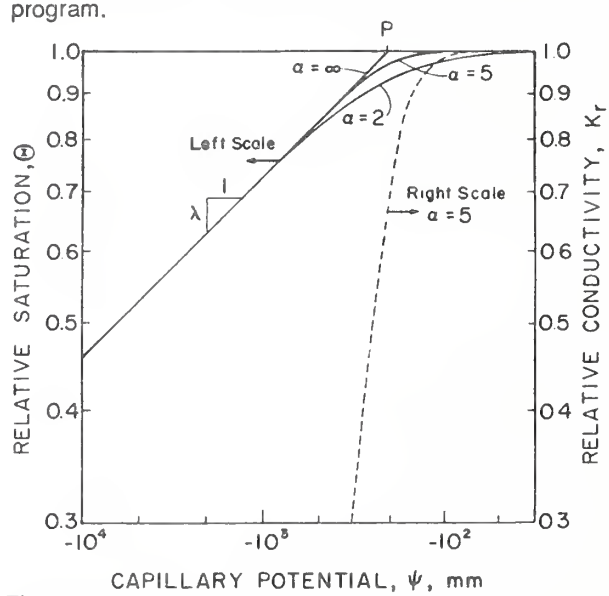

Figure 12.
The unsaturated soil hydraulic characteristics are represented by an analytic expression that allows fitting to most soil types. Water content is normalized to relative saturation, Θ, as shown in equation [3].

The field unit simulated by Opus may be thought of as an ecosystem, including the plants and soil down through the root zone. In this conceptual framework, the meteorological processes are the driving forces for this system, and the description of those processes is a crucial part of the simulation process. The meteorological variables that "drive" or excite the system here include daily solar radiation (measured in langleys), daily maximum temperature, and precipitation. These "drivers" may be input or in some cases may be generated from input statistical parameters representing an analysis of local historical records.

Alternatives for Weather Simulation

Whenever available, records of daily maximum and minimum temperatures, daily radiation, and rainfall for a location are input to drive the simulation. The input format is described in the User Manual (vol. II). In practice, all required data (on meteorological variables) may not be available for many locations for which simulation studies are desired, or may not have been collected frequently enough to allow physically sound simulations. Most likely the user will have only Weather Bureau summary data perhaps including monthly means of temperatures, or will have only daily precipitation records, or will have some combination of these data. So Opus has been designed to accept a variety of combinations of such actual records, including daily values or historical monthly means of any of the maximum temperatures, minimum temperatures, and net radiation.

The weather model in Opus is built around a variation of the WGEN model (Richardson and Wright 1984), which requires as a minimum no additional data, but falls back on a set of furnished parameter maps for the continental United States. In addition, Opus accepts data on monthly average temperatures and radiation, and reconstructs either a smoothly changing record or a serially correlated random record with the given characteristics. Thus a variety of available data can be used in conjunction with the WGEN model to produce the necessary weather record for simulation.

Fundamental to this model is the idea that these weather parameters are intrinsically linked--that temperature variations and radiation variations from day to day should be related to each other and to the occurrence pattern of rainfall. The model can maintain both the statistical features of observed time series and the generally observed interdependencies between physically related variables.

The data-generating process and its assumptions are summarized below. In many cases, although daily temperatures and radiation values are available for a certain period of record, the user may choose to generate data when longer simulations are desired, instead of creating and handling massive files of input data.

Simulation of a Precipitation Record

When either daily or pattern ("breakpoint") data for rainfall are available for the period for which the simulation is to be performed, the data are given to the model in the form of a sequential data file. If such data are not available or if it is desired to simulate for periods longer than the available record, a statistical model of the occurrence and depth of daily rainfall may be used to generate rainfall sequences appropriate to the local climate. Note that only daily rainfall can presently be stochastically generated; breakpoint data must be provided.

Simulating Occurrence of Daily Rain

The occurrence of daily rainfall is modeled by WGEN as a Markov chain process, simulating the binary sequence of wet days and dry days. On rainfall days, or wet days, the amount is randomly distributed according to a two-parameter gamma distribution. A wet day is defined as one on which more than 0.25 mm (0.1 inch) of rain falls. The following description is a summary of the WGEN methodology, and the reader is referred to Richardson (1981) or Richardson and Wright (1984) for a more complete discussion.

The Markov chain model of a binary process deals with transition probabilities, that is, the probability of the transition from a wet day yesterday, for example, to a dry day today. Let $p_i(w|d)$ represent the probability of a dry day following a wet day on day i. Then clearly,

$$p_i(w|w) = 1 - p_i(d|w) \qquad [6]$$

and

$$p_i(d|d) = 1 - p_i(w|d) \qquad [7]$$

Thus, specifying two of these four transition probabilities, $p(d|w)$ and $p(d|d)$, fully defines the model. These probabilities change with seasonal climatic changes. With enough historical data, one can get a good picture of the change in transition probabilities in some climates over periods as short as 5 days to 1 week. For purposes of Opus (and in WGEN) it is considered adequate to define weather trends by month. Thus i is used in equations [6] and [7] as a monthly index, and the rainfall-occurrence model requires a total of 24 parameters. Richardson and Wright (1984) have tabulated these parameters for many locations in the United States. These data help in modeling for ungaged basins and are reproduced in the User Manual.

Simulating Depth of Daily Rainfall

The probability of the amount of rain, v, on wet days, p(v), is estimated by a two-parameter function for gamma probability density:

$$p(v) = \frac{v^{\alpha-1} e^{-v/\beta}}{\beta^{\alpha} \Gamma(\alpha)}, \quad v, \alpha, \beta > 0 \qquad [8]$$

The symbols α and β are the parameters for shape and scale, respectively. Like the transition probabilities, they are assumed to vary by month at each location. Stochastic simulation of a daily amount involves generating, on days for which runoff is predicted to occur, a random variate Y: $0<Y<1$. Then Y is made to have the distribution

$$Y(v) = \int_0^v p(v)\, dv \qquad [9]$$

which is inverted to solve for the precipitation value v satisfying this relation. When equations [8] and [9] estimate values of v less than 0.25 mm, they are ignored and another value is produced. This procedure is consistent with the definition of a wet day given above.

Simulation of Daily Radiation and Temperature

The simulation of daily radiation (in langleys), daily maximum temperature, and daily minimum temperature depends on options chosen by the user and on the existence of any input records of those variables. The basic model for the variation of these three variables (heretofore referred to as "weather" variables) assumes that in the mean they follow a sinusoidal annual variation, have a random variation about this mean pattern, are cross-correlated, and are correlated with the wet/dry pattern of rainfall. This part of the model is also taken from the WGEN model of Richardson (1981) and is briefly described below. Richardson's methods have been slightly modified to allow operation in the Celsius scale of temperatures. The changes to this basic weather model to account for recorded input data are described in the following section.

Generating Mean Values for Daily Temperature and Radiation

If monthly data on temperature and radiation are provided, the simplest method for obtaining estimates of record-averaged daily weather values is to interpolate between the monthly mean values obtained from the input data, assuming that the monthly mean applies on the day at the middle of the month. This provides a smoothly changing value for each record of maximum and minimum daily temperatures and daily solar radiation. With

this method, the value for these parameters on a given date will be identical for each year. For some simulation purposes, this estimate of weather data will be adequate. For this and other options, Opus applies a bias upward or downward, depending on whether the day is dry or wet, respectively.

Generating a Stochastic Record of Daily Temperature and Radiation

To obtain a more realistic sequence of daily weather variables, with or without dependence on recorded monthly mean values, an autoregressive generation scheme may be used for each of these weather variables. Monthly mean values may be used, but daily values are generated based on the model described by equations [6] through [9] above. Parameters are obtained from Richardson's parameter maps of standard deviations and variable cross-correlations (in app. D of the User Manual). Thus daily radiation, for example, can be a random variable that has the mean and standard deviation as specified by the input data, but also is correlated with yesterday's value. The value for daily radiation shifts downward if rainfall occurs.

The procedure for generating daily values of T_{max}, T_{min}, and R_i (maximum temperature, minimum temperature, and solar radiation, respectively) was presented by Richardson (1981). Each of these daily values is assumed to be related to its value yesterday in an autoregressive manner as

$$x_i(j) = Ax_{i-1}(j) + B\chi_i(j) \qquad [10]$$

where

$x_i(j)$ is the vector of residuals of T_{max} $(j = 1)$, T_{min} $(j = 2)$, and R_i $(j = 3)$ on day i,
χ_i is a size-3 vector of independent random components, and
A and B are 3X3 matrices whose elements define the serial and cross-correlation properties of these variables.

Richardson (1981) found that although means and standard deviations vary in space and time, it is a very acceptable approximation to assume constant values of correlation relations described by matrices A and B. Opus uses such fixed matrices.

Since x_i is a residual value, with mean 0 and standard deviation 1.0, the generated value of any given variable, $v_i(j)$, is then found as

$$v_i(j) = \bar{v}_i(j) + x_i(j)\sigma_i(j) \qquad [11]$$

where j indices are as defined above,

$\bar{v}_i$ is the mean value of v for day i, and

σ_i is the standard deviation of v for day i.

The generation model distinguishes two sets of parameters for each location: one is for wet days and one is for dry days. Each set includes parameters for the mean and amplitude of the Fourier two-term series description of the mean value of each variable, plus a mean and amplitude for a Fourier model of the coefficient of variation of each. The mean and amplitude of the coefficient of variation for radiation are assumed the same for all locations, based on analysis of the U.S. data. In operation, Opus converts coefficient of variation into standard deviation, to avoid possible division by zero when operating in the Celsius temperature scale.

Using Recorded Monthly Data

When monthly mean recorded data are available for any of the three weather variables, Opus adjusts generated values to have monthly mean values equal to the corresponding recorded means. The model uses recorded data in comparison with the Fourier means for each month, and determines a shift factor that keeps the generated mean values consistent with the input values of monthly means. The weather-generating parameters may be taken from parameter maps referred to above, and are supplied as input to Opus in any case.

Reading Recorded Daily Data

When recorded daily data are available, an option in Opus allows the user to bypass the weather-generating model and to read actual recorded weather data on a day-by-day basis. A separate input file is used for this option. Such recorded weather data may include the three weather variables (described above), the runoff, and the daily sediment production. This option is included for users wishing to simulate only ancillary processes such as plant growth, transport of nutrients, or transport and decay of pesticides.

Potential Evapotranspiration

The values of temperature and radiation on a given day can be used to calculate the potential evapotranspiration (E_t) on that day. Actual transpiration plus soil evaporation is less than or equal to E_t, and depends on plant and soil conditions. The method used in Opus to calculate E_t is a modified form of the equation used in CREAMS. It was developed by Ritchie (1972), starting from the relations of Penman. The equation and its components are

$$E_t = (1 + c_w)\ \Delta H_o/(\Delta + 0.68) \qquad [12]$$

where

c_w is a coefficient expressing effects of wind and humidity,

Δ is slope of curve for saturation vapor pressure at mean air temperature, represented as

$$\Delta = 5304.0 \exp(21.255\text{-}5304.0/T_K)/T_K^2 \qquad [13]$$

in which

T_K is daily mean Kelvin temperature

The value of c_w is 0.28 in Ritchie's equation, but Opus allows the user to modify it to account for local conditions. Conceptually, humid conditions reduce this factor, and windy conditions increase it (Ritchie et al. 1976).

The second variable in the E_t equation is defined as

$$H_o = R_i(1 - \xi)/58.3 \qquad [14]$$

where

ξ is albedo of field surface (described below), and

R_i is incoming solar radiation, in langleys/day

In these expressions, R_i is the daily solar radiation in langleys/day. Equation [14] is an estimating algorithm for the daily net effective radiant energy (H_o). The units of E_t are millimeters of water, and E_t can be thought of as a derived daily variable for weather. Note that 1 langley/day = 0.041868 $mj/m^2/day$.

The field albedo (ξ) is calculated as a combination of area-weighted factors for plant and mulch cover, snow cover, and surface soil. The albedo of dry surface soil is an input parameter. Snow albedo is presumed to vary with time (in days) after snowfall (t_s), as follows:

$$\xi_{snow} = .4 + .5\ e^{(-t_s/12)} \qquad [15]$$

Soil albedo varies with normalized moisture content (Θ) and compares with the dry soil albedo (ξ_{ds}) as follows:

$$\xi_{soil} = \xi_{ds}(1.0 - 0.4\ \Theta^2) \qquad [16]$$

Plant and mulch albedo is assumed constant at 0.23.

Time Distribution of PE_t

Figure 13 schematically illustrates how Opus assumes the major weather variables to be distributed in time. Time distribution is important because computational time intervals, which vary with the hydrologic conditions, may consist of any portion of a day. On days that include a rainfall event, the beginning and ending times of that event are found or assumed, and the E_t for that day is assumed to be that occurring in the nonrainfall portion of the daylight hours. Radiation is assumed to be distributed sinusoidally between dawn and dusk (as shown in fig. 13) on rainless days. From equations [12] and [14], this implies a sinusoidal distribution of E_t as well. A small time interval near dusk or dawn contributes considerably less incremental E_t than does an equal time near noon.

Division of PE_t Between Plant and Soil Surface

For an estimated daily E_t, the soil and plant conditions determine the daily proportion expected to be evaporated from the soil surface or transpired through the plant leaves, or in winter the amount evaporated from snow surfaces. In addition, some of the E_t will be used when water is intercepted from precipitation and stored on plants or surface material. Such intercepted water has first access to E_t. The remaining E_t, which we here refer to as E_t', is divided among soil and plants.

Transpiration is estimated on the basis of total area of leaves. That portion of E_t' consumed by plants is estimated as

$$E_p = E_t' F_p c_s \quad [17]$$

where

F_p is relative surface area shaded by plants, and

c_s is relative effectiveness of plant cover as a function of leaf area index, as follows:

$$c_s = 1/\ [1 + (2.5/F_L)^5]^{0.2} \quad [18]$$

where F_L is leaf area index.

Leaf area index is defined as the ratio of the total leaf surface of a plant to the ground area projection or shade under the plant. Equation [17], through F_p, also accounts for sparse plant cover (when plants do not cover the entire ground surface). The value of c_s can vary from 0 to 1. Further discussion of the use of plant water is in chapter 7.

Soil evaporation is estimated from the portion of soil surface not shaded by plants or surface litter (mulch). The total shaded area includes both live plant cover and surface mulch cover, and is estimated as

$$F_s = F_p + (1 - 0.5F_p)F_m \quad [19]$$

where F_m is relative area covered by mulch.

The relative amount of E_t' assigned to soil evaporation is controlled by the soil-water content in the near-surface region. Without this latter control, the potential soil evaporation part of E_t' (E_{ps}) is

$$E_{ps} = E_t' \exp(-1.2F_s) \quad [20]$$

Soil evaporation proceeds in the two-stage process assumed by Ritchie (1972) and used in CREAMS (USDA 1980). The first stage is short and proceeds at the potential rate (E_{ps}) based on micrometeorologic conditions. The second stage represents soil-limited evaporation, and the rate is reduced proportionally to the square root of time, provided soil water can move toward the surface at this rate. This process reduces the actual soil evaporation (E_s) below the potential represented by E_{ps}.

From equations [18] through [20], $E_s + E_p$ do not always necessarily sum to E_t. If the sum is greater, the deficit is allocated so that the sum becomes E_t. Of course, the plant may also not be able to transpire at its potential due to limited soil water in its root zone, but this is not reflected in any increase in the soil-surface evaporation. If $E_s + E_p$ is less than or equal to E_t, no adjustment is required.

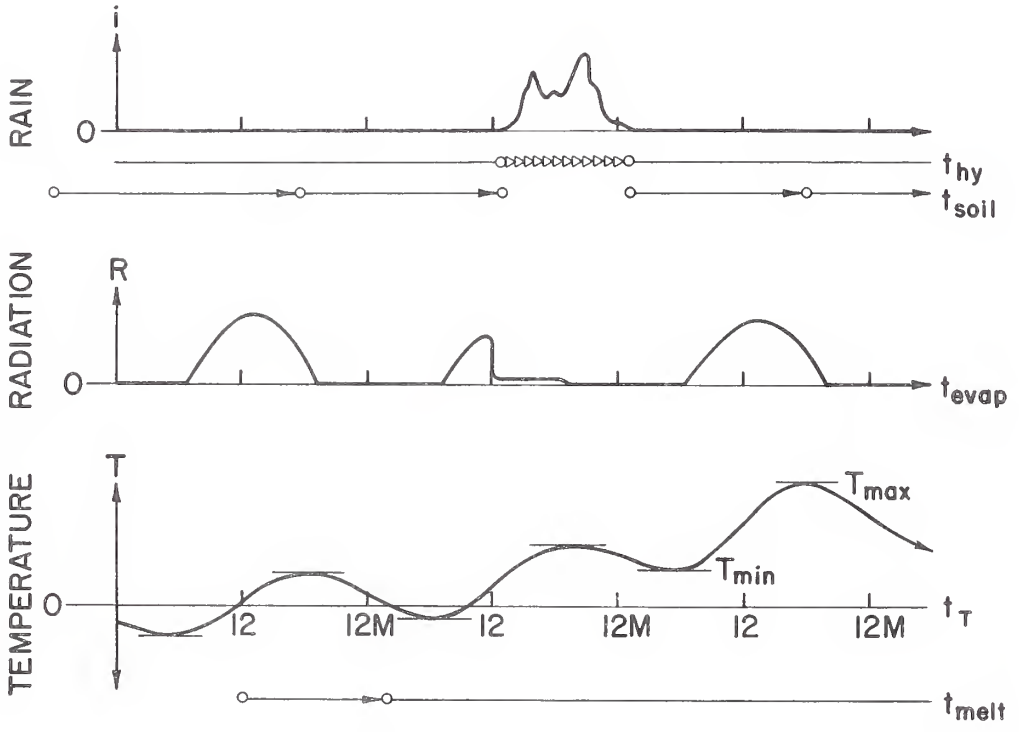

Figure 13.
Time distribution of major weather variables in Opus.
Radiation is assumed to vary with solar angle as shown, and temperature is assumed to follow a daily sinusoidal cycle. Radiation is reduced during a rain, and rain also reduces the daily maximum temperatures.

4. FLOW AND TRANSPORT BY SUBSURFACE WATER

Soil-water dynamics involves most of the precipitation falling on the agricultural catchment and is thus a key element in the water transport of pollutants, both directly and indirectly. The zone of unsaturated flow extends from the soil surface down to the water table. In most cases, the solution region in Opus will extend to only a few centimeters below the maximum root depth. In the case of high water tables with artificial drainage, the solution region will extend to the lower boundary control, which is usually the drain tile depth.

Simulating Flow of Unsaturated Water

Opus uses Richards' equation to describe flow in the unsaturated soil profile. This mathematical expression is based on a dynamic, one-dimensional form of soil-water conservation with Darcy flux, expressed as

$$\frac{\partial \theta}{\partial t} + \frac{\partial q}{\partial z} = q_e \qquad [21]$$

where

θ is volumetric soil water content,
t is time (min),
z is depth from surface (mm),
q is flux (mm/min), and
q_e is local inflow (min^{-1}).

The value q is assumed to be described by Darcy's law, which relates flux to gradient of total potential (H) as follows:

$$q = -K(\theta)\frac{\partial H}{\partial z} \qquad [22]$$

where

K is hydraulic conductivity (mm/min), and
H is total soil (gravitational and matric) potential ($\psi + z$) so that

$$\frac{\partial H}{\partial z} = \frac{\partial \psi}{\partial z} + 1 \qquad [23]$$

Richards' equation assumes that the unsaturated, one-dimensional vertical flow of water is unaffected by the counterflow of air. The equation does not attempt to account for other soil-water-movement processes involving thermodynamics, such as vapor movement or local soil freezing. These assumptions are not considered restrictive in the context of the principal applications envisioned for Opus, and in comparison with other sources of error.

Simulating Redistribution of Soil Water

All common numerical solutions to equation [21] divide the soil depth (z) into finite increments within which ψ and therefore θ and $K(\theta)$ are considered locally uniform. One of the recurring problems in the numerical solution of equation [21] is characterizing an effective local value of $K(\theta)$ for flow between the adjacent finite increments making up the numerical grid. $K(\theta)$ is a highly nonlinear function and is often changing rapidly in space and time, whether or not the soil texture changes between layers. Haverkamp and Vauclin (1979) have summarized and compared several published techniques for $K(\theta)$ averaging within numerical solutions.

For Opus, with relatively large z increments, the problem is even more acute, and the method used takes unique advantage of the analytic knowledge of unsaturated gravitational soil flow. Taking equations [22] and [23] together, we can consider the flux (q) as being made up of two flux components corresponding to the two components of the total potential H (diffusive flux, q_u, and gravitational flux, q_g) as follows:

$$q = q_u + q_g = -K_u(\theta)\frac{\partial \psi}{\partial z} + K_g(\theta) \qquad [24]$$

The two different subscripts on $K(\theta)$ (u = diffusive and g = gravitational) represent two different methods of calculating the effective K between finite difference nodes. The gravitational q_g is always downward (positive z). From kinematic analysis[g](Smith 1983b), K_g for flow between nodes i and i+1 is best approximated for numerical solution by heavily weighting toward $K(\theta)_i$, the K at the upper node.

For diffusive flux, an efficient value for $K_u(i,i+1)$ can be found by assuming that ψ varies uniformly between z_i and z_{i+1}. Thus, while $\partial\psi/\partial z$ is uniform between nodes and is continuous within a given soil horizon, $\partial\theta/\partial z$ will nevertheless be discontinuous when soils change at the layer interface between i and i+1. This is illustrated in figure 14. Since $K(\theta)$ is a relatively simple relation (equation [4]), the net K is calculated as the first moment of $K(\theta)$ over the computational interval. To describe the case of changing soils at the interface, θ_{bj} is defined as water content at the j side of interface b, with j = i or i+1. Then the first moment of $K(\theta)$ between i and i+1 is

$$K_u(i,i+1) = \frac{1}{\theta_i - \theta_{b,i}} \int_{\theta_{b,i}}^{\theta_i} K_i(v)dv + \frac{1}{\theta_{b,i+1} - \theta_{i+1}} \int_{\theta_{i+1}}^{\theta_{b,i+1}} K_{i+1}(v)dv \qquad [25]$$

With the soil's relation for $K(\theta)$ characterized simply as described in chapter 2, the solution of equation [25] is relatively straightforward.

Using the conceptual division of q from equation [24], equation [21] becomes

$$s_c(\theta)_i \frac{\partial \psi}{\partial t} i = \frac{\partial}{\partial z}[K_u \frac{\partial \psi}{\partial z} + K_g]_i + q_{ei} \qquad [26]$$

where $s_c(\theta)$ is the local slope of the hydraulic characteristic, i.e., $d\theta/d\psi$. This method is termed the Separable Flux (SF) method of numerical treatment.

The first step of the solution procedure for Opus is a time step (Δt) selection. This is accomplished by calculating q in equation [24] for the flow between all nodes at existing conditions, and choosing a Δt by examining the resulting net rate of change of θ in each computational layer. The critical conditions that are examined include (a) drying to near θ_r at the surface and (b) potential (artificial) gradient reversals that would arise for large time steps with locally large differences in q. An iterative, partially linearized, implicit method is used, which estimates values of K that are fixed for the time step, but provides mass-conserving correspondence between the new array of ψ values and the new values of θ. This means that values of $s_c(\theta)$ are chosen as chord slopes between old and new points on the $\theta(\psi)$ relation, and are kept correct across the time step by iteration. The nonlinear nature of the $\theta(\psi)$ relation and its reversal of curvature require the use of a relaxation technique, and the relaxation factor becomes larger for cases in which several iterations are required. Solution proceeds with the automatic selection of time steps until the time interval of soil-water redistribution (not longer than 1 day) is exhausted. Because of the vast array of soil conditions met and also the severe nonlinearity of the characteristic relations, time steps can and do vary as needed between 0.01 and 1440 minutes.

Local inflow (q_e) is negative for both evaporation in the surface increment and plant root extraction in all lower increments. The total root-water use is distributed according to the water potential seen by the plant at each level, which is proportional to $z_i - \psi_i$. Continuous accounting is made of the available water in the root zone. On a daily basis, this is compared with the water demand of the plant and with the estimated "wilting point" water content, to limit plant uptake in response to stress. (This is discussed in more detail in ch. 7.) Surface-soil evaporation is estimated by the modified method of Ritchie (1972) (ch. 3). Surface-soil evaporation is computationally limited when the surface nears 15-bar water content, by the soil's ability to furnish water to the surface through upward flux.

The lower boundary condition for equation [26], as indicated above, is located either at two computation nodes below the root zone or at the drain depth when field drains are simulated. In the former case, ψ is allowed to rise at the boundary in a kinematic manner when a θ "wave" passes below the roots (positive $d\psi/dz$). Conversely, ψ may decrease as this "wave" passes out of the root zone (negative $d\psi/dz$). At the boundary, ψ is not allowed to decrease below the value that represents a hydrostatic profile condition relative to the water table. Periods of relative drought, or large root-zone demands, can therefore cause upward movement from water in the soil below the root zone. This potential flux is reduced with increasing depth to the water table. If draintiles are included, the unsaturated-zone solution includes the saturated region above the drain tiles.

In model simulation, soil water is redistributed over periods of about 1 day. When a day includes a storm, the soil-water simulation period will go to only the beginning of the storm. The next period will include the remainder of the day plus the period to 6:00 p.m. the next day, or to the start of the next storm, whichever comes first. The time of 6:00 p.m. is an arbitrary division point for nonstorm days. Equation [26] is not solved during storm input; it is not felt necessary or appropriate to use this method in lieu of the physically based infiltration option. In any case, flux-rate information is not available when the daily hydrology option is used. Both hydrology options estimate the total runoff, total infiltrated depth, and time base of the event.

Simulating Rain Wetting Profiles

When runoff occurs, saturation of surface soil must have occurred, and a first-order estimate of the resulting wetted-soil profile is step input of depth equal to the infiltrated amount divided by $(\theta_s - \theta_i)$. The prestorm value of θ is θ_i at each depth. When runoff does not occur for the daily option, the effective average rate of rainfall is estimated by the amount of rain divided by the amount needed for runoff to occur. This ratio, less than 1, can be used as a relative rate (r_*), and a profile water content can be estimated from using this value of r_* in an inversion of the $K(\theta)$ relation (equation [4]). This provides an estimated $\theta(r)$ for the step profile estimate. It extends to that depth necessary to provide for the amount of infiltrated rainwater. In either case the estimated profile becomes the starting point for subsequent soil-water redistribution. For the breakpoint hydrology option, when runoff does not occur, the rainfall data provide an average value for r, which is used as above to estimate a θ from the inverted $K(\theta)$ relation, for the surface-wetted profile.

The relative efficiency of the solution method in computation, using the large z increments, is exemplified in figure 15. The initial condition profile is shown as a dashed line. The SF method described here is compared with a precise, fine-mesh solution by an implicit finite-difference Crank-Nicholson method (Smith 1970). Given the vast difference in finite increment scale, the SF method is quite a faithful simulation compared to the fine-scale solution, which takes about 2 orders of magnitude more computation time. What is not demonstrated here is the additional fact, with comparable large-scale increments, that the use of common K-averaging schemes and standard numerical methods (such as the Crank-Nicholson scheme) would not produce an acceptable approximation to the behavior of equation [21].

Simulating Draintile Control

When draintile management methods are used in areas of a high water table, the action and effect of the draintiles as lower boundary controls on the unsaturated flow region may be approximated using an analytical expression. Figure 16 illustrates the approach used to link the saturated and unsaturated flow regions. The superelevation of the water table above the parallel drains is assumed to describe a half-ellipse in shape. Thus the mean superelevation of the water table ($\bar{h}$) can be made a simple function of the maximum superelevation (h_m). From an expression of Bouwer and van Schilfgaarde (1963), the flux through the draintiles is a quadratic function of this maximum superelevation (h_m). The unsaturated flux from above, $q(z,t)$, at level h_m, can be assumed constant over the period Δt of interest (usually equal to the period of unsaturated-flow redistribution). It is hereafter termed q_m and can be found from the unsaturated-flow solution. The controlling water-balance equation for the basic portion of the system shown can be written as

$$\phi y_s \frac{d\bar{h}}{dt} = y_s q_m - q_d(\bar{h}) \qquad [27]$$

in which

y_s is drain spacing (mm),
q_d is drain discharge ($mm^3/mm^2/min$), and
ϕ is effective soil porosity in drain region.

From Bouwer and van Schilfegaard (1963), we use Houghoudt's quadratic equation for q_d, which may be written as

$$q_d = c_a h_m^2 + c_b h_m \qquad [28]$$

in which c_a and c_b are geometrically calculable parameters as follows:

$$c_a = 4K_s/y_s^2 \qquad [29a]$$

$$c_b = 8K_s z_e/y_s^2 \qquad [29b]$$

The quantity z_e is a function of z_d (the distance below drains to a limiting interface), and is calculated internally by Opus following graphical results from Bouwer and van Schilfgaarde (1963).

Equation [27] can be formed into a lower boundary condition to use in conjunction with the numerical solution of equation [24] for the case of draintile control. This boundary condition is active whenever there is a positive value of H at the drain-tiles. Assuming the superelevation to have an elliptical shape, h_m is related to H by a constant ratio of $4/\pi$. The expression is partially linearized for solution in the tridiagonal matrix by using $h_m(j\text{-}1)h_m(j)$ in place of $h_m^2(j)$. The sumbols j and j-1 refer here to time-step indices for current and previous times, respectively. This allows the quadratic equation to be put in the same form as the finite difference equations for solution. Very little accuracy is lost in the linearization, because in almost all practical cases, the second-order term is 2 orders of magnitude smaller than the linear term.

Flow toward active roots and surface evaporation can cause the water table for some cases to drop below the drain level. Opus treats this condition as it does a profile without drains. The relation between water deficit below the drains and the negative H at the drains is assumed to be equal to the relation of a soil column in equilibrium with the potential H at the drain level. This varies as necessary for the solution of the balance in equation [26]. When the water table again rises to the drain level due to leaching from above, the boundary condition reverts to the drain equation [27]. Use of a fixed but very small positive value for s_c when $\psi > 0$ allows Opus to successfully solve for positive as well as negative matric heads.

Transport of Soil Heat

Simulation of the biological processes in the soil of a field area requires knowledge of the temperature at each depth and time. Both plant growth and microbial activity are temperature dependent, and these processes are involved in several aspects of the transport and decay of pollutants. Although large changes occur through the day in the near-surface region of the soil profile (due to diurnal temperature changes in the air and diurnal variation in soil radiant heating), Opus focuses on the simulation of variations in mean daily temperatures. Heat moves through the soil by convective transport with water and

by diffusion from temperature gradients induced by temperature changes at the soil surface. In Opus, these changes are treated in a manner similar to the movement of water, with thermal redistribution between storms treated in consideration of diffusive-type flows, and rapid waterborne heat convection during a storm treated as if it were a single pulse flow.

Diffusion of Soil Heat

The soil profile is a significant heat-storage mass, and changes in daily surface air temperature cause diffusion of heat into and out of the soil. The general one-dimensional equation for heat diffusion is

$$\frac{\partial T}{\partial t} = D_T(\rho,\theta)\frac{\partial^2 T}{\partial z^2} \qquad [30]$$

with boundary conditions

$$T(0,t) = T_o,\ 0 < t < 1440 \text{ min, and}$$
$$T(L,t) = T_{av},$$

and initially

$$T(z,0) = T(z) \text{ arbitrary}$$

in which

T	is temperature (^oC),
L	is maximum depth of simulation,
D_T	is thermal diffusivity (mm^2/min),
t	is time (min),
z	is depth (mm),
ρ	is soil density (gm/cm^3),
θ	is volumetric soil-water content, and
T_{av}	is average annual temperature.

Soil thermal diffusivity (D_T) is theoretically a function of the mineral composition, the shape and orientation of soil particles, and water content (de Vries 1966). Mineral thermal diffusivity can be computed approximately from knowledge of clay content, assuming randomly shaped and oriented particles. Following the procedure for this computation from de Vries (1966) and assuming that the soil-water content is nonuniform but constant over the time steps of interest, D_T can be determined for each soil computational layer, and the difference form of equation [30] can be quickly solved at each time interval with a direct Gauss-Seidel method. This T is found at the intersection of the soil computational layers, and T at z = L is taken for simplicity as the annual mean air temperature. At depths of a few meters, this is a reasonable assumption for the

lower boundary condition. Although equation [30] could be solved through the day to simulate the diurnal excursions in near-surface temperatures, that detail is not necessary for the purposes of simulating processes that depend on soil temperature over the time scale of interest in Opus.

Convection of Soil Heat With Water

Heat may be input to the soil with the influx of water at the soil surface, and heat may be transported within the soil by the movement of soil water. Complete thermal mixing is assumed within each incremental layer of the flowing water, and initial soil-water temperature is assumed to be in equilibrium with soil mass. The convective heat budget for a control volume of soil may be written as

$$\gamma_w(T_i q_i - T_o q_o) = \frac{d}{dt}\left[(\gamma_w V_w + \gamma_s V_s)T_o\right] \qquad [31]$$

in which

T_i = temperature of inflow water (^oC),
T_o = temperature of outflow and control-element water (^oC)
γ_w = heat capacity of water (cal/cm^3/deg),
V_w = volume of control-element water (cm^3),
γ_s = volumetric heat capacity of soil (cal/cm^3/deg),
V_s = volume of soil in control element (cm^3),
q_i = flux of inflow water (cm^3/min), and
q_o = flux of outflow water (cm^3/min).

The left side of equation [31] is the net input of heat, and the right side is the change in heat in the control element.

The general solution to this linear differential equation may be written as

$$T_o = T_i + (T_{oz} - T_i)\left(\frac{V_{wz}+bV_s+\Delta V}{V_{wz}+bV_s}\right)^{-V_{wz}/\Delta V} \qquad [32]$$

in which

T_{oz} = initial value of T_o,
V_{wz} = initial water in element at $t = t_z$,
b = γ_s/γ_w,
Δt = $t - t_z$ (min), and
ΔV = $(q_i - q_o)\Delta t = \Delta q \Delta t$.

For the special case $\Delta V \to 0$, one obtains the following from equation [31]:

$$T_o = T_i + (T_{oz} - T_i)\exp[-q\Delta t/(V_w + bV_s)] \qquad [33]$$

Equation [32] is solved for each computational element in the soil column in which water moves during a time step. Values for the initial and final water contents are obtained from the waterflow calculations. The most dramatic heat convection occurs in the influx of generally cooler rainwater. In the absence of actual data, rainwater temperature is assumed to be equal to the minimum daily temperature for the day of occurrence.

Transport of Solutes Through Soil

Opus includes the capability of calculating the transport of partially soluble and partially adsorbed chemicals in flow of unsaturated soil water. One of two kinds of solute adsorption may be simulated: (a) Adsorption assumed to be characterized by equilibrium chemistry. This adsorption is described by a linear adsorption isotherm. (b) Adsorption assumed to be kinetic, with the rate of transfer between adsorbed and solution phases a linear function of the current phase ratio compared to the equilibrium ratio.

Equilibrium adsorption assumes an invariant equilibrium ratio between the solute adsorbed on the soil solids and the solute in solution in the soil water. Equilibrium adsorption can also be taken to mean that the kinetic transfer rate (discussed below) is very rapid compared with the processes of soil-water movement. The equilibrium ratio is termed K_d, and is expressed as

$$K_d = \frac{C_a}{C_w} = \frac{\text{adsorbed concentration}}{\text{concentration in water}} \qquad [34]$$

Since C_a has units of kg/liter, and C_w has units of kg/kg, the ratio K_d is in liters per kilogram. Further, the K_d for pesticides is assumed to be directly proportional to the local content of organic carbon (f_b), as follows:

$$K_d = f_b K_{oc} \qquad [35]$$

with K_{oc} being a pesticide-dependent absorption constant. If this formulation were universally accurate, K_{oc} would depend only on the type of chemical. Although some variation remains, this expression does explain much of the observed variation in adsorption properties of many chemicals. Values of K_{oc} suggested by studies for many pesticides are given in the User Manual (vol. II).

The assumption of kinetic adsorption accepts the concept of K_d but specifies a rate of transfer between the dissolved phase and the adsorbed phase as being proportional to the extent to which the existing ratio differs from the equilibrium ratio. Expressing the transfer as the change in concentration of adsorbed material (C_a) per unit time, this rate may be represented in the kinetic assumption as

$$\frac{dC_a}{dt} = \nu(C_w K_d - C_a) \qquad [36]$$

in which ν is rate coefficient with units of minutes^{-1}.

Transport With Equilibrium Adsorption

A definition sketch for the transport of solutes through an arbitrary numerical layer in Opus is given in figure 17. If equilibrium is assumed to always hold between the adsorbed and dissolved materials, then equation [36] reduces to $C_a = K_d C_w$, and a differential mass-conservation equation is written for the total amount of material in the layer as follows:

$$\frac{d}{dt} C_w(V + c_h K_d M_S) = C_i Q_i - C_o Q_o \qquad [37]$$

in which

C_w	is concentration in solution (kg/liter),
K_d	is adsorption coefficient (liter/kg),
M_s	is mass of soil layer (kg/ha),
c_h	is a conversion factor: ha-mm/liter (0.0001),
q	is flow in or out of a layer, and
C	is concentration in or out of a layer, designated by subscripts as follows:
i	is subscript representing inflow, and
o	is subscript representing outflow.

With complete mixing in each layer assumed, and when q_o and q_i are both positive, $C_o = C_w$, and one term of equation [37] disappears. Expanding the differential on the left, noting that dV/dt is ΔQ, and grouping terms, equation [37] becomes

$$\frac{dC_w}{C_i - C_w} = \frac{q_i dt}{V_{wz} + \Delta qt + K_d M_s c_h} \qquad [38]$$

This equation also holds for the case of reversal of both inflow flux and outflow flux, by symmetry. When both flows are into the layer, this equation will not hold, but C can be found by simple summation, because the layer is a sink. When both flows are out of the layer, their concentrations and the source-layer concentration will be unchanged over the time step.

Solving equation [38] for nonzero Δq, the equation for change in local solute concentration (C) after a time (Δt), beginning at time (t_z) at which $C = C_z$, is

$$C(\Delta t) = C_i + (C_z - C_i)\left(\frac{V_{wz}+K_d M_s c_h+\Delta V}{V_{wz}+K_d M_s c_h}\right)^{-V_i/\Delta V} \qquad [39]$$

in which

V_i = volume of water entering layer (mm),
ΔV = change in water volume in layer during Δt, and
C_z = solute concentration at initial time (t_z).

Again, uniform mixing of layer water and inflow water is assumed within the layer. Values of q_o and q_i are obtained from calculation of soil-water movement for the soil profile over the period Δt. The Δt for equation [39] is the same time interval as that for soil-water redistribution or storm inflow, and is not greater than 1 day (as described above).

The outflow concentration from any layer may vary with time, according to equation [39]. To simplify computation over long periods of time, outflow concentration from a layer is averaged over the computation interval, to become an input-flux concentration for the adjacent layer. While equation [39] may be integrated over time to obtain the mean value, it is more straightforward to obtain the time-average outflow concentration by mass balance as follows:

$$C_m = \{C_z(V_z+K_d M_s c_h) - C(\Delta t)[V(\Delta t)+K_d M_s c_h] + q_i c_i \Delta t\}/q_o \Delta t \qquad [40]$$

in which

C_m = mean outflow concentration over Δt,
$V(\Delta t)$ = liquid volume in layer at end of Δt,
$C(\Delta t)$ = concentration in layer at end of Δt, and
V_z = initial liquid volume in layer

For the special case of through flow without volume change, or $q_i = q_o$, equation [38] simplifies and the solution for $C(\Delta t)$ is

$$C(\Delta t) = C_i + (C_z - C_i)\exp[-q\Delta t/(V(\Delta t) + K_d M_s c_h)] \qquad [41]$$

The solution procedure begins at a layer(s) that is a "source" (has only outflow) and proceeds from each source in either direction until meeting a "sink" layer (which has only inflows).

Transport With Kinetic Adsorption

The option for transport with kinetic adsorption assumes that the transfer of material between adsorbed and dissolved phases is not instantaneous and follows equation [36]. Because of this assumption, a mass-balance equation including both adsorbed and dissolved materials must be written. Figure 17 illustrates the linked systems. For the dissolved phase, one can write

$$\frac{d}{dt}(C_w V) = -c_h \frac{dC_a}{dt} + q_i C_i - q_o C_o \qquad [42]$$

where V is assumed to be a steadily increasing or decreasing function of time during the increment of computation

This equation can be solved in tandem with equation [36] for kinetic gain or loss of adsorbed material. The form of the solution varies somewhat with the various conditions of inflow and outflow. Special cases exist at the boundary, where evaporative outflow will transport no dissolved material and where input may be free of solutes.

In general, when the terms of the equation are of equal order, the Runge-Kutta method can be used in a piecewise manner over time intervals as great as 1 day or more to simulate the kinetic transfer of partially adsorbed solutes. However, many pesticides of interest are highly adsorbed to organic material and clays in the soil, and for realistic values of ν, the relative change of C_a over a computational interval can be considered negligible. In that case, the equation reduces in general form to

$$\frac{d}{dt}(C_w V) = c_h \nu (K_d C_w - C_a) + q_i C_i - q_o C_w \qquad [43]$$

Here C_w is written for C_o, which is true for complete layer mixing except when q_o is evaporative outflow. Even for slowly changing C_a, this equation can be superior in stability to a Runge-Kutta solution. The general solution to this linear differential equation, starting with C_z for interval Δt, is written as

$$C_w(\Delta t) = C_b + (C_z - C_b)\left(\frac{V_z}{V_z + \Delta q \Delta t}\right)^{b/\Delta q} \qquad [44]$$

where C_b is a steady-state concentration defined by

$$C_b = \frac{q_i C_i + \nu c_h C_a}{q_i - q_e + \nu c_h K_d} \qquad [45]$$

and b in the exponent of equation [44] is equal to the denominator on the right side of equation [45]. For small values of Δq (which make the exponent in equation [44] very large), the solution reduces to

$$C_w(t) = C_b + (C_z - C_b)\exp(-b\Delta t/V_z) \qquad [46]$$

For either equation [44] or [46], one can obtain the mean outflow concentration for the interval by integrating as was done in obtaining equation [40]. Opus uses one of these two equations when K_d is larger than 40, and selects equation [46] when the exponent $(b/\Delta q)$ exceeds 10 in equation [44]. In either case, the time steps used follow the solution appropriately, and the small changes in C_a that occur with the large values of K_d are computed stepwise by a mass-balance equation. The kinetic option is useful for only values of ν smaller than 0.01, because larger values are, on a daily basis, practically indistinguishable from the equilibrium case.

Implementation by Computer

Simulating the ensemble of many soil computational layers over a time interval requires consideration of one or more cases, depending on direction of flow and solute transfer. A layer may act as (a) a sink, with flow entering from both above and below, (b) a source, with flow moving away in both directions, (c) a flow-through, with water flowing in one side and out the other, (d) a surface "source," with solutes leaving at the bottom and only water leaving at the top, (e) a surface flow-through, with water and solute entering below but only water moving out at the top, or (f) the reverse flow of case e. For each case, equation [37] or [42] will be modified by elimination of terms or zero coefficients. Solution of either the kinetic equation or equilibrium equation is implemented when the equation has been properly resolved for the local conditions. For each case, the solution order must be determined properly in advance, proceeding in both directions from each source layer. Information on inflow concentrations from adjacent layers is not required for only source layers. Thus, input values are determined in advance for every layer. The solution finds the new local concentrations of both adsorbed chemical and dissolved chemical, and solves for the time-averaged value of outflow concentration for use in the adjacent layer solution. The kinetic-solution algorithm uses internally determined time subdivisions when dC/dt is a rapidly changing function over the interval of interest.

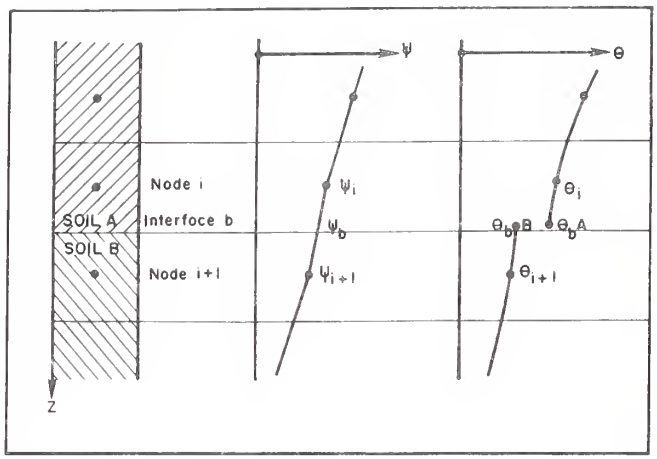

Figure 14.
Diagram of changes in Ψ and Θ across the interface of two different soils, and values used at adjacent computational nodes.

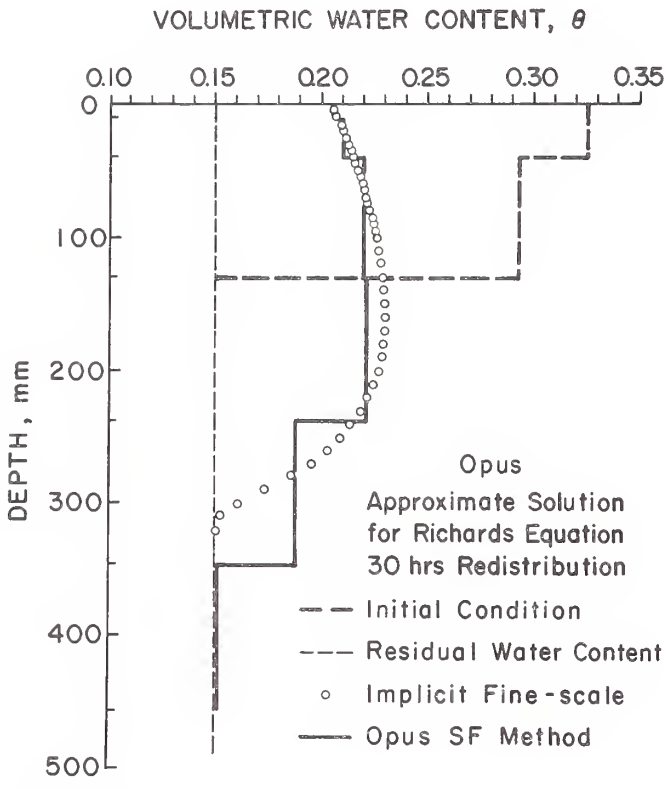

Figure 15.
Comparison of the Separable Flux numerical method of Opus (with large depth increments) with a numerical solution of the standard Richards' equation formulation (with very small depth increments). The SF method does a good job of simulating the general distribution of soil water. Use of very large increments with standard numerical methods produces biased estimates of soil-water redistribution.

DRAINTILE SIMULATION

Dynamic balance of saturated zone:

$$V = \phi \int_0^{y_s} h_m \, dy \approx \phi \bar{h} \, y_s$$

unsaturated flux = $q(z,t)$

$$\frac{dV}{dt} = \phi y_s \frac{d\bar{h}}{dt} = y_s \, q(z,t) - q_d(h_m)$$

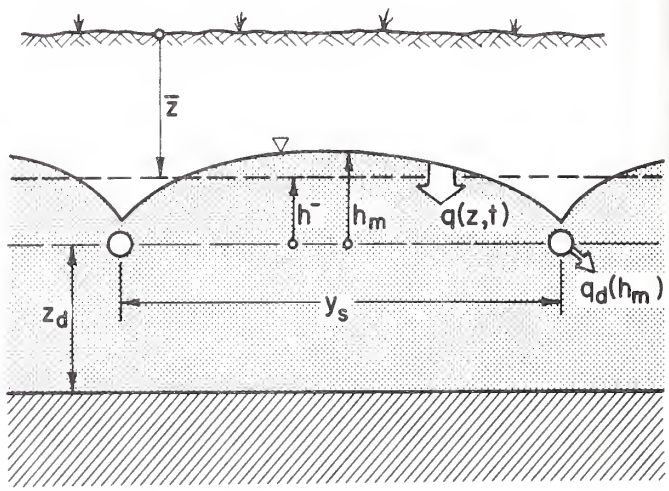

Figure 16.
Estimation of drainage for perched or high water table with draintiles. Approximate equations taken from Bouwer and van Schilfgaarde (1963) are used as a lower boundary condition for the unsaturated zone redistribution calculations.

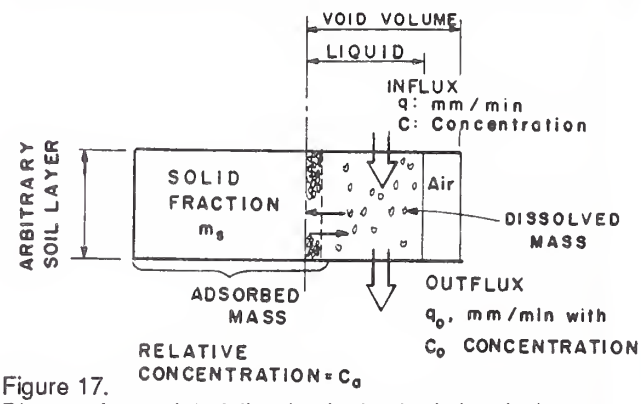

Figure 17.
Diagram for model of dissolved/adsorbed chemical movement using the soil increments and interlayer fluxes from the soil water flow model. This figure shows the major terms used in the equations.

5. SURFACE-WATER FLOW PROCESSES

Much of the pollution from agricultural areas is carried in runoff from precipitation events. Surface runoff interacts with the soil and transports dissolved or suspended pollutants off the field or catchment area. Although many of the potential pollutants may be within the soil profile, they are often concentrated near the soil surface. Clearly a useful simulation of the pollution from a field requires an accurate practical simulation of the movement of water on the field surface as well as within the soil.

The difficulty in simulating surface-water processes is not so much in our knowledge of the water-movement mechanisms, but rather in having data appropriate to our ability to represent the mathematics of these processes. Specifically, even when data on topography and soil are abundant, knowledge of only daily totals or even storm totals of rainfall is inadequate for accurate simulation of either infiltration rates or runoff rates. A storm of given depth could produce large amounts of runoff for high-intensity rainfall but produce no runoff if the same depth of rain comes at low intensity.

Nevertheless, it is most often the case that situations in which simulation is a useful tool do not provide the modeler with the rainfall-intensity data that are necessary for using infiltration methods. For this reason, Opus (like CREAMS in this respect) allows the user to choose a surface-hydrology method that is appropriate to lumped, daily rainfall data. In addition, since the processes of surface-water transport are so dependent on surface-water-flow information, the daily hydrology option also uses a "lumped" method for estimating erosion and sediment production from the catchment. The user's choice of hydrologic option will depend on both the quality of the data available and the particular objectives of the model user.

Because of the limited information contained in daily rain summaries and also the lumped nature of the resulting runoff-estimation methodology, the information on field topology (ch. 2) finds only limited use in the daily hydrology option. Nevertheless, advantage is taken of all information from the field topology that can be used to improve the accuracy of daily runoff prediction. This improvement includes a refined estimate of the relative time of concentration, which is used to estimate the peak runoff rate.

Simulation of Runoff From Daily Rainfall Data

The minimum hydrologic information needed for Opus from a precipitation event is the amount and peak rate of runoff. Given only daily total rainfall, these must be estimated with conceptual methods based on hydrologic experience. The methods used in EPIC (Williams et al. 1984) for estimation based on daily rainfall are used here with minor modification.

The EPIC model uses the Soil Conservation Service (SCS) Curve Number (CN) runoff-estimation method, with some important modifications. The basic method is fully explained in the SCS Hydrology Handbook (USDA SCS, 1972). Briefly, runoff amount (Q) is related conceptually to precipitation amount (P), a soil-water storage value (s_w), and an initial abstraction (I_a) as follows:

$$Q = \frac{(P - I_a)^2}{P + s_w - I_a} \qquad [47]$$

$$I_a = 0.2 s_w \qquad [48]$$

$$s_w = 254\left(\frac{100}{CN} - 1\right) \qquad [49]$$

The method gets its name from the curve number parameter, CN. As indicated in equation [49], CN may vary from 1 to 100. P, Q, I_a, and s_w are expressed here in millimeters.

Equation [47] was originally described (USDA SCS, 1972) as estimating storm runoff amounts rather than daily amounts. Nevertheless, it is applicable just as well (or better) for larger-period rainfalls. The CN is conceived as a soil parameter, with a mean value for average soil conditions. A specified method modifies the curve number for wet or for dry initial soil conditions. The EPIC modifications used in the daily option of Opus relate the value of CN to current soil-water content (Williams et al. 1984). Opus also uses the method of EPIC to estimate peak runoff rates for runoff events, based on estimated time of concentration, monthly distribution of rainfall intensities, and ratio of maximum 30-minute and 24-hour rainfall depths for the location of interest (Williams et al. 1984).

Unlike EPIC, Opus provides (and the authors encourage the use of) an option to use the CN rainfall/runoff relation described above as an expected value rather than a prediction. Thus for long-term simulation sequences, individual runoff amounts are randomly selected from a rational distribution about this mean. The physical limits of a runoff/rainfall ratio are 0 and 1, and a two-parameter beta distribution with these limits is used. Figure 18 illustrates the shape of the curve described by equation [47] and also the typical scatter of runoff data from two catchments with rather long records (Montgomery 1980). Some scatter of CN-estimated runoff occurs because the CN changes with initial soil water content. But as figure 19 shows, this scatter is a minor amount compared to scatter in recorded data. Scatter about such a rainfall-runoff curve is to be expected for many reasons but especially because of the variation in storm intensities. This variation is important

information not measured by daily or storm rainfall totals. Figure 20 illustrates the beta function distribution of runoff used in Opus for several given runoff/rainfall ratios.

Simulation of Runoff From Breakpoint Rainfall Data

Given adequate rainfall data, an entirely different simulation method is available with Opus. A deterministic, distributed simulation of the dynamic response of soil and surface-water flows is done when breakpoint or pluviograph data are provided.

Infiltration

Flow within the soil itself is assumed to be described by Darcy's law and continuity of mass as expressed in equation [21]. Infiltration is flow through the soil surface, and the fundamental relation for infiltration is also based on Darcy's law and an expression of continuity for flow across the surface. Assuming that initial water content θ_i is relatively uniform in the surface region, and with infiltration rate f(t), the basic relation for infiltration (Smith 1981b) is

$$I(f) = \int_{\theta_i}^{\theta_s} (\theta - \theta_i) \frac{D(\theta)}{f - K_s} d\theta \qquad [50]$$

in which

$D(\theta)$ is diffusivity, defined as $K(\theta)d\psi/d\theta$ (mm^2/min),
I is depth of infiltration from start of rainfall (mm),
f is rate of infiltration (mm/min)

and other symbols are defined in chapter 4.

Two types of infiltration conditions may be encountered at the soil surface. The first is an imposed ponding condition, such as with flood irrigation. This condition effectively imposes a fixed soil-water head at the surface, and equation [50] describes infiltration rate (f) for all values of $I > 0$ under these conditions. The other condition is the common rainfall, or flux boundary condition. For this case, I at first increases as

$$I = \int_{o}^{t} r(t)dt \qquad [51]$$

until the surface becomes saturated, and the boundary condition changes to a fixed head of 0. Consequently, at that time and beyond, the infiltration capacity is controlled by the condi-

tions near the soil surface. The time of this change of control is the time of ponding (t_p), after which equation [50] describes the decay of f with increasing I. These two relations are illustrated in figure 21. In other words, at $t = t_p$, equation [50] indicates the relation between rainfall rate, initial water content (θ_i), and ponding depth, because the lower limit of the validity of equation [50] is reached when $f = r$ and I at ponding = I_p. An analytic function is obtained from equation [50] by making assumptions on the functional form of D that allow integration (Parlange and Smith 1976). The function used in Opus is that developed by Smith and Parlange (1978), which assumes exponential behavior of K near θ_s, so that $D(\theta)$ is approximately proportional to $dK/d\theta$, and equation [50] can be integrated to obtain

$$I(f) = G(\theta_i) \ln \left[\frac{f}{f-K_s}\right] \qquad [52]$$

Capillary parameter $G(\theta_i)$ is a coefficient depending on initial conditions and is related to the integral properties of the soil capillary characteristics. For most initial water contents, it can be represented by

$$G(\theta_i) = H_c(\theta_s - \theta_i) \qquad [53]$$

in which H_c is a capillary scale parameter and is relatively independent of initial water content (Smith 1983a). The value of H_c can be obtained from infiltrometer experiments, or from the soil characteristics as

$$H_c = \frac{1}{K_s} \int_{-\infty}^{0} K(\psi) d\psi \qquad [54]$$

Thus a rough estimate of H_c can also be regressed from soil texture as was done for unsaturated soil hydraulic parameters (Rawls et al. 1983). Equation [52] is universal in the sense that it applies to the determination of ponding occurrence and to the rate of infiltration after ponding, and also describes infiltration from initially ponded (flooded) soil conditions. Other closely related "universal" relations may be similarly obtained by making different assumptions on the nature of D in the integration of equation [50].

When inverted as an f(I) relation, equation [52] becomes

$$f = K_s \frac{\exp(I/G)}{\exp(I/G)-1} \qquad [55]$$

A relation for f as an explicit function of t that is accurate to within a very few percent over most time ranges of interest can be obtained from any of the "universal" relations (Smith 1981b). In particular, for equation [55], the first two terms of the Taylor expansion of exp(x) may be used to solve for an expression useful in simulation. Equation [55] is first integrated with f expressed as dI/dt, to obtain

$$K_s t = I + G[\exp(-I/G) - 1] \qquad [56]$$

Then using the Taylor expansion and the finite differential expression that $f \rightarrow \Delta I/\Delta t = [I(t+\Delta t) - I(t)]/\Delta t$, we obtain

$$\Delta I = G \sqrt{B^2 - 2K_s \Delta T/(b_e G)} - B \qquad [57]$$

in which

$$B = (1-b_e)/b_e, \text{ and}$$
$$b_e = \exp(I/G)$$

This expression is convenient for advancing in small time steps during model simulation, with maximum errors on the order of 1 percent. Mean time-step infiltration-rate f is taken as $\Delta I/\Delta t$. Note that this expression is asymptotically correct at both small and large times. At small I, f is proportional to 1/I, or I is proportional to the square root of time. As $I \rightarrow \infty$, f approaches K_s asymptotically.

Treating Storm and Soil Complications

To use this infiltration theory in field runoff simulation, one should be able to account for a variety of complexities presented in nature. This section describes how some common complexities are treated by Opus. It should be kept in mind that allowance for deterministic complications by the methods outlined here can improve simulation accuracy only to a certain degree. The major ground between mathematical simulation and natural system performance is occupied by the complexities of spatial and temporal variations that are always found in catchment characteristics. Treatment of such variability is within our capability, given large capabilities of computational time and storage, but the collection of information to describe natural spatial variability is usually quite uneconomic. In some cases, the variability of nature coupled with the sensitivity and nonlinearity of hydrologic processes can cause the variability to dominate the response characteristics of a system. This possibility should not be used, however, to dismiss the value of physically sound simulation models.

Rainfall Hiatus. One common complication is the occurrence of periods within a storm in which rainfall rate falls below K_s. Runoff is not generated during these periods, and any runoff water on the surface from previous rainfall will remain subject to infiltration. The desaturation of the surface soil proceeds in accordance with Richards' equation, subject to complexities of soil structure including soil-water hysteresis. At large times after the beginning of such a draining period, given that r is constant and less than K_s, the surface-water content (θ_o) approaches the kinematic value (Smith 1983b), which is

$$\theta_o = \theta_r + (r/K_s)^{-1/\epsilon}(r_s - \theta_r) \qquad [58]$$

For a rainfall hiatus in Opus, θ_o is computed from r as this equation shows, and is approached asymptotically with a transition half-life of approximately 30 minutes. The asymptotic approach is made to be a function of the proportion of surface still covered with water, the amount of rainfall already infiltrated, and the hydraulic conductivity of the soil, as follows (Woolhiser et al. 1990):

$$\theta^j = \theta^{j-1} + [\theta_o - \theta^{j-1}][1 - \exp(-c_r \Delta t)] \qquad [59]$$

in which

j is an index for successive time steps,

Δt is $t_j - t_{j-1}$,

c_r is a rate parameter estimated as

$$c_r = K_s/(I+0.1) \qquad [60]$$

This is a conceptual relation but is similar to one that has proved successful in simulating data from Walnut Gulch Experimental Watershed. This relation provides that redistribution proceeds more slowly for large rains (large I) and for tighter soils (small K_s).

This approximation of surface-water desaturation is applied only during the course of a storm, with total poststorm redistribution calculated by Richards' equation as described above.

Infiltration Through a Surface Crust Layer. Another important complication to be treated in natural conditions is vertical anisotropy in the soil profile. Opus treats a general three-layer case in the simulation of infiltration dynamics. The surface soil is assumed to lie above a subsoil layer, which may be assigned properties by the model user to represent a plowpan condition. The lower soil is assumed by the infiltration calculations to be either equal to or less than the surface soil

in hydraulic conductivity. This assumption is not required for calculation of soil-water movement (equation [26]). In addition, agricultural soils are assumed to form surface crust after mechanical disturbance, due to the impact of energy of subsequent rainfall. The following method of treating the effect of this crust is not theoretically complete, but it does provide for modification of infiltration performance in response to management changes of the surface-soil conditions.

The crust layer, when formed, is arbitrarily assumed to comprise the top 10 mm of surface soil. Although this is certainly not accurate for all cases and all soils, it should be noted that the crust thickness and the crust hydraulic conductivity (expressible jointly as a crust resistance) play partly interchangeable roles in infiltration dynamics (Smith 1990).

The Opus infiltration model assumes that the effective saturated hydraulic conductivity of the crust (K_{sc}) is equal to or less than that of the underlying surface soil (K_{s1}). The case of $K_{sc} > K_{s1}$ is both unusual and relatively unimportant in its effect on infiltration. When the ratio of r to K_{sc} is large, ponding could occur while the wetting front is still within the crust layer, $I < I_c$. I_c is I required to just fill the crust layer. In this case, calculation of t_p is straightforward, using K_{sc} in equation [56].

Ponding can more commonly occur after the wetting front has passed the crust layer, $I > I_c$. This is the more complicated case, because the crust and underlying soil both play important roles in the net infiltration dynamics (Smith 1983b, 1990). Since the hydraulic conductivity of the crust layer has been assumed to be lower than that of the underlying soil, the final infiltration rate, or effective K_s, can be obtained by analysis of steady unsaturated flow across isotropic layers (Smith 1990).

The vertical distribution of matric water potential in the surface region will generally be as shown in figure 22. At longer times, the gradient in the underlying soil becomes small, the value of K_{s1} becomes closely uniform, and the greater gradient of ψ occurs in the crust. The following equation arises from matching fluxes into and out of the boundary between crust and subsoil, assuming that head at the bottom of the crust (ψ_c) equals head at the top of the subsoil (ψ_1) (this potential is termed ψ_b):

$$K_c(\psi)\left[1 - \frac{d\psi}{dz}\right] = K_1(\psi_b) \qquad [61]$$

Since the right side of equation [61] is a constant at steady flow, this equation applies throughout the crust layer at large times. It may be integrated from 0 to ψ_b to yield

$$z_c = \int_0^{\psi_b} \frac{d\psi}{K_1(\psi_b)/K_c(\psi) - 1} \qquad [62]$$

The function $K_c(\psi)$ is described in equations [2] plus [4], and $K_1(\psi_b)$ is a single value satisfying this equation. Equation [62] is integrated by trial or iteration to find ψ_b and $K_1(\psi_b)$, which is the asymtotic infiltration rate for this crusted profile (K_{se}).

In most cases, the best single value of G to use when the wetting front has passed into the subsoil from a crust is that of the subsoil (G_1). This conclusion comes from a study of infiltration under various conditions with various crust properties using solutions of equation [26]. At short times, equation [55] is accurately approximated by the expression

$$f = K_s G/I \qquad [63]$$

This indicates that soils with equal products $K_s G(\theta_i)$ act similarly at short times. When the subsoil has a higher K_s, and the value of $K_{se} G_1$ is lower than $K_s G$ (using K_{se} determined from solution of equation [62]), the value G_1 should be used to simulate infiltration after the crust has been passed. When $K_{se} G_1$ is larger than $K_s G$, it is more accurate to use a weighted value of G for $I > I_c$. To estimate this weighting, G′ is calculated, which is the value of G such that $G'K_{se} = GK_s$ at $I = I_c$. Then as I increases beyond I_c, G for use in estimating f(I) is found as a weighted average of G′ and G_1 (Smith 1990), as follows:

$$G_e = (I - I_c)G'/I + I_c G_1/I \qquad [64]$$

in which G_e is the effective value to use in estimation. Although this procedure may seem obscure, it is handled automatically in Opus. Validity of this weighting method is illustrated for one case in figure 23.

Crust Development. The mechanics of transient surface-crust layer development in agricultural conditions is not understood sufficiently to allow reliable quantification based on measurable soil parameters. Crust development apparently depends on such things as particle-size distribution, content of clay and organic matter, exposure to rainfall energy, and distribution of rainfall energy (Chevalier 1984). This is a subject needing much more investigation. It is known that the hydraulic conductivity of crusts developed under rainfall is commonly an

order of magnitude less than that of the parent soil, with some noted exceptions (Chevalier 1984). Further, in the absence of soil cohesion, the crust development is probably limited to simple increases in bulk density due to packing.

The hypotheses used in Opus to estimate crust formation are illustrated in figure 24. The upper graph represents a hypothesis for the effect of clay content on the ultimate crust hydraulic conductivity that can be formed by the action of rainfall. The lower graph illustrates a hypothesis for the rate of crust formation; it is assumed that the crust formation is an exhaustion function related to the accumulated amount of rainfall energy-intensity (EI) as described for the USLE factor in predicting erosion. The storm effective EI used in crust-formation estimates is directly reduced by the ratio of covered (plants and mulch) surface to total surface of the catchment. Opus uses the EPIC regression estimate (Williams et al. 1984) to obtain an estimate of EI when daily rainfall data are used, and finds approximate storm EI using

$$EI = 10\ r^2$$

when breakpoint rainfall rates (r) are given in millimeters per minute.

Crusts are assumed to be destroyed by cultivation operations that disturb the soil to any depth. Because some operations will not completely destroy an existing condition, the specified efficiency of cultivation (e_c) determines the starting state (EI_o), as follows:

$$EI_o = -400\sqrt{e_c} \qquad [65]$$

In part, this conceptually represents the effect that cultivation has on opening the soil, which goes beyond merely destroying a previously formed crust. Thus the soil hydraulic conductivity is briefly enhanced (negative EI_o) as a leftward extension of the lower graph in figure 24. Succeeding rains quickly increase the summed EI into the positive region (e.g., clod dissolution).

Dynamics of Surface Water

When the infiltration simulation model begins to produce rainfall excess, water begins to move over the surface (excepting the case of surface furrow storage) along the described topography as discussed above. Because Opus is limited to areas containing insignificant spatial variability of soil conditions, all parts of the catchment are assumed to begin to produce runoff at the same time. The tracking of spatial and temporal variations in surface-water-flow conditions is crucial

in simulating not only the discharge at the catchment outlet, but also the transport processes within the catchment that produce the pollutant load of dissolved and suspended material at the outlet.

The de Saint-Venant equations for surface water flow have proven to be a reasonably accurate and efficient means to describe the dynamics of catchment runoff. Two alternate well-known approximations are used in Opus to solve these equations. The kinematic method assumes that an equation of mass balance and a rating equation are sufficient for all but very flat slopes to describe the flow of surface water. The rating equation describes a consistent relation between discharge and flow depth or area for a given section geometry. The Manning uniform flow relation is such a rating and is the one used in this model. It relates flow velocity to hydraulic radius. Hydraulic radius is defined as the flow cross-section area divided by the wetted perimeter. For very low slopes, a diffusive wave equation is used, slightly more complicated than the kinematic wave equation, but amenable to rapid solution.

Mass balance can be expressed in differential form as

$$\frac{\partial a}{\partial t} + \frac{\partial q}{\partial x} = r - f \qquad [66]$$

in which

a is cross-sectional area of flow (m^2),
x is distance from beginning of runoff path (m),
q is local discharge (m^3/min),
t is time in minutes,
r is current rainfall rate (m/min), and
f is local current infiltration rate (m/min).

The Manning equation for normal flow can be expressed as

$$q = 60 \frac{\sqrt{S}}{n} \rho R^b \qquad [67]$$

in which

S(x) is local water energy slope,
n is Manning roughness coefficient,
ρ is wetted perimeter (m),
R is hydraulic radius (m), and
b is hydraulic exponent, = 5/3 for Manning relation.

Equations [66] and [67] are also tied together by the fact that $a = \rho R$. Thus, equation [66] may be written in finite difference form for solution as follows:

$$[\rho R]_i^{j+1} - [\rho R]_i^j + \frac{\Delta t}{\Delta x}\,\omega[q_i - q_{i-1}]^{j+1} + (1-\omega)[q_i - q_{i-1}]^j$$

$$- w\,\omega[r-f]^{j+1} + (1-\omega)[r-f]_i^j = F(R_i) = 0 \qquad [68]$$

in which

- i refers to sequential increments along the x path, i=1 to N,
- j refers to sequential time increments,
- w is width of the section from which rainfall excess contributes (m),
- ω is time step weight (0 to 1),
- Δx is incremental flow length = L/(N-1).

When the flow section geometry is given, the relation between a, R, and ρ can be obtained since $q_i = q(R_i)$. Thus equation [68] can be solved for R_i^{j+1} by iteratively making $F(R_i) = 0$. The Newton-Raphson method for sets of equations is used, and the matrix equation has the form

$$J(3,n)\delta(\underline{R}) = F(\underline{R}) \qquad [69]$$

where

- J(3,n) is the tridiagonal Jacobian matrix, containing terms of $\partial F/\partial R$,
- $\delta(\underline{R})$ is the vector of estimated corrections to $\underline{R}$, and
- $F(\underline{R})$ is the vector of residuals as in equation [68].

The upstream boundary condition and the downstream boundary condition depend on the flow type as discussed below.

Kinematic Wave Flow

Morris and Woolhiser (1980) demonstrated that one can properly assume kinematic flow for larger slopes or for shallower depths. Their criterion is expressed as a dimensionless number k_o, as follows:

$$k_o = S_o L/h_o \qquad [70]$$

in which

S_o is bed slope,
L_o is flow surface length (m), and
h_o is normal flow depth (m).

When k_o is greater than about 5 for low Froude numbers, the kinematic wave approximation can be made. That is, the slope term in equation [67] can be assumed to be the bed slope: $S(x) = S_o(x)$. For rainfall on a kinematic slope with an upstream divide, the upper boundary condition is simply that $q(x=0)$ or $R(x=0) = 0$. For cases where a small channel has an upstream input (q_o), the upstream boundary can be specified as $R(x=0) = R(q_o)$. This requires an algorithm to invert the q(R) relation (equation [67]) for a given flow geometry. The kinematic flow assumption requires no downstream boundary condition. The formulation given above for the finite-difference solution allows either sequential solution of equation [68] from i=1 to the downstream boundary (i=N) or a matrix solution for all i at once as in equation [69].

Diffusive Wave Flow

When k_o is smaller than 5, the kinematic-wave approximation is generally inadequate, and the energy slope may be expressed as

$$S = S_o(x) - \frac{dh}{dx} \qquad [71]$$

Use of equation [71] in equation [68] makes the formulation more complicated and nonlinear, so that sequential solution is not possible as in the kinematic-wave case. In Opus, equation [71] is approximated by $S = S_o(x) - \Delta R/\Delta x$. In addition, a relaxation coefficient is required in iteration. This means that stability of convergence requires that, for the (k+1)th iteration,

$$R_{k+1} = \beta(\delta R_{k+1}) + R_k$$

in which δR_{k+1} is the correction to R found from equation [69], and k is the iteration number. The upstream boundary condition for runoff from a plane beginning at a divide or for a channel with no upstream inflow is $S(0) = 0$, or $dh/dx(x=0) = -S_o(0)$. For flow with upstream inflow, the upper boundary condition at $x = 0$ is the normal flow depth for that inflow and flow geometry (equation [67]). The usual downstream boundary condition diffusive wave flow is a critical depth condition, which assumes an overfall of some kind. This is not presumed to be universally true, but it is not a severe assumption and allows convenient computation of a flow-depth relation. The alternative is more complex backwater calculations.

Estimation of Hydraulic Roughness

The user of Opus may specify a value of Manning n to represent roughness, which is used until a surface-altering management operation takes place. For natural untilled catchments or for simulating other fixed surfaces, this value applies throughout the simulation.

When the field is tilled, an empirical method is used to estimate the resultant value of n. It is assumed to be the sum of four factors: a bare soil value for a smooth, clean soil surface; a roughness caused by surface residue; a form roughness caused by clods and surface irregularities formed during plowing; and for unfurrowed surfaces, the roughness effect of plant stems. For many partially cohesive soils, the actual form roughness from plowing can vary considerably, depending on soil wetness at plowing. The relationship is unknown and is the subject of considerable research. The relation here is not presumed to be universal.

The value of n for bare smooth soil is assumed to be 0.02. Form roughness (f_f) varies with the type of operation and equipment. A table of values as a guideline is given in the User Manual (vol. II), taken partly from work done for EPIC (Williams et al. 1984). Values range from 6 to 50 and represent mean height of microroughness forms produced (in mm). The resulting roughness effect, in terms of a partial Manning n (n_f), is estimated (G.R. Foster, personal communication) as:

$$n_f = 0.00087 f_f^{1.25} \qquad [72]$$

The roughness resulting from surface residue is estimated following the work of Foster et al. (1982). It is a function of effective residue weight (m_{res}) (kg/ha) and a coefficient (c_{res}) that changes between furrowed and unfurrowed flows. The effective mulch cover (F_m) is first estimated as

$$F_m = 1 - \exp(-m_{res}/4428) \qquad [73]$$

The partial residue roughness (n_{res}) is then estimated according to the data from Foster et al. (1982) by

$$n_{res} = 1/[1 + (c_{res}/m_{res})^2]^{0.61} \qquad [74]$$

The value of c_{res} is 10.67 for furrowed surfaces and 3.43 for unfurrowed surfaces. Finally, the weighted sum of form and mulch factors becomes a partial n value represented by

$$n_{rf} = F_m n_{res} + (1-F_m) n_f \qquad [75]$$

The net n also includes a factor for estimated stem density when the surface is unfurrowed and flow must pass by plant stems. This is a function of the plant mass per unit area of surface. The final estimating equation becomes

$$n = [n_{rf}^{1.5} + n_b^{1.5}]^{0.667} + 3.6E\text{-}6M_{lv}/y_p \qquad [76]$$

in which M_{lv} is mass of plant above ground (in kg/ha) and y_p is height of plant (in m).

Flow Geometry Relations

The flow section geometry for which equation [68] can be applied is quite arbitrary, including plane flow; furrows; and trapezoidal, triangular, or rectangular channels. When a furrow or channel is treated, often a relatively flat bottom is formed by local transport and/or deposition of sediment. This surface can have a very different roughness than do the sides of the section. In such a case, the local net value of Manning roughness ($\bar{n}$) may be formed as a weighted sum of the roughness (n) of each part of the wetted perimeter, as follows:

$$\bar{n} = \left\{[\rho_b n_b^2 + \rho_z n_z^2]/\rho\right\}^{0.5} \qquad [77]$$

in which subscript b refers to the bottom section, and subscript z refers to side slopes of the section.

Time Steps

For surface-water routing with this scheme, time steps are the same as those for the infiltration calculations, described above. Hydraulic conditions on the catchment are checked at each time step, and time intervals are reduced if velocities between x increments are large enough to cause potential instabilities. These reduced time steps are then used in the next time increment for infiltration simulation. The largest time steps allowed are those read from the breakpoint rainfall record.

Irrigation Flows

The numerical scheme described above is applicable for estimating (a) the advance of water down a furrow from border irrigation or (b) any runoff produced by sprinkler irrigation. Sprinkler irrigations are treated like rainfall inputs, except that they are assumed to be controlled so that runoff is not produced. For border irrigation, the limits of practicality do not allow Opus to divide long furrows into enough distance increments to produce a precise prediction of flow advance, but

Opus provides a reasonable numerical approximation. The principal additional feature required for irrigation-advance simulation is the proper calculation of the spatial variation of infiltration rate, which depends on the time of initial wetting of a given point along the furrow. Thus, infiltration rate (f) and depth (I) are separately calculated for each increment node (x_i) along the plane. Net infiltration for water-balance calculations is obtained by summing over all locations along the field.

Erosion and Transport of Sediment

The methods used by Opus to estimate sediment production resulting from rain on a catchment correspond in approach to the methods available for estimating runoff. The sediment option accompanying the daily runoff method is a lumped-parameter expression that corresponds in sophistication to the SCS Curve Number runoff method. The corresponding option associated with breakpoint rainfall is a spatially distributed treatment of sediment transport similar to KINEROS (Smith 1981a). The option has been expanded to allow simulation of sediment with up to five representative classes of particle size.

For all cases, information on the rate of erosion (or deposition) as a function of soil, surface, cover, and local hydraulic conditions is crucial for accurate estimation of sediment transport. Opus makes use of information on the local conditions that is available from other parts of the model; included is information on plant and mulch cover, and soil-surface conditions.

Sediment Production for Daily Simulation

The daily amount of sediment that is produced by the daily runoff is estimated with a variation of the well-known USLE (Wischmeier and Smith 1978), which is MUSLE (Williams 1975). USLE is a lumped-parameter method of estimating net erosion by use of a log-regression expression involving a parameter estimate of each of several major erosion factors, as follows:

$$Q_s = R_u K_u L_u S_u \phi P_u \qquad [78]$$

in which

Q_s is net storm or daily soil loss (kg/m^2),
R_u is storm or daily erosivity (Newtons/hr),
K_u is soil erodibility factor ($kg \cdot hr/Newton/m^2$),
L_u is slope length factor,
S_u is slope steepness factor,
ϕ is coefficient for cover and management,
P_u is a factor for effects of supporting management practices.

Use of USLE and detailed discussion of the coefficients and their values is provided in a USDA Handbook on the subject (Wischmeier and Smith 1978). In MUSLE, R_u is modified from the original USLE to account for both rainfall erosivity and runoff erosivity. The estimating equation is (Williams and Berndt 1977):

$$R_u = 90.5(Q \cdot q_p)^{0.56} \qquad [79]$$

in which

Q is runoff volume (m^3), and
q_p is peak runoff rate (m^3/s).

Clearly this is a lumped approximation, but the method is tested and has complexity appropriate to match the daily hydrology estimation. The effects of impoundments such as tile outlet terraces or holding ponds are simulated by modifications to the parameter (P_u).

Distributed Erosion and Sediment Transport

When breakpoint rainfall is used, spatial and temporal distribution of runoff hydraulics is simulated and can be used to estimate spatial and temporal erosion and sediment transport. The general governing equation for sediment transport (Bennett 1974) in time (t) and along distance (x) can be written as

$$\frac{\partial}{\partial t}(aC_{sk}) + \frac{\partial}{\partial x}(qC_{sk}) - d(x,t)_k = q_s(x,t)_k \qquad [80]$$

in which

C_s is sediment concentration,
a is cross-sectional area of flow (m^2),
q is water discharge per unit width (m^2/min),
d is rate of erosion or deposition at the bed (m/min),
q_s is local input of sediment ($m^3/m^2/min$), and
k is a subscript referring to a particle size class.

This equation may be applied and solved through time and space in conjunction with the information on hydraulic conditions in time and space. It is solved in conjunction with the numerical solution for runoff water. If the user knows the hydraulic variables for a time step, the change in concentration with time over space can be found directly.

Surface Erosion and Sediment Transport

Whether the surface is furrowed or unfurrowed, flow can be thought of as composed of both "sheet" and rill flow. Erosion is caused by the shear of flowing water and by the disturbance of surface soil by raindrop impact. For this case, Foster (1982), based on existing experimental data, proposed an equation for the detachment of soil particles by rainfall as follows:

$$d_i = 0.0138\ K_u\ r_e^2[2.96(S_i)^{0.79} + 0.56]\ \phi_i \qquad [81]$$

where

r_e is effective rain intensity (mm/hr),
S_i is sine of the interrill surface-slope angle, and
ϕ_i is the interrill soil/crop coefficient as follows:

$$\phi_i = \phi_u\ (1-F_s)\exp[-0.21(h_c/h_b - 1)^{1.18}] \qquad [82]$$

where

F_s is fractional total cover (plant and mulch) over soil,
h_c is water flow depth for given cover conditions (m),
h_b is water flow depth for bare soil (m),
ϕ_u is a surface-soil residue factor defined as

$$\phi_u = B_s(c_a + c_b t_m)\exp(-120 f_{rs}) \qquad [83]$$

in which

B_s is a soil consolidation factor,
c_a and c_b are coefficients,
t_m is time since last tillage, and
f_{rs} is residue concentration in surface soil (10-100 mm) ($kg/m^2/mm$).

Foster's concepts grew out of the USLE to some extent, and the ϕ factors are related in concept to the ϕ of the USLE, insofar as they represent effects of management on the erosion process. The coefficients are discussed in Foster et al. (1983).

Interactions of rill erosion and transport capacity are calculated with a linear deficit-reaction relationship as follows:

$$d_{rk} = (d_{pr}/g_c)[g_c - g_s]_k \qquad [84]$$

in which

d_r is actual local rill-detachment rate (kg/m^2/min),
d_{pr} is potential rill detachment rate (kg/m^2/min),
g_c is transport capacity for particle class k (kg/m^2/min)
g_s is current transport rate for particle class k, (kg/m^2/min), and
k is an index for each particle-size class.

For this option, Foster et al. (1983) proposed d_{pr} to be related to local hydraulic shear, as follows:

$$d_{pr} = b_D \tau_s^{3/2} \quad [85]$$

and he also proposed that transport capacity is similarly related to shear, as follows:

$$g_c = b_t \tau_s^{3/2} \quad [86]$$

in which parameters b_D and b_T are defined in the following (Foster et al. 1983):

$$b_D = 139 K_u \phi_u \phi_r \quad [87]$$

$$b_T = 188 - 468 f_c + 907 f_c^2 \quad ; f_c \leq 0.22 \quad [88a]$$

$$b_T = 130 \quad ; f_c > 0.22 \quad [88b]$$

in which

f_c is clay fraction in soil, and

$$\phi_r = \exp[-1.8 M_m] \quad [89]$$

which is similar to the factor ϕ_u. M_m is mulch-cover density (in kg/m^2).

With the shear terms in equations [85] and [86] dividing out in equation [84], d_{pr}/g_c becomes a constant related to factors ϕ and clay content. Thus equation [84] is very similar to the equation used in KINEROS (Woolhiser et al. 1990) except that variations in the coefficient are still found from changes in the ϕ factors as shown in equations [87] and [88].

Potential transport capacity is found using the transport capacity relation of Engelund and Hansen (1967) as follows:

$$C_{smx} = \frac{0.05 \, S \, u \, u_*^3}{g^2 \, h \, y_d \, (\rho_s - 1)^2} \quad [90]$$

in which

u = flow velocity (m/min),
u_* = shear velocity (m/min),
y_d = mean particle size (m),
ρ_s = particle specific gravity,
g = acceleration of gravity (m/min^2),
h = flow depth (m), and
C_{smx} = transport capacity concentration for given particle and hydraulic conditions.

This relation is used because it has shown itself to be as robust as any for shallow flows and high slopes, which may often be encountered (Alonso et al. 1981). It has been discussed thoroughly elsewhere (Alonso 1978).

Concentrated Flow Erosion and Sediment Transport

Even in catchments of relatively simple geometry, distributed surface flows soon become concentrated into rivulets or small channels. On managed areas these channels may be the furrows themselves, or they may be formed when flow in furrows finds a local swale and forms a cross-furrow flow. These cases often result in ephemeral gullies in areas where erosion potential is high. They are ephemeral in cultivated lands because they are obliterated by mechanical cultivation. Conversely, these swales may be places for upland eroded material to deposit. Foster et al. (1983) suggested that erosion rates in small channels are best modeled by a relation based on the hydraulic bed shear and including consideration of a critical or threshold value, as follows:

$$D_f = c_f(1.35\tau_s - \tau_{cr}) \qquad [91]$$

in which

D_f is local concentrated flow-detachment rate (in kg/m^2/min),
c_f is a coefficient,
τ_s is hydraulic shear on the wetted perimeter of flow (Newtons/m^2), and
τ_{cr} is critical shear above which erosion occurs, (in Newtons/m^2).

This value is considered a potential detachment rate and is used in equation [84] along with transport capacity for distributed flow to determine actual local erosion (or deposition) rate. The value c_f is suggested by Foster et al. (1980b) to be estimable as proportional to USLE erodibility (k_u); in Opus, c_f is taken to be $0.246*k_u$ (metric units).

Erosion and Deposition With Mixed Particle Sizes

The transport of sediment particles is possible because of the dissipation of hydraulic energy from the flowing water. In the erosion and transport of soils and sediments of a mixture or range of particle sizes, different particle sizes will exhibit very different transport capacities (see equation [90]). Although there are yet no definitive, experimentally based laws governing the apportionment of transport energy among particle sizes of a mixture, some reasonable assumptions can make possible a useful model for the process. Opus treats a distribution of particle sizes as did CREAMS, that is, by using up to five different classes of particle size. The methods of Foster et al. (1985), for estimating the distribution of classes in the absence of specific information, are available as a default in Opus.

In the distribution of transport capacity among sediment-size mixtures, three general cases exist. In the first case, the transport capacity of flow may exceed the current sediment load of flow for all particle sizes involved. Here it is reasonable to assume that erosion will act on all the particles of the soil, so that particle sizes are eroded in direct proportion to their availability.

In the second possible case, the transport capacity of flow is inadequate to transport the sediment load for any particle sizes involved. For this case, deposition of all sizes will occur.

In the third case, conceptual assumptions are required, and present erosion theory is incomplete. Here the transport capacity may be greater than the sediment load if composed of only the smallest particle class, but the reverse is true for a load composed entirely of the largest particle size. The model must distribute the hydraulic energy among the particle sizes that make up the actual sediment load. In Opus, the total transport capacity is assumed to be a weighted sum of the transport capacities calculated for each class of particle size. The particle-size-class capacity weightings are assumed to be inversely proportional to the fall velocities of the class of particle size. Thus, a particle size with relatively high transportability will tend to be enriched in the total mix of particles. Since smaller particles almost always have a smaller fall velocity relative to their proportion of the soil, they tend to be always enriched in the sediment in runoff. This occurs not by excessive erosion, but by preferential deposition of heavier particles.

In determining the local conditions for transport of several particle-size classes, the total transport capacity is compared with the total sediment load. If excess capacity exists, a net erosion is indicated, but Opus assumes that erosion must take

all particles in proportion to their distribution in the soil, or else erosion would be self-limiting by surface armoring. Thus erosion is distributed according to the proportion of particle sizes, with a rate necessarily controlled by the rate determined for the largest (and least transportable) size. On the other hand, when there is an excess of total load over total transport capacity, selective deposition may take place. In this case, deposition will occur for the larger particle sizes, to the extent that total load exceeds total capacity. It is possible for net hydraulic erosion to be zero but with excess of capacity for small sizes and deficit of capacity for large sizes. This is conceptually analogous to armoring for riverbeds, but the rapid changes in shallow flow from rainfall runoff make actual armoring unlikely as an extensive or significant watershed phenomenon. However, selective deposition and consequent enrichment of fines is common and is simulated by Opus as described above.

Evolution of Flow Sections With Erosion and Deposition

Erosion and deposition often occur alternately during a runoff event at a given location, and will alter the geometry of a furrow formed by a farming implement. Also, small channels in a catchment will tend to have a geometry that is characteristic of the balance of erosive and depositional forces. With some simplifying assumptions, one can estimate the direction that will be taken in erosive or depositional changes. Opus includes an algorithm to estimate the changes in a furrow or channel section that result from the loss or gain of a certain eroded or deposited volume (expressed as m^3/m).

It is assumed that the channel cross section starts as a simple trapezoid formed as a furrow or as the intersection of two slopes, and is reset by mechanical operations. The width of the bed is assumed to adjust itself until critical shear is exceeded only on the bottom of the section. Changes of section shape are not computed during a runoff event, but are effected after the event when flow means and erosion or deposition totals are known. Erosion of a trapezoidal section can be accompanied by either widening or narrowing of the bottom section. The same is true with deposition or reduction in section area.

In CREAMS, Foster et al. (1980a) assumed a simple distribution of the local shear force along the wetted perimeter and developed an algebraic method to predict bottom width based on that

assumption. If the flow section is assumed to be rectangular, the hydraulic radius is related to the section factor as follows:

$$R = [SF]^{3/8} c_m \qquad [92]$$

in which

SF is a section factor, $Qn/\sqrt{S_o}$, and
c_m is a coefficient that depends on the section geometry.

The local shear stress is assumed to be distributed along the wetted perimeter, increasing from zero at the water edge to a maximum at the middle of the bottom. To describe this distribution we define a normalized distance along the wetted perimeter (here called y_*), which is obtained by dividing the distance along the perimeter by the wetted perimeter (ρ). The local shear stress can be expressed in terms of critical shear stress as

$$\tau = \tau_c B$$

with

$$\tau_c = \text{critical shear stress} = \gamma S_o R \qquad [93]$$

in which

γ is specific weight of water, and
B is a weighting function found so that

$$1.0 = \int_0^{\rho/2} B dx$$

These equations merely express the concept that shear stress is distributed along the distance from the water edge to the middle of the rectangular channel ($y = 0$ to $\rho/2$, or $y_* = 0$ to $y_* = 0.5$), and weighted in such a way that the total shear stress is still expressed by equation [93]. If c_m and R in equation [92] are expressed in terms of y_* and combined with equation [93], a combined factor b_c can be obtained as follows:

$$b_c(y_*) = [SF]^{3/8} (\gamma S_o/\tau_c) \qquad [94]$$

The terms on the right can be obtained independently of the section proportions, and the function $b_c(y_*)$ is inverted so that y_* is found as the dimensionless depth of the rectangle with τ at the edge of the bottom just equal to τ_c. The bottom width immediately follows from the rectangular-shape assumption and can be expressed as

$$w_f = [SF(1-2h)]^{3/8} y_*^{-5/8} \qquad [95]$$

This provides a means to estimate the width of the bottom when the shape of the section is being altered by scour or deposition. This method is used in Opus with sloping sides rather than rectangular sections. Figure 25 illustrates how the section is assumed to change. At the end of a runoff event, the amount eroded or deposited at each section has been accumulated and expressed in terms of a cross-sectional area. This is used along with the width found from equations [94] and [95] to solve for the required cross section. Given a change in section area and new bottom width, the change in bottom elevation is the single unknown dimension.

Impoundment Storage

One significant management practice that may often be used in controlling pollution from agricultural catchments is the inclusion of an impoundment element in the field. This may take the form of a tile outlet terrace or a series of them, or it may be as simple as a pond at the lower end of the field. Of course, ponds may also be natural parts of unmanaged catchments. For experimental catchments, a pond may be formed as backwater to a measuring weir or flume.

The option for daily rainfall sediment (described above) simulates the effects of a pond on sediment and sediment-associated pollution by modification of the USLE "P" factor (P_u), as specified in USLE methodology. The USLE handbook describes the appropriate P_u factor changes for pond effects.

Routing of Water Through a Pond

Given the time distribution of inflows of water and sediment to a pond, the hydrologic effects of the pond on both hydrograph and sediment-concentration distribution can be analytically simulated. This is done in the option for breakpoint rainfall hydrology and sediment.

The pond is described for purposes of simulation either by an equation for depth-area relationship, or by the slope geometry of the surfaces converging at the pond location. That is, the description of the slope of two planes and the slope of their intersection (presumably a channel to which they contribute, plus the slope of the face of a dam across the channel) can be converted into an equation for the relation between depth of water and surface area contained in this inverted-pyramid-shaped "basin."

Either method produces an equation with three parameters relating pond water surface area (A) to depth (h) as follows:

$$A(h) = A_p + b_p h^{c_p} \qquad [96]$$

in which A_p, b_p, and c_p are the descriptor parameters for the pond.

The other information needed to route water and sediment through the pond is the outlet-rating relation. This is an equation relating discharge from the pond to depth, and includes a threshold depth below which the discharge is zero. The pond is assumed to seep water into the soil at all depths, using the saturated hydraulic conductivity of the surface-soil layer or other user-specified limiting conductivity as the rate of seepage.

The outflow rating may be given either as an explicit relation of discharge to depth or in the form of an orifice coefficient, which is translated by the program into an explicit relation. The general rating relation for outlet discharge is

$$Q_o = c_o(h-h_z)^{d_q} \qquad [97]$$

in which

Q_o is outlet discharge (m^3/min),
h is pond depth (m),
h_z is the threshold depth for outflow (m), and
c_o, d_q are parameters.

The routing of runoff through the pond is simply the solution of the differential equation for a linear storage system, as follows:

$$\frac{dV}{dt} = Q_{in} - Q_o \qquad [98]$$

in which

Q_{in} is pond inflow discharge (m^3/min),
V is storage in pond (m^3).

$Q_{in}(t)$ is known, and the solution is obtained through the relation between $Q_o(t)$ and h of equation [97], plus the relation between the pond volume V and depth y(t), which comes from the following integration of the area-depth relation equation [96]:

$$V(h) = \int_0^h A(h)dh = A_p h + \frac{b_p}{c_p+1} h^{(c_p+1)} \qquad [99]$$

In Opus, the solution is obtained on successive small time steps (Δt) during which Q_{in} is assumed constant. Using $dV(h) = A(h)dh$, the solution is actually obtained in the form

$$\frac{dh}{dt} = \frac{Q_{in} - Q_o(h)}{A(h)} \qquad [100]$$

Pond storage (except for the smallest ponds) will often have a considerable damping effect on the peak discharge from a small catchment. A significant value of h_z indicates that runoff from small flows can be trapped, and pondages in general can trap most sediment carried by all but the largest flows.

Routing of Sediment Through a Pond

Each class of particle size from the sediment-transport simulation is considered separately in routing sediment through a pond. A given sediment particle entering the pond is assumed to settle at its fall velocity. The general equation for mass balance of the sediment particle class j, with concentration C_j and settling velocity v_{sj}, can be written as

$$\frac{d(C_j V)}{dt} = C_{ji} Q_{in} - C_j Q_o(h) - A(h) C_j v_{sj} \qquad [101]$$

We assume (as above for pond depth) solution during a small time step in which Q_o and Q_{in} are locally constant. Noting that dV/dt is $Q_{in} - Q_o$, the general equation in terms of C_j becomes

$$\frac{dC_j}{dt} = \frac{C_{ji} Q_{in} - C_j (Q_{in} + A v_s)}{V(t)} \qquad [102]$$

in which C_{ji} is input value of C_j. Equation [102] is solved by a transformation of variables, and the solution takes one of three forms, depending on the relative size of various variable terms. The forms are

Form 1: For relatively constant V, or $Q_{in} \simeq Q_o$, the solution for C_j after an interval Δt is

$$C_j = C_{jx} + (C_{jo} - C_{jx}) \exp(-b\Delta t/V) \qquad [103]$$

in which

C_{jo} is C_j at time 0,

b is $Q_{in} + Av_{sj}$, and

C_{jx} is $C_{ji}Q_{in}/b$

Form 2: For $|b/\Delta Q|$ greater than 10,

$$C_j = C_{jx} + (C_{jo} - C_{jx})V/(b\Delta t)[1-\exp(-b\Delta t/V)] \qquad [104]$$

Form 3: For $|b/\Delta Q|$ less than 10,

$$C_j = C_{jx} + (C_{jo} - C_{jx})[V_o/(V_o+\Delta Q\Delta t)]^{b/\Delta Q} \qquad [105]$$

The value ΔQ is $Q_{in} - Q_o$. Time steps Δt are those chosen as appropriate for the solution of equation [100] above.

From the point of view of the various flow paths across the impoundment, given a variety of flow-entrance locations and outlet location, the pond is actually a spatially lumped element in the method as described.

After the cessation of input to the pond, its settling and outflow are simulated until outflow ceases, with time steps chosen to optimize the computations. The fact that the pond is on soil with a finite loss rate assures that outflow returns to zero at a finite time.

Simulation of Snow Budget

Precipitation records very rarely include data on whether the precipitation in winter periods occurs in the form of snow or rain. Further, since Opus is designed to not require detailed daily records of temperature, there is no way to accurately predict the occurrence of snow. Even when records of daily maximum and minimum temperatures accompany the precipitation record, often it cannot be ascertained whether a precipitation event was snow or rain. Thus the model in Opus is only approximate.

Accumulation of Snow

In Opus, snow is assumed to be the precipitation form when the (typically) regenerated (or measured) sequence of daily maximum and minimum temperatures indicates that the mean daily temperature at the soil surface is less than 0^oC. Snowpack is accumulated from any precipitation occurring as long as mean daily temperature remains below 0^oC.

Simulation of Snowmelt

Snow melt is calculated on days when a snowpack exists and when daily maximum temperature rises above 0. Figure 26 illustrates the processes that Opus considers in estimating the melt and evaporation of snow. As with rainfall, a certain amount of snow is intercepted on any plant or standing dry material. This intercepted snow is subject to early evaporation by available solar and thermal energy. Snowpack evaporation is calculated to be analogous to bare-wet-soil evaporation, with PET obtained using the estimated albedo for snow-covered surfaces.

The daily effective melt temperature is apportioned for that part of the day that is estimated to have temperature above $0^{o}C$, assuming sinusoidal temperature variation. Melt is assumed to come from two potential heat sources: air heat convection and soil diffusive heat flux. Air heat melt is estimated using a degree-day method modified by shade and snow depth (Linsley et al. 1958). Snow depth is used as a simple surrogate for snow-heat storage and ripening, which cannot be properly simulated without more detailed temperature information and heat-transfer simulation within the snow cover. The Opus approximation of the effect of snowpack's latent heat storage is illustrated in figure 27.

Melt due to soil-heat flux is estimated whenever the surface-soil temperature is greater than the assumed snow temperature ($0^{o}C$). Transfer of heat from soil to snow is assumed to be reduced by the presence of surface residue and mulch. The combined equation for estimating daily snowmelt potential (x_M) (mm) is

$$x_M = 4.5(1-0.4F_p^2)T_m\Delta t_m c_f + 10.8T_{s^2}\kappa_s(1-F_m^2)\Delta t \qquad [106]$$

in which

F_p is relative cover shading in snow,
T^m is effective mean melting temperature ($>0^{o}C$),
Δt_m is effective time of melting (days),
c_f is $\exp(-.005W_s)^2$,
W_s is snowpack water equivalence (mm),
T_{s^2} is soil temperature at 10 mm depth,
κ_s is surface-soil thermal conductivity (mcal/cm/sec/^{o}C),
F_m is relative mulch cover on soil, and
Δt is time interval (days).

The first term on the right of equation [106] is the degree-day estimate of melt from atmospheric heat. The second term is the estimate of melt due to thermal flux from the soil. The coefficient 4.5 is the degree-day melt coefficient (Linsley et al. 1958), and the 10.8 is a unit conversion factor for the latent heat melt for heat from the soil. The term c_f (illustrated in

fig. 27) is the surrogate effect of the greater coldness of the deeper snowpacks.

Estimated snowmelt water is added as surface input during calculation of the daily soil water flow, with sinusoidal distribution through the day for days of melt. The amount that is estimated to be excess, when melt rates are high, is treated as runoff in the surface-hydrology section of the model. When rain falls on a day when snow is melting, the two inputs are treated in sum in the hydrologic simulation.

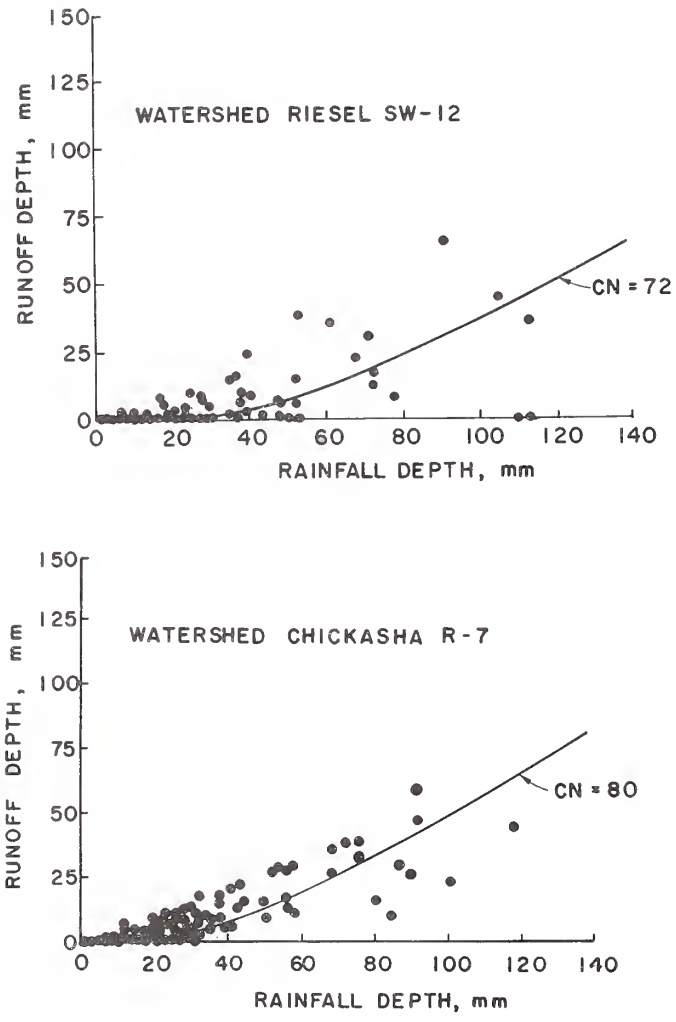

Figure 18.
Two examples of curve number relation compared with actual rainfall-runoff data. Measured daily rainfall and runoff, when plotted in this way, always show considerable scatter, which the more simple or lumped runoff relations cannot simulate accurately.

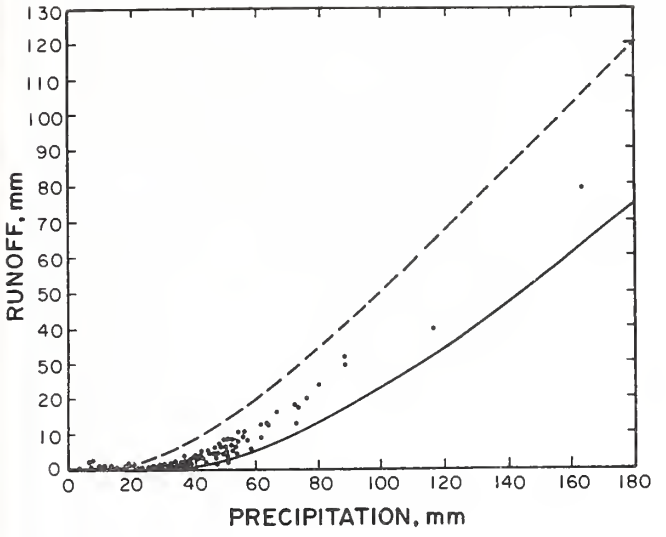

Figure 19.
The SCS method for treating initial soil-water condition results in only a very small relative variation in predicted runoff. The two curves shown are the CN relations for antecedent conditions I and II.The case simulated is Watkinsville, GA.

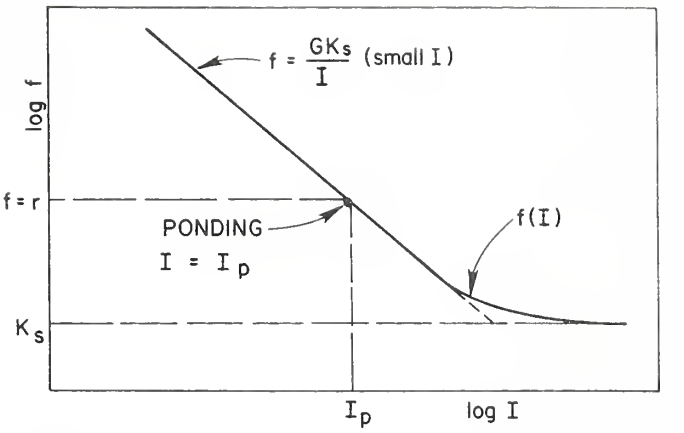

Figure 21.
The Opus breadpoint hydrology relates infiltration capacity (f) to infiltrated depth (I). At short times this relation is an inverse one as shown. Actual infiltration rate is the smaller of f or rainfall rate (r). At larger times or at larger values of I, the relation becomes asymptotic to the constant K_s.

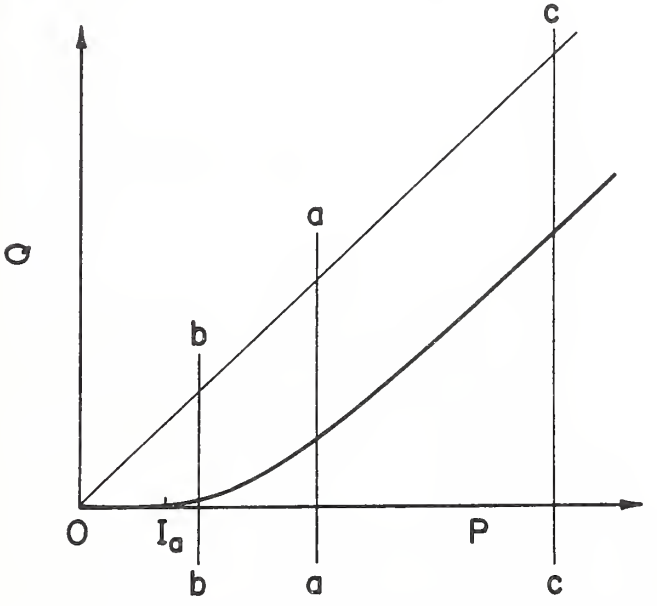

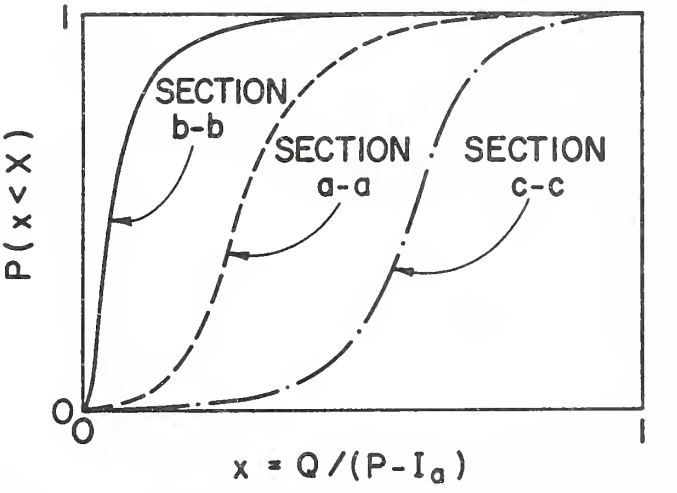

Figure 20.
The probabilistic method in Opus assumes that the Curve Number method estimates an expected value of runoff. At any level of rain (P) in left figure (a, b, or c) there is actually a random distribution of runoff (Q). A two-parameter beta distribution can represent a reasonable distribution for relative runoff amount, as shown in the right figure.

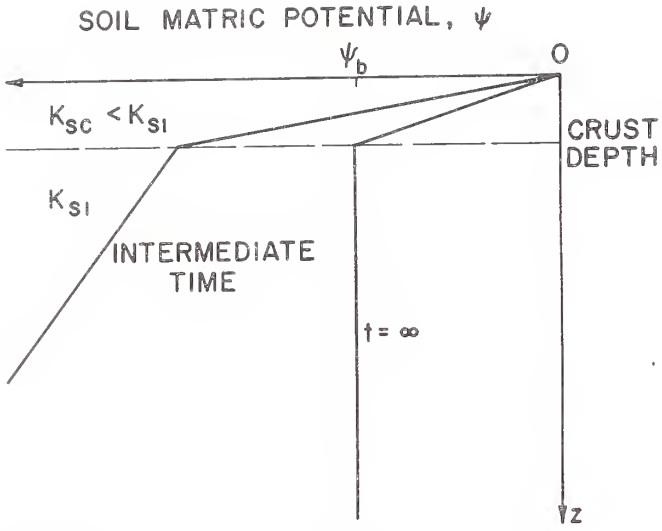

Figure 22.
The effect of a surface soil crust on potential gradient in infiltrating soil. This effect is important in simulating the infiltration relation for the crusted soil case, which requires knowing the ultimate value of f.

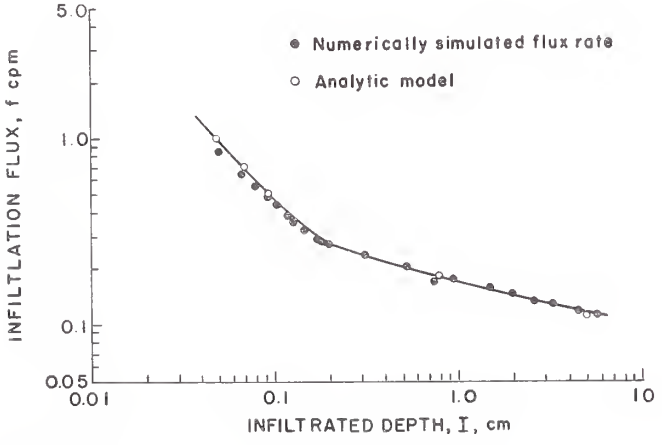

Figure 23.
An analytic weighting method used in Opus for estimating infiltration in crusted soils. It is compared here with the numerical solution of Richards' equation for the same case.

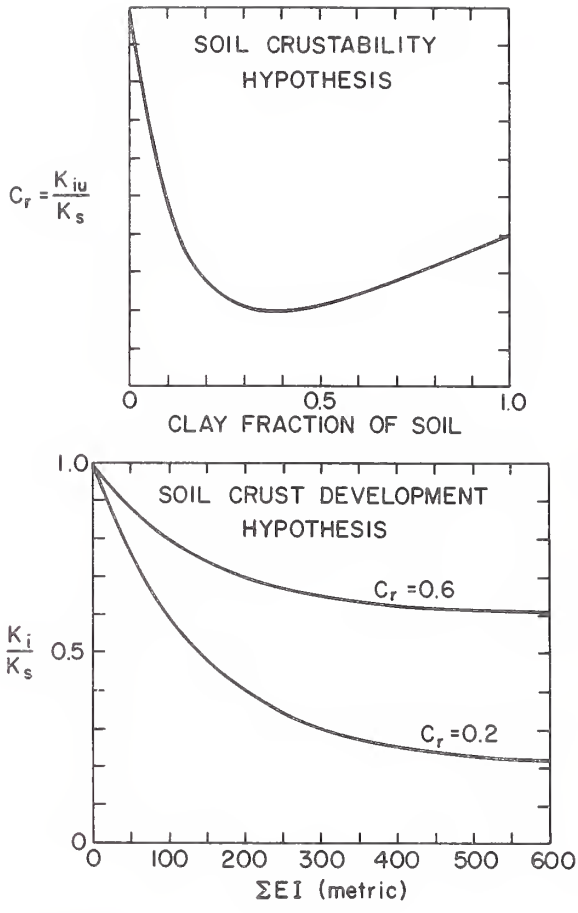

Figure 24.
Two curves representing hypotheses used by Opus to estimate the relation between soil clay content, accumulated rainfall energy, and formation of restricted crust layers at the surface of cultivated soil. K_i is value of K_s in surface layer at any time.

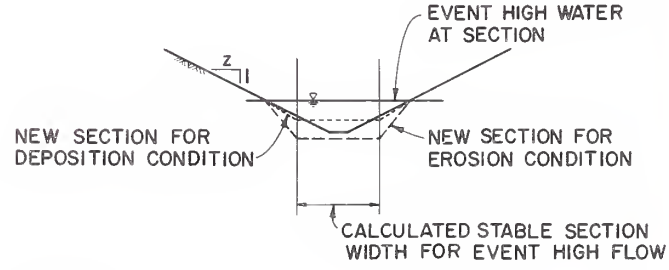

Figure 25.
Section changes estimated by Opus based on an estimate of altered section bottom width for distribution of bottom shear. Erosion and sedimentation occur in different amounts at different locations along a channel or furrow, and cause changes in the furrow geometry.

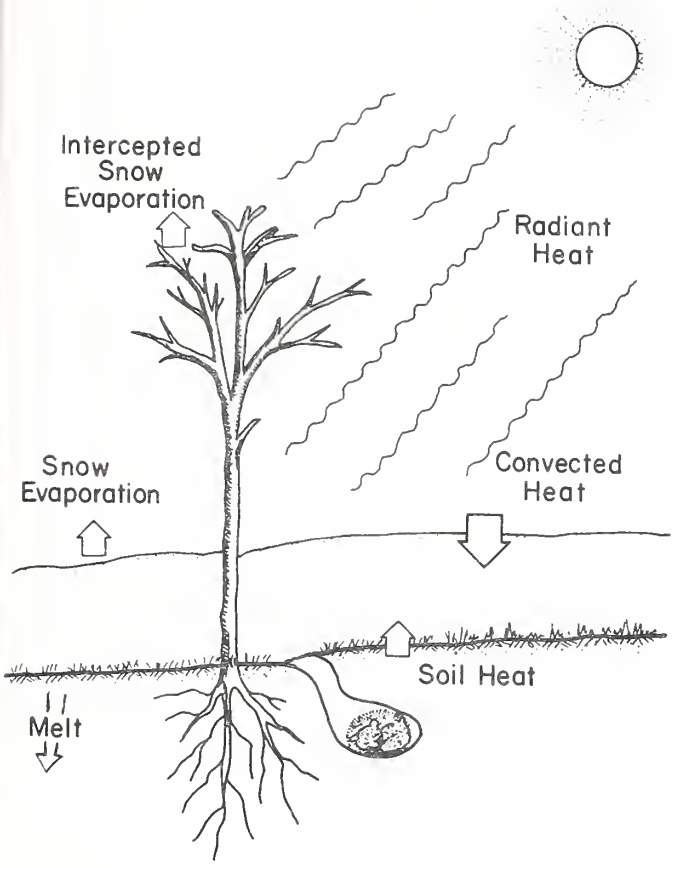

Figure 26.
Various processes that affect snowmelt and snow evaporation. Snowmelt is assumed to include loss of intercepted snow from vegetation. Surface accumulations are melted from convective, radiative, and soil heat energy sources.

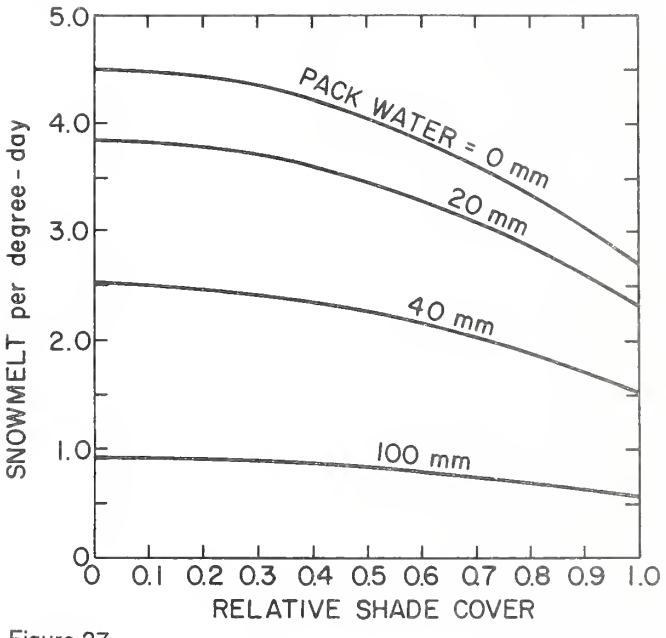

Figure 27.
Opus approximation of effects of latent heat and shading on snowmelt.

Transformations of Nutrients

Because nutrients are a major contributor to agricultural non-point-source pollution, it is important to accurately simulate cycles of nutrients in the agricultural system. These cycles describe the exchange of nutrients (including those in applied chemicals and manures) between plants, soil, and microbes. Along with the transformation cycles of phosphorus, carbon, and nitrogen, the movement of all nutrients in tillage, mixing, and transport in soil-water movement should be considered in the nutrient model. All of these processes together determine the amount of movable material present at the surface when runoff occurs, and the amount transportable with moving soil water.

Organic matter is central to the cycling of plant nutrients, and the simulation of nutrient transformations in Opus is done by a version of the "Century" organic-matter model of Parton et al. (1988b). The model simulates both labile and stabilized organic-matter fractions, and thus simulates the nutrient-supplying capacity of the soil organic matter (SOM) as well as the local amount of mobile nutrients. A more complete discussion of the modeling approach and the background for the model can be obtained in Parton et al. (1988b).

The nutrient model contains three SOM fractions (fig. 28), as follows:

(a) An **active** SOM fraction of soil carbon (C), nitrogen (N), and phosphorus (P). This consists of live microbial matter and microbial products, along with partially humified soil organic matter with a short turnover time (1 to 5 y).

(b) A **slow** SOM fraction of C, N, and P that is physically protected or more biologically resistant to decomposition. This fraction has an intermediate turnover time (20 to 40 y).

(c) A **passive** SOM fraction that is chemically resistant and may also be physically protected. This fraction has the longest turnover time (200 to 1500 y).

Plant residue (above and below ground) is divided into two fractions: **Structural** carbon and nutrient pools that have 1- to 5-y turnover times, and **metabolic** carbon and nutrient pools that have 0.1- to 1-y turnover times before transfer into SOM pools. Decomposition products from these pools are added to the SOM pools described above.

Decomposition of each of the organic-matter fractions is calculated using the following equation:

$$\frac{d(m_{rc})_i}{dt} = k_i \cdot f_w \cdot f_T \cdot (m_{rC})_i \qquad [107]$$

where

$(m_{rC})_i$ = carbon in the respective pools (gm/m^2),
i = pool index: 1 for structural and 2 for metabolic soil surface litter; 3 for structural and 4 for metabolic soil litter; and 5, 6, and 7 for active, slow, and passive SOM, respectively;
t = time (days);
k_i = parameter of maximum daily decomposition rate for the ith state variable;
f_w = effect of relative soil-water content on decomposition (see fig. 29 top); and
f_T = relative effect of daily mean soil temperature on decomposition (see fig. 29 bottom).

The factors of temperature and water content were developed based on laboratory and field observations (Parton et al. 1987).

The decomposition-rate parameter (k_i) is constant except for k_1 and k_3, which are functions of the lignin content of the structural material, and K_5 (the active SOM decay rate), which is a function of the soil texture. Decay rates of surface litter are slower than those of soil litter, based on the assumption that soil-moisture conditions are consistently less advantageous for decomposition at the surface.

The model assumes that all pool transfers from carbon decomposition are a result of microbial activity and that microbial respiration is associated with each of these transfers. The relative amounts of loss of m_{rC} from respiration are shown in figure 28. The split of plant residue into structural and metabolic fractions as a function of the ratio of lignin (m_{rL}) to nitrogen (m_{rN}) was determined experimentally by incubation studies (Pinck et al. 1950). This split is determined using the following equation:

$$f_{rm} = 0.83 - 0.018(m_{rL}/m_{rN}) \quad [108]$$

where f_{rm} is the fraction of residue that is metabolic. The fraction that is structural (f_{rs}) equals 1 - f_{rm}. The split occurs when plant residue is transferred into litter material or plowed into soil residue. The fraction of structural material in the litter that is lignin (f_{rL}) affects the decomposition rate coefficients k_1 and k_3 in the following manner:

$$k_1 = k_{1c} \exp(-3f_{rL}) \quad [109]$$

$$k_3 = k_{3c} \exp(-3f_{rL}) \quad [110]$$

where k_{1c} and k_{3c} are appropriate constants.

These relations cause the decay rates of structural material to decrease as the relative lignin content increases. The relations are based on the assumption that the microbes can more easily decompose certain substrates when lignin contents are lower (Melillo et al. 1984). Values of parameters in equations [109] and [110] were obtained from laboratory incubation data.

Laboratory incubation data were also used to determine functional forms for the effect of soil texture (Sorenson 1981). Texture, in terms of sand fraction (f_s), is assumed to affect respiration efficiency (e_r) of the active SOM pool and its decay rate (k_5), as follows:

$$k_5 = k_{5c} \ (0.25 + 0.75 f_s) \qquad [111]$$

$$e_r = 0.17 + 0.68 f_S \qquad [112]$$

The relations shown above have been verified by several studies (Parton et al. 1987). Determination of a value for k_7 could not be done by laboratory exercises but was found by observations on stable SOM levels at several sites and model-tuning procedures (Parton et al. 1987).

The model operates on a daily time step, which is a modification over other versions of the same model. Accumulations of added residue material and losses from crop harvesting and grazing are accounted for each day, if generated by the management component. The location of the SOM pools is the top 200 mm of soil, assumed to be the active decay region of soil. Usually little residue decay takes place below this level. The mineral N pool is subject to transport through this zone as water moves through it. This is accomplished by the subsurface-water-transport component of the model (ch. 4). The model is linked to the plant-growth component for uptake of mineral N and P and for input to litter of residue after senescence, or input of soil residue from plowing.

Submodel for Nitrogen

The nitrogen model has the same flow or state-transfer structure as the carbon model (see fig. 30). It is assumed that most N is bonded to carbon. Ratios of C/N for structural, active, slow, and passive soil fractions are assumed to remain fixed for a given site. Ratios of C/N for structural and active SOM are set at 150 and 8, respectively, and the C/N ratios for slow and passive SOM are 11. These ratios are based on soil pedon data analysis and other data (Parton et al. 1987). The N content of the metabolic pool is allowed to vary; any incoming plant N material not needed for the structural C/N ratio goes to metabolic N. N transfers are stoichiometrically related to carbon transfers, with N transfer being equal to

carbon transfer divided by the C/N ratio. Transfers between pools can result in mineralization or immobilization, depending on the C/N ratios of the donating and receiving pools and also the fraction of carbon lost as CO_2 respiration (30% to 80%).

Nitrogen is added to the system as fertilizer mineral N, as plant residue N (discussed above), or by biological fixation. Fertilizer N comes in bulk as an addition to the mineral N content (NO_3 or NH_4) of a given soil layer, usually the top of the soil.

Other N-transforming processes include fixation by air and plant processes and also nitrification and denitrification (Parton et al. 1988a). Daily fixation from the atmosphere (m_{NA}) (g/m^2) is estimated by

$$m_{NA} = c_A + b_A(P) \qquad [113]$$

in which c_A and b_A are fixed coefficients and P is daily precipitation. Fixation by nitrogen-fixing plants is assumed to occur to the extent necessary to prevent N stress on such plants.

Nitrification, which changes NH_4 N to NO_3 N, is assumed to occur continuously in response to soil water content, temperature, and concentration of NH_4, as follows:

$$m_{Ni} = c_{Ni}\ f_W\ f_T\ f_{NH} \qquad [114]$$

in which the f coefficients are factors of water, temperature, and NH_4 concentrations, respectively. The quantity c_{Ni} is a coefficient with a value of 0.1 for estimating m_{Ni} in $gm/m^2/day$. Figure 31 illustrates the f functions used in equation [114]. Denitrification is modeled similarly, with an additional soil-texture factor based on content of sand. Denitrification causes mineral NO_3 to be volatilized in oxygen-poor situations. Oxygen poverty is usually associated with high water contents, and denitrification is assumed to be approximated as follows (Parton et al. 1988b):

$$m_{Di} = c_{dn}\ f_W\ f_T\ f_{SN}\ NO_3 \qquad [115]$$

with factors f similar to those for nitrification but based on nitrate content (NO_3) (in parts per million) rather than on NH_4 concentration. The quantity f_{SN} is an approximator of texture and is defined as $4.66 - 4.8f_S$ (f_S = sand fraction). The coefficient c_{dn} is 0.0004. Figure 32 shows the factor f_W for this process as a function of water content. The factor f_T is the same as for nitrification. Units of m_{Di} are again in $gm/m^2/day$, with the computed amount being taken from the soil's

total NO_3 content and lost as gas. Amount of N volatilized is assumed to be 5 percent of the total N mineralization flows that accompany decomposition of metabolic residue and SOM fractions.

Submodel for Phosphorus

The model for phosphorus is similar to that of nitrogen, with some small differences (fig. 33) (Parton et al. 1988b). Ratios of C/P are used to trace P transformations that accompany C transformations between the various pools. The primary mineral source of P is weathering of soil apatite. During weathering, labile P is taken up by organisms at the same time that secondary and occluded forms of P are produced (fig. 33). The SOM pools are assumed to have characteristic C/P ratios, and the amount of P moving between pools is determined, as for N flows, by use of C/P ratios. Also as for N, P involved in respiration is assumed to be mineralized, and decomposition of structural residue (which is low in N and P) is assumed to involve immobilization.

Transformations of Pesticides

As outlined in chapter 8, pesticides are applied in several ways, and they enter the simulation by deposition on plants, deposition on surface soil and residue, or incorporation into soil at some depth. The portion of a pesticide on a plant surface is subject to both environmental decay and partial washoff during subsequent rain. Description of a pesticide in input data includes the fraction of plant-adsorbed pesticide subject to washoff and also the first-order decay-rate coefficient for this plant fraction.

Pesticides within the soil are assumed to be subject to environmental decay. The decay rate is modified by temperature and water content, but is assumed to be described by a first-order rate equation (exponential decay) with coefficient k_{ps}, as follows:

$$dm_p/dt = k_{ps}\ m_p \qquad [116]$$

in which m_p is local pesticide mass. The effects of water and temperature are assumed to be described by the Arrhenius equation (Walker 1974), as follows:

$$k_{ps} = k_{psb}\ f_w(\theta)\ \exp(b_{ar}/1.99[1/T_{Kb}-1/T_K]) \qquad [117]$$

in which

T_K is current Kelvin temperature,
T_{Kb} is a reference Kelvin temperature,
f_w is a water-activity function used for microbial degradation (see fig. 29),
b_{ar} is a constant, and
k_{psb} is decay coefficient at temperature T_{Kb}.

The coefficient b_{ar} is calibrated if data are given for a measured K_{psb} at a given temperature or water content, or else is assumed to have a default value taken from published values (Walker 1974). Without better and more widely available knowledge of the individual processes, Opus does not attempt to separate the various processes of environmental degradation and transformation of pesticides (such as hydrolysis and photochemical action). Decay is assumed to be highly related to microbiological activity, so it follows that a pesticide leached beyond the depth of active decay (approximately 200 mm) is decayed at a fraction of the decay rate of pesticides in the active region.

Pickup of Chemicals by Rainfall and Runoff

The movement of both soil and surface water is involved in the transport of chemicals in the agricultural environment. However, the occurrence of a runoff-producing rain has the primary role in actually moving chemicals off the field. Nonrunoff rainfall events can also move chemicals from plant and residue surfaces into the soil surface.

Several processes are simulated in the Opus model in connection with the production of chemicals in runoff water. The simulation methods are designed to operate equally well with both of the sediment transport/hydrology options available. This dictates that the methods are lumped. It is doubtful that detailed, spatially distributed calculations have general value because of many nonuniformities and our imprecise knowledge of the exact mechanisms in the various processes.

The following paragraphs outline the methods used in Opus to estimate the load of nitrate, phosphorus, and ammonia in runoff water, and the amount of each that washes into the soil from the surface. These constituents are treated identically, with few noted exceptions. The following discussion, for simplicity, uses labile phosphorus (P) as an example.

Leaching of Canopy Chemicals

For all rainfalls that exceed the interception storage of the current canopy, a certain small fraction of the nitrate and phosphorus contained in the plant is assumed to wash off the plant with the rainwater. For living plants, this fraction is assumed to be 0.02; for standing residue, or plants undergoing senescence, it is assumed to be 0.03 (Schrieber 1990). If the period since the last rainfall or washing event [Δt_d (days)] is greater than 1.0, the fraction is reduced by a factor (f_{pw}) as follows:

$$f_{pw} = 1 - \exp(6\Delta t_d) \qquad [118]$$

In addition, the amount of plant leachout is proportional to the percent cover that the crop represents compared to the field surface (F_p). Thus, the estimated field value of labile phosphorus leached from the canopy [$m_p(cl)$, in kg/ha] is

$$m_p(cl) = 0.02 m_p(c) f_{pw} F_p [LF_L / F_{LT}] \quad [119]$$

in which

$m_p(c)$ is P content in crop (c) (kg/ha),
F_L is leaf area index for that crop, and
F_{LT} is total field Leaf Area Index (F_L) for all plants.

Leaching of Residue

Rainwater also leaches decomposition-product nutrients from residue on the surface of the soil. This process is assumed to be similar to the clarification of a simple reservoir. Adding water to a solution in an overflowing reservoir results in exponential decay of concentration, assuming a fixed mixing efficiency. The leaching constant for residue is assumed to be .05 per mm of rainfall. The amount of P in the residue that is leached in a given storm [$m_p(rsl)$] is assumed (re Schrieber 1990) to be

$$m_p(rsl) = m_p(rs)(1-\exp[-.05V_p]) \quad [120]$$

where

$m_p(rs)$ is current content of P in surface residue (kg/ha), and
V_p is rainfall passing through residue (mm).

Routing Chemicals by Infiltration and Runoff

Phosphorus or other nutrients from the above sources, plus natural nitrate in rainwater, will either enter the soil or leave the catchment in runoff. The path of a solute is estimated according to the division of rainfall in the infiltration process. The first part of the rainfall will all infiltrate into the soil. This portion (I_p) is then distributed downward from the soil surface (along with chemicals contained in the water) to the depth reached by the wetting front at ponding (z_p). A more detailed, spatially distributed, and dynamic study has been made by Havis (1986). The model here is necessarily lumped.

Rainfall and washed solutes reaching the soil surface after ponding will be divided between infiltration and runoff, but all incoming rain will interact with the flowing surface water.

First, the concentration of chemicals in the surface active layer is calculated at the time when runoff begins, based on the amount I_p, which has washed through it. Then the rainwater that exceeds I_p interacts with this surface zone as a simple reservoir during runoff. For chemicals such as phosphorus and ammonium, this interaction assumes the behavior of an equilibrium adsorption isotherm. The depth of the interactive soil is related to soil disturbance, porosity, and infiltration characteristics. The depth is user specified as a fraction (f_z) of the 10-mm-deep surface layer.

The mixing interaction is assumed to be similar to that in soil-water transport. The estimated concentration of runoff water (C_{ro}) is

$$C_{ro} = C_{Pi} + [C_{Po} - C_{Pi}]\ F_e(r_e, M_w) \qquad [121]$$

in which

C_{Pi} is P in water reaching surface after runoff begins,

C_{Po} is P concentration in active zone of soil surface at beginning of runoff, and

$$F_e(r_e, M_w) = [1-\exp(-r_e/M_w)]M_w/r_e \qquad [122]$$

in which

M_w = total water for equivalent dissolved labile P at equilibrium in active layer (mm),
$= 10\theta(1) + 1000\ K_{dp}M(1)$,

K_{dP} = equilibrium adsorption isotherm for P (liter/kg),

$M(1)$ = mass of soil in top 10 mm (kg/ha),

$\theta(1)$ = water content in first (10-mm) layer after infiltration,

r_e = rainfall reaching soil after surface ponding (mm).

Finally, the amount of P in this example is assumed to equilibrate with the transported sediment according to the equilibrium adsorptivity described by K_{dP}, which partitions the P in runoff between that adsorbed on sediment particles and that in solution.

Pesticides enter runoff water by very similar assumed mechanisms. Some pesticides may contribute part of their concentration by washoff from plants. In Opus, this portion is kept separate from interactions between runoff water and soil

pesticides, for simplicity. An additional complexity for pesticides enters when kinetic adsorption dynamics is assumed. For that reason, the equilibrium distribution used in equations [121] and [122] cannot be treated. An estimate is first made of the average concentration of the dissolved and adsorbed amounts of each pesticide in the upper layer during the runoff time. A weighted average is used. The weighting is proportional to the ratio of infiltrated water to the water content of the first layer. More infiltrated water will more heavily weight the concentrations at the end of the runoff event. Then the pesticide is assumed to interact with the runoff water, using a surface active fraction as above, and assuming a reduced equilibration mass fraction based on the kinetic adsorption rate factor (ν) and length of rainfall (t), as follows:

$$f_b = \exp[t(.01-\nu)] \qquad [123]$$

The factor f_b is multiplied by the surface interactive fraction (f_z) to obtain the equivalent amount of soil from which the adsorbed pesticide will equilibrate with the runoff water. For the equilibrium option, f_b is 1. The total pesticide from the soil available for runoff interaction (M_{pt}) is then

$$M_{pt} = f_z[M_{ps} + f_b C_a M(1)] \qquad [124]$$

where

M_{ps} is the mass of pesticide in soil solution in the upper layer (1), and

C_a is adsorbed concentration of pesticide.

Writing an equation for this amount equilibrated with the total runoff water depth Q (mm), and solving for the concentration of runoff dissolved pesticide (C_{ro}), we obtain

$$C_{ro} = M_{pt}/[1/c_h + f_z f_b M(1) K_d] \qquad [125]$$

in which c_h is the conversion factor defined below equation [37]. The amount of pesticide dissolved in runoff in kg/ha is this concentration times Q divided by the conversion factor c_h. The concentration on sediment (C_{pm}) results from surface soil that has released pesticide into runoff, according to fraction f_b, plus transported particles with adsorbed material, as follows:

$$C_{pm} = K_d C_{ro} f_b + (1 - f_b) C_a \qquad [126]$$

where C_a refers to effective surface-soil-adsorbed concentration during the runoff event, as discussed above. This concentration is then multiplied by the enrichment ratio and the sediment mass to obtain the estimated amount of pesticide of each species that leaves the catchment on sediment. The amounts adsorbed and dissolved in surface soil are then adjusted for this loss by mass balance.

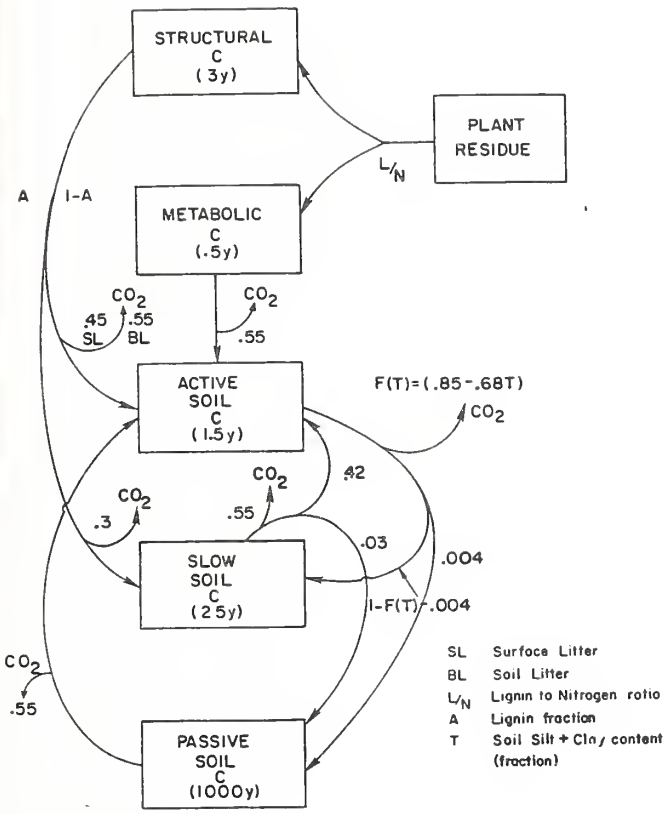

Figure 28.
Diagram for the century model of the organic carbon cycle (used in Opus) and the flow of carbon between the various pools. (Reproduced with permission from Parton et al. 1988b.)

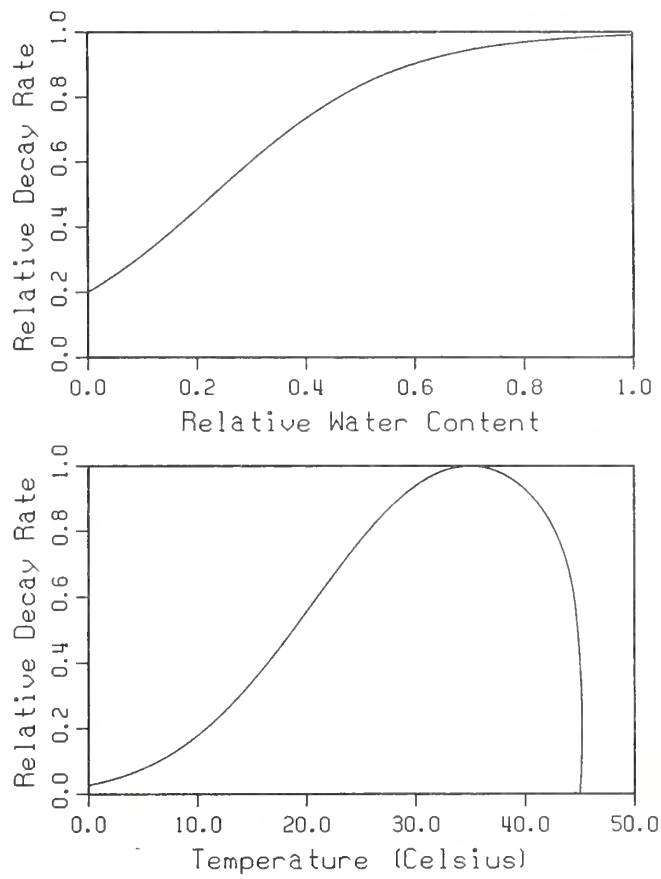

Figure 29.
Relative effect of soil moisture (top) and soil temperature (bottom) on microbial decay process for the Century model for soil carbon and nutrient cycles.

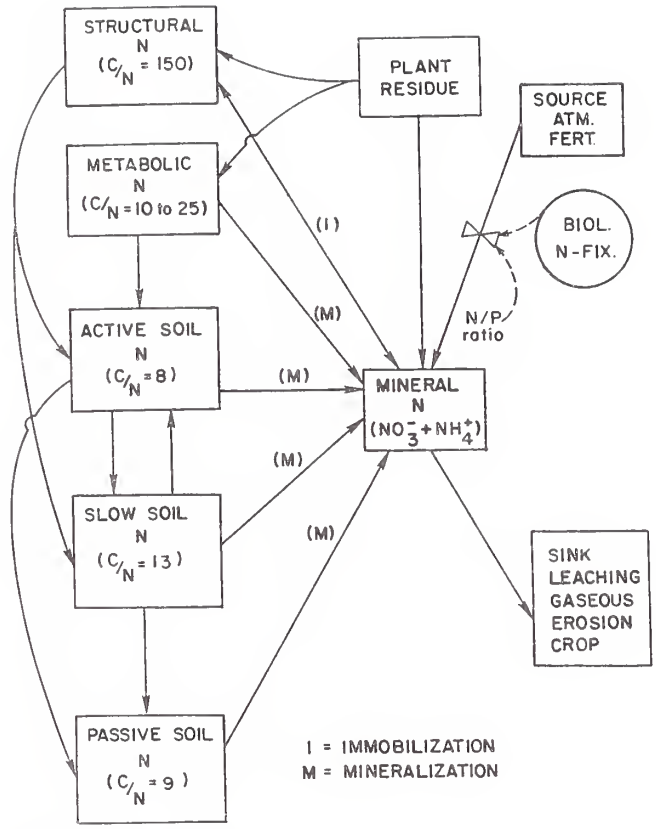

Figure 30.
Diagram for the Century model for organic nitrogen cycle and the flow paths for exchange of N between pools. (Modified from Parton et al. 1988b.)

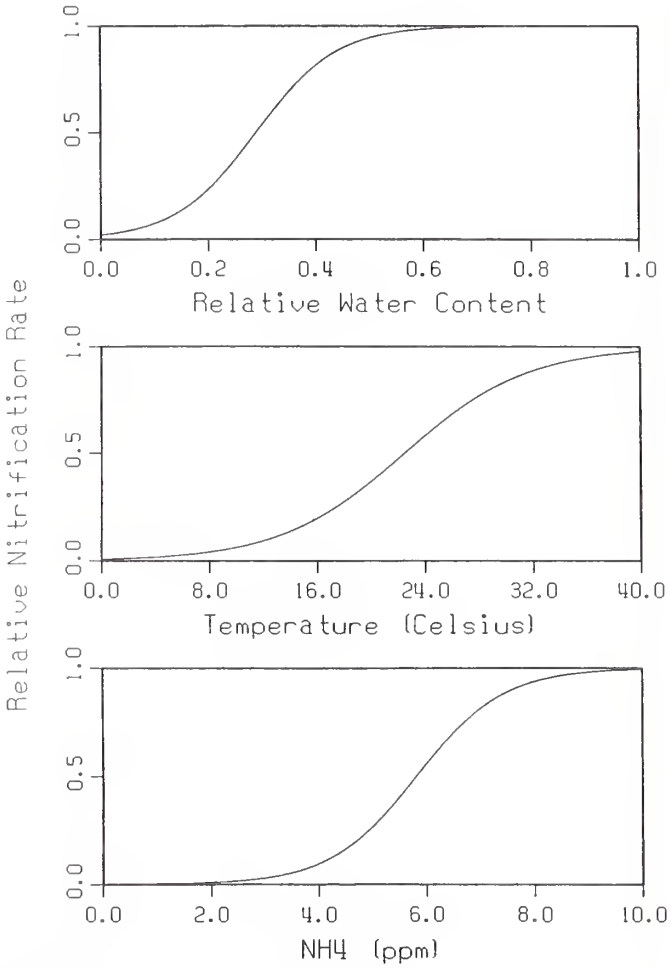

Figure 31.
Functions for the effects of the soil water content (upper), soil temperature (middle), and soil ammonia (lower) on relative rates of nitrification.

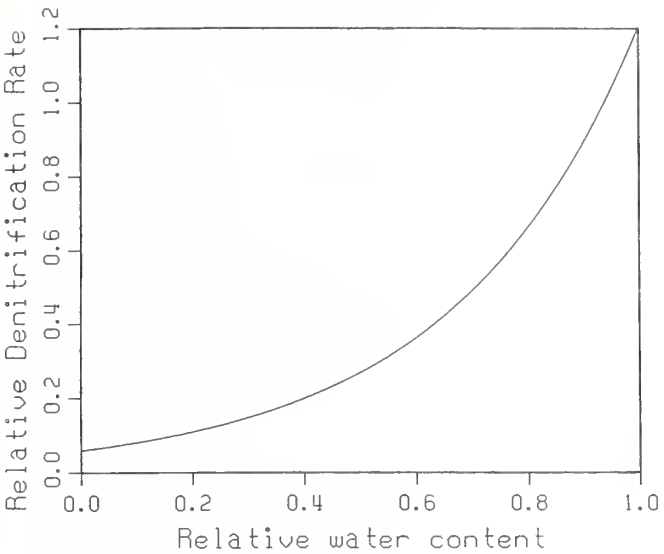

Figure 32.
Relative effect of water content on rate of denitrification in the Century model for nitrogen cycling.

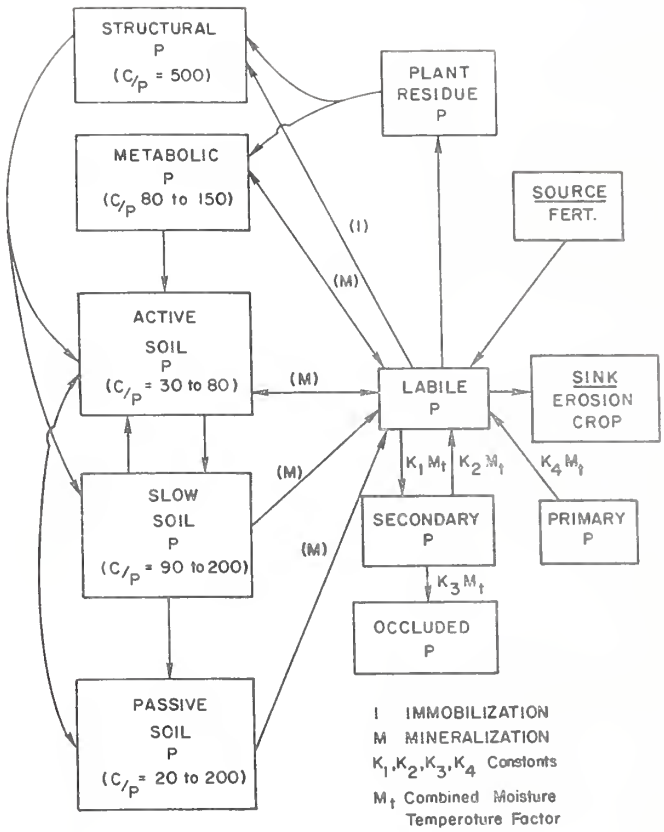

Figure 33.
Diagram for flows between various pools in the Century model for phosphorus in Opus. (Reproduced with permission from Parton et al. 1988b.)

7. SIMULATION OF PLANT GROWTH

Opus uses a mechanistic plant model to simulate the growth of plants or crops in response to four major factors related to plant development: radiation, nutrients, temperature, and water availability. The model may be used for either annual or perennial crops, and it responds to grazing, harvest, and stresses in a relatively realistic manner. It is distantly related to the plant-growth model in the EPIC model (Williams et al. 1984), and many of the Opus concepts were inspired by early versions of the EPIC plant model (Williams, personal communication).

Growth Model

In general, the plant model can be expressed as a relation between various factors and the incremental production of plant material (Δpm) in a time period (Δt), as follows:

$$\Delta pm = c_e \, f_e \, f_a \, f_m \, \tau \, R_i \, \Delta t \qquad [127]$$

in which

c_e = photosynthetic conversion coefficient for production of plant material from radiant energy (kg/ha/langley),

f_e = factor (0 to 1) for energy-conversion efficiency,

f_a = factor (0 to 1) for plant age,

f_m = factor (0 to 1) for plant size,

τ = stress factor (0 to 1), considering water, nutrients, and temperature stresses,

R_i = daily radiation (langleys),

Δt = time increment (days).

The value c_e is a time-invariant, crop-related parameter, with the conversion efficiency varying over a limited range from plant to plant. The values f_a and f_m are functions that auto-regulate the plant growth; they are illustrated in figure 34. The value f_a slows the plant growth as degree-day age approaches maturity, and f_m slows the plant growth as maximum genetic size is approached. These functions are mechanistic rather than experimentally determined, but they produce a plant response that imitates observed plant behavior.

Self-Dependent Growth

The value f_e reflects change over time in the plant's ability to intercept radiation and photosynthesize new material as the leaf area increases toward that at leaf maturity. Growth

depends on the amount of radiation that can be intercepted by the leaves and thus on the amount of leaf area. The relation of leaf-area index (F_L) to leaf mass is discussed below. Because of shading and the variable nature of maximum F_L (referred to here as F_{LM}), the relation of F_e to $F_L \backslash F_{LM}$ is direct at small values of F_L, but is asymptotic to the upper limit of 1. The equation, illustrated in figure 35, is

$$f_e = 1 - \exp(-3F_L/F_{LM} - v_e - c_i) \qquad [128]$$

In perennial plants and some multiple-harvest plants (such as alfalfa), root mass can be large relative to aboveground mass, and stored energy can be used to produce leaves and plant material. This is modeled here by a factor v_e (defined below), which boosts growth efficiency above that limited by the leaf area. The factor c_i acts similarly to represent the initial production of leaves from seeds. This factor shrinks to zero as the plant grows. It is mathematically necessary to initiate seedling growth. In mathematical terms, equation [127] is in simplest form a linear differential equation at small values of pm (or F_L), and cannot exhibit growth for pm = 0, without a value for c_i. Equation [128] reduces to $f_e = F_L + v_e + c_i$ at small values of F_L.

As leaf-area index increases, growth rate can increase, expressing a self-dependent growth rate. The parameter on the curves in figure 35 indicates the simulated effect of excess root/leaf ratio. The value v_e is the ratio of mass of roots to mass of leaves in <u>excess</u> of that called for by a normal root/leaf ratio. Positive values of v_e can occur under hay or alfalfa harvest or grazing. This ratio also expresses an early spring start for perennials with an established root system, compared with plants starting from seed. A value of $v_e = 0$ indicates normal root/leaf ratio for annuals.

Growth-Limiting Stresses

The stress factor (τ) is the minimum of individually considered stress-coefficient approximations for water, temperature, and nutrients. It is 1.0 for no stress and 0 for complete cessation of plant growth. The lower the value of this factor, the greater the stress the plant is experiencing in that time period. The time period for growth computation is typically 1 day.

Water Stress

The water stress factor (τ_w) is 1 for net contents of root-zone water down to 20 percent greater than 15-bar water content (θ_{15}), and declines linearly between that point and θ_{15}, as follows:

$$\begin{aligned} \tau_w &= 1.0 && ; \quad \theta > 1.2\theta_{15} \\ \tau_w &= (\theta - \theta_{15})/(0.2\theta_{15}) && ; \quad \theta_{15} < \theta < 1.2\theta_{15} \\ \tau_w &= 0. && ; \quad \theta < \theta_{15} \end{aligned} \qquad [129]$$

Nutrient Uptake and Stress

The nutrient stress factor (τ_N) is a function of the ratio of actual to potential use of plant nitrogen. Phosphorous stress is not simulated. Plants maintain a given N/P ratio, which is used in the residue-decay model (ch. 6). Potential use of plant nitrogen is obtained from information on the N content of the plant at various growth sizes, as illustrated in figure 36. Plants typically contain more N at emergence than at maturity. The relation of fractional N content to relative size [n(d)] can be expressed as a three-parameter function, based on N contents at emergence and maturity, plus a shape factor, as follows:

$$n(d) = n_m + (n_o - n_m)\exp(-c_d d) \qquad [130]$$

in which

- d is dimensionless plant size expressed as ratio of dry matter or plant material (pm) to potential maximum plant material (ppm), = pm/ppm
- n_o is content of plant nitrogen at emergence,
- n_m is a parameter set so that n(d) equals mature N content for d = 1, and
- c_d is a coefficient controlling decay rate of the function.

This allows estimation of the potential content of plant N at any point. If root-zone soil N is insufficient to meet the daily N demand thus estimated, the N stress factor (τ_N) is calculated as

$$\tau_N = 2\,\frac{\text{actual N use}}{\text{potential N use}} - 1 \qquad [131]$$

It is assumed that plant roots are able to selectively garner nitrogen from soil water if the N demand by the plant exceeds that amount present in the daily water uptake. Plant use cannot exceed the nitrate and ammonia in the soil water ambient to the roots.

Temperature Stress

The plant-temperature stress factor (τ_T) is a dimensionless function of the daily mean air temperature (T), the minimum growth temperature (T_b), and the optimum growth temperature (T_{op}) (illustrated in fig. 37). Several types of curve functions are candidates to represent observed plant-temperature responses, and plants naturally differ somewhat. The τ_T function used in Opus may not exactly represent every type of plant. The normalized temperature (T_*) used in figure 37 is defined on the abscissa.

Allocation of Plant Material

Plant material produced by the model thus described is divided among leaf/stalk, root, and fruit/seed material according to the plant's relative age and size. A general division function is presently used for all plants, and is illustrated in figure 38. Relative root/leaf ratio is a function of relative mass (lower scale), and relative seed or fruit production is a function of relative age in degree-days (upper scale).

The plant material in leaves and roots must be interpreted to estimate leaf area (or F_L) and rooting depth to complete the plant description. The relation between the mass of plant material in leaves/stems (pm_{lv}) and the leaf area index (F_L) is assumed to follow a nonlinear function as follows:

$$F_L = F_{LM} \sin[\pi/2 \; pm_{lv}/ppm_{lv}] \qquad [132]$$

in which

F_{LM} is maximum potential leaf-area index for the plant type, and

ppm_{lv} is maximum potential leaf/stem dry matter for the plant type.

The plant material allocated to root mass (pm_r) results in a gradual increase in depth of root penetration into the soil (Z_r) up to a maximum potential root depth (Z_{pr}), as follows:

$$Z_r = 10 + (Z_{pr}-10)\{1-\exp[-2(\exp[1.5pm_r/ppm_r]-1)]\} \qquad [133]$$

in which ppm_r is potential maximum root mass for the plant. This function includes the allowance for planting of the seed for annual crops at least 10 mm deep.

Interaction of Plant Growth Factors

If the leaf-intercept area were directly proportional to plant dry matter and if the age and senescence factor are ignored, equation [127] would be a linear differential equation. Growth could not initiate without the presence of c_i, which may be thought of as representing the ability of the plant to produce leaves from seed material. As described above, the plant material produced is divided between root and nonroot (leaf+stem, and fruit) material. If we assume for the moment that factors f_a, f_m, and R_i are constants, and that f_e is proportional to F_L plus the value c_i (as is true at small F_L), the equations [132] and [133] can be combined and simplified to illustrate the underlying basic growth-rate function as

$$\frac{dM_*}{dt} = B[\sin(M_*) + b] \qquad [134]$$

in which (recalling that pm is plant material and ppm is potential maximum plant material)

M_* is $\pi/2(pm/ppm)$,
B is $\pi/2(Y/ppm)$,
b is c_i/Y, and
Y is $f_a f_m R_i c_e$.

The solution of equation [134] has the form

$$t = \frac{1}{B\ v} \ln \frac{b \tan(m*/2) + 1-v}{b \tan(m_*/2) + 1+v} \cdot \frac{1+v}{1-v} \qquad [135]$$

in which

$$v = \sqrt{1-b^2}$$

Although equation [135] includes assumptions neglecting senescence factors, it can help obtain an index of the optimum time to maturity for a set of plant parameters, by solving for t when M_* reaches its peak of $\pi/2$. Notice that although the solution is scaled, the time is inversely proportional to B and is thus proportional to ppm. This is reasonable because a fixed amount of radiant energy is available, which causes larger plants to reach maturity at later dates than small ones, all other factors being equal.

Senescence

After maturity, failing a harvest operation that removes the plant, active leaves will turn to "standing dry matter" at a rate specified as a parameter by the user. Roots of annual plants are converted to soil residue when active leaf area falls to zero. For perennial plants, roots are assumed to recycle and regenerate 10 percent of their mass over winter.

No doubt this figure actually varies widely with plant type and climate.

In summary, the major parameters needed by this model to describe a plant include the following:

(a) seasonal lifetime in degree-days to onset of senescence,

(b) age at emergence in degree-days (measured from planting for annuals or from January 1 for perennials),

(c) potential production of total plant material for unstressed condition (τ=1),

(d) N content with growth stage (three parameters),

(e) potential weight of fruit/seeds at maturity,

(f) maximum depth of rooting, and

(g) conversion efficiency of photosynthetic energy.

Discussion

Like some other parts of the Opus model, the plant model is well behaved (or bounded in its response to inputs) but also difficult to exhaustively test because of the paucity of data on the growth response of plants to known amounts of stress. Few data exist for other than a few crops for the simultaneous values of plant mass, leaf area, water content, and nitrogen available in the root zone. Typically, experimental objectives are limited to only a few of these factors. The model described above has been compared with various types of plant data from several climates around the continental United States, and parameters are given in the User Manual (vol. II). That tabulation should guide the user in estimating values for related crops and climate zones.

Example of Plant Growth Simulation

Figure 39 illustrates the plant-model simulation of a hypothetical corn crop, with only temperature stress imposed. The combined action of the factors f_e, f_m, and f_a is manifest in

the shape and timing of the growth pattern that results. The same corn-parameter set produces significantly less when the stresses of limited water and nutrients are included, as illustrated in figure 40. This particular year, 1973, was a relatively dry one. Application of the plant model to a multiple-harvest-grass field crop is illustrated in figure 41.

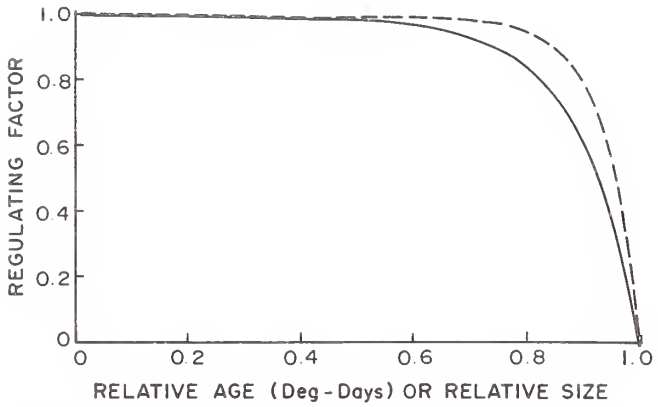

Figure 34.
The relative growth factors f_a and f_m, representing relative aging and relative size used in the mechanistic plant model.

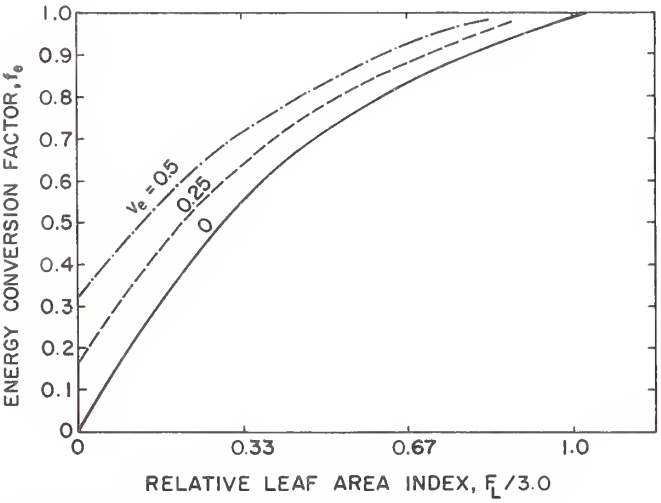

Figure 35.
Illustration of equation [128]. As leaf area index increases, the relative ability of the plant to intercept radiation and produce new plant material increases at a decreasing rate, with an upper limit of 1. For perennial plants or cropped grasses, energy stored in roots can effectively increase this rate; V_e is relative proportion of roots to aboveground material in excess of normal ratio.

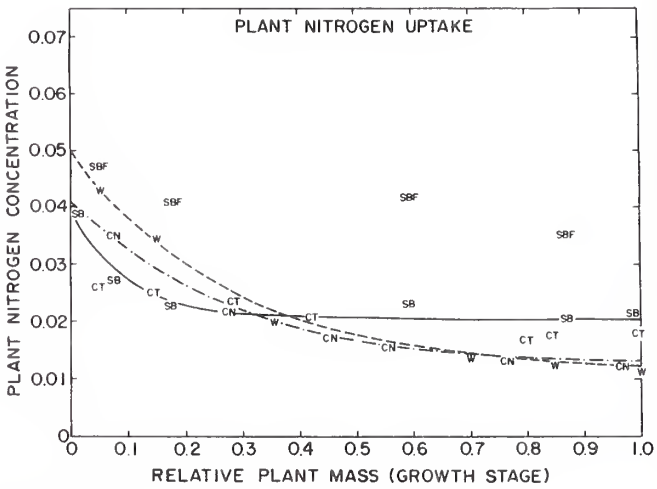

Figure 36.
Concentration of plant nitrogen as a function of relative size or growth stage for several common crops. Symbols are from published data: W = wheat (Boatwright and Haas 1961), CN = corn (Hanaway 1962), SB = soybeans (Hanaway and Weber 1971), SBF = fertilized soybeans (Hanaway and Weber 1971), CT = cotton (Bassett et al.1970).

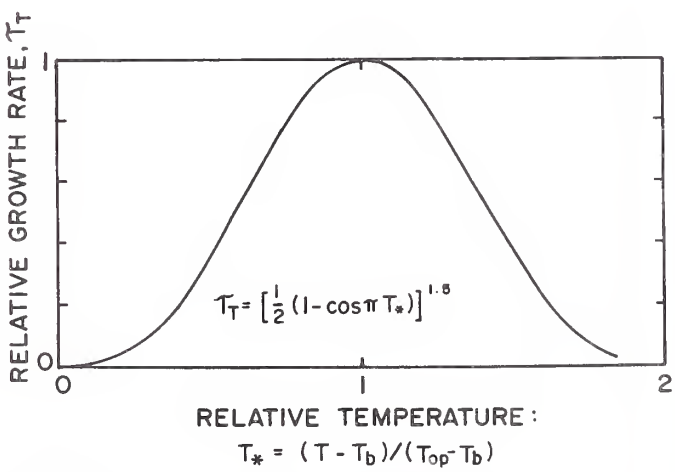

Figure 37.
Relative effect of temperature on growth rate of plants, based on a scaled or relative temperature. T_b is lowest and T_{op} is optimum temperature for plant growth.

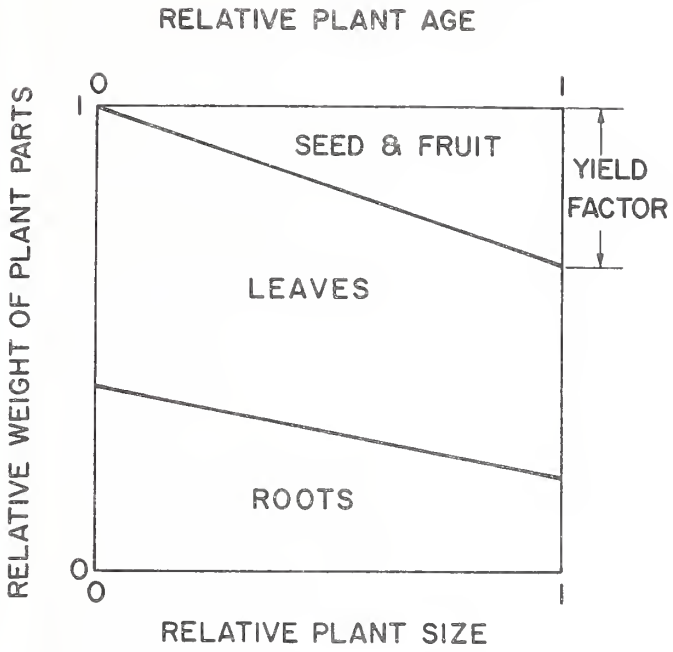

Figure 38.
Division of plant material by the plant growth model in Opus. Plant material produced by the plant is divided between leaves, roots, and fruit according to the relative size of the plant or the relative age of the plant (upper scale) in the case of fruit.

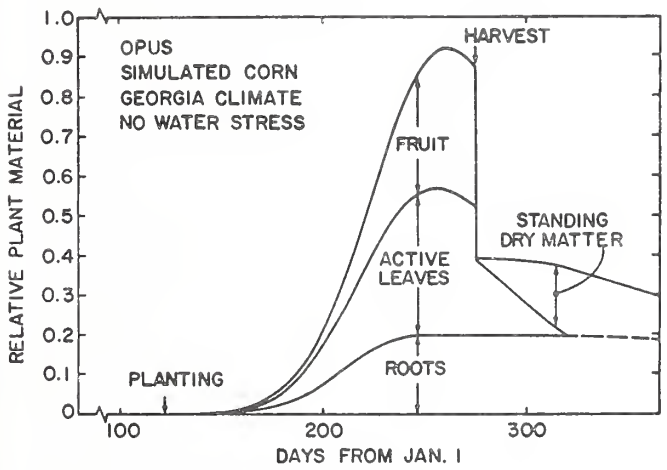

Figure 39.
Plant model simulation of ideal growth (no stress) of a corn crop in Georgia.

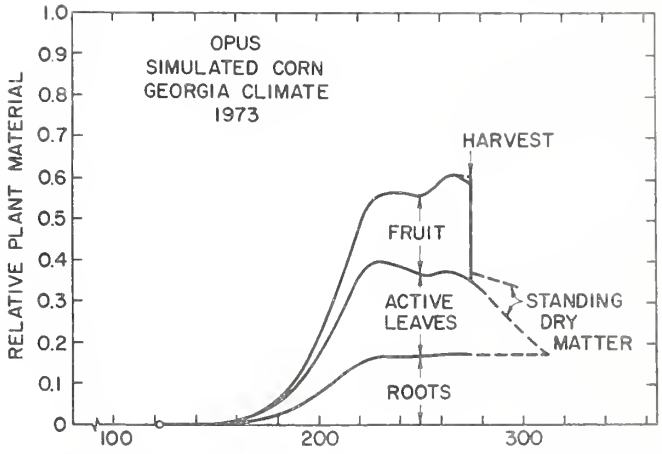

Figure 40.
The same simulation as in figure 39 except that water stress was included, reducing growth and yield.

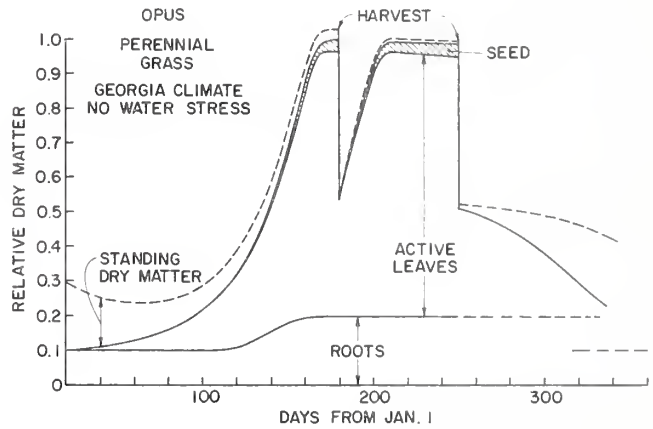

Figure 41.
Example Opus plant model simulation of the growth of a multiply harvested grass crop. This figure illustrates the rapid regrowth feature where root resources are available.

8. SPECIFYING MANAGEMENT OPERATIONS

Several major options for the use and treatment of land are specified as part of the field description, discussed in chapter 2. These include the direction of tillage and the use of terracing, an impoundment, and/or various grass buffer strips. Other management operations, especially those with specific dates of application, are discussed below. Management is assumed to occur on a multiyear rotation basis.

Management operations are specified by a list of operations and their characteristics plus a schedule of operation amounts and target dates. The list describes the major physical changes that each operation effects in the condition of the field or crop. The schedule specifies the date on which that operation should occur and any variable amounts involved. Each year in the rotation cycle has a schedule, and the rotation period can include as many as 5 years.

Lists of Choices

Opus allows users to choose from among crops to grow, tillage procedures to use, and pesticides and animal wastes to apply. Certain characteristics of members of these four lists are specified and remain fixed, independent of when the farming operations involving the choices are implemented.

List of Crops

The set of parameters representing a crop or plant (as given in ch. 7 in connection with the plant model) are listed for each plant species that is grown during the management rotation period. For a perennial, a mix of perennials, or an unmanaged catchment, the rotation period is 1 year, and the plant characteristics are listed for the major plants or plant families found on the catchment. A maximum of four plant species may be treated simultaneously. When an annual is planted, the parameters in this list are used by the plant model to simulate its growth. The crop parameters list includes specification of a type for each plant. The plant types are annual, harvested perennial, grazed perennial, and annual meadow or no-till. This type controls how the plant model operates and how instructions for planting and harvesting or grazing are interpreted. These features are more fully explained in the User's Manual (vol. II).

List of Tillage Operations

Mechanical operations in the field are classed into four types, numbered as follows:

(1) Planting: A plant seed or seedling is placed in the ground at a specified depth, during which some mixing of the soil may

occur. A row spacing is specified, which may not be changed until harvest. Plant degree-day "timers" (ch. 7) are started on the planting day.

(2) Cultivation: The field soil is disturbed with a specified mixing efficiency to a specified "plow" depth. Plant material standing at the time is assumed to be unaffected. Row spacing is unchanged, but furrow depths may be changed. Any shape changes from past erosion or deposition are eliminated. These characteristics distinguish cultivation from plowing operations. Mixing includes all soil constituents down to the given "plow" depth.

(3) Harvesting: A specified proportion of the plant is removed, including at least the seed/fruit portion existing at harvest time. The soil is not mixed, and row spacing and furrow depth are not affected. A special code allows harvesting of the plant plus roots for root crops. For grazed crops, this operation specifies time interval (days) and rate of removal of leaf and stem material by animal grazing.

(4) Plowing: Characteristics for plowing operations are similar to those for cultivation except that live or dead standing plant material, surface litter, and plants now growing are also mixed into the soil to a given depth with a given efficiency. Row spacing may be changed arbitrarily.

Data for operation types 1 and 3 must include naming a crop from the crop list. If harvest-operation type is specified for a date with a crop that has been designated a grazed perennial, then it is assumed that a period of grazing is started on that day and extends a specified number of days with a specified grazing rate.

Mixing that accompanies management types 1, 2, and 4 causes major changes in the soil material. Soil bulk density is returned to a minimum value. A mixing-efficiency parameter determines the degree of mixing, so that soil-water content and all dissolved and adsorbed materials (nitrate, labile phosphate, pesticides, and residue material) will be mixed to the specified efficiency. It is assumed that the plowing does not extend significantly beyond the 200-mm depth of microbial activity and that nutrient-model pools are not altered. It is also assumed that plow depth does not exceed the depth at the upper soil horizon: Opus cannot predict the results of mixing two different soil types.

List of Pesticides

The characteristics of all pesticides to be used during the rotation period are specified in a list. This includes natural-decay-rate constant, solubility, adsorption coefficient (K_{oc}), relative washability of the portion reaching plant leaves, and Arrhenius constant if known (equation [117]).

List of Animal Wastes

Each manure that is applied during a rotation cycle is described in a parameter list. The list gives data on percent organic matter, total N content, ammonia N, and phosphorus. A list, including nine common animal wastes, is incorporated as default data in the program. The user may change any of these or add a tenth, specifying the material's content of organic matter, ammonia, phosphorus, and nitrate. Inorganic fertilizers are more simple; they are specified by their content of nitrate, ammonia, and phosphorus. The amounts of each used are given in the operations schedule, discussed below.

Schedule of Operations

The lists described above are for fixed characteristics of the management operations that may be repeated by several similar operations. Variable aspects, if any, of those operations and their dates are given in the operations schedule. There are separate schedules for tillage operations, fertilizations, pesticide applications, and irrigation. A different schedule is read for each year of the rotation period, and these operations are repeated in the same sequence for the number of rotations required by the simulation interval.

The schedules needed include the following:

(a) Tillages are specified by number from the tillage operations list above and by date of implementation.

(b) Fertilizations are specified by date plus the rate of application of each of N, P, and ammonia (in lb/acre or kg/ha). In addition, if animal wastes are the fertilizer applied, the number from the above list is given and the type of application is specified, including depth of incorporation or injection if used.

(c) Pesticides are applied by specifying the pesticide number and a date, a code for method of application, and an application rate (in kg/ha or lb/acre).

(d) Irrigation schedules include specification of the type and amount of water applied and the method used.

Three types of irrigation may be simulated, as follows: (a) Sprinkling on demand according to soil water in the root zone; (b) furrow irrigation on demand based on a soil-water state; and (c) ditch supply irrigation for a specified period of the year, where water is available on a rotating calendrical basis and with data given on total annual supply. Furrow irrigations are routed along the furrow from a field edge as described in chapter 5. For sprinkler irrigations, it is assumed for simplicity that all applied water infiltrates into the soil. A wetted profile is created and subsequently redistributed just as for water entering the profile from a rainfall.

Each fertilization can apply any or all of N, P, and NH_4 in the same application. Fertilization and cultivation or plowing, or any other mixture of management operations can occur on the same date. However, each schedule must list operations in chronological order.

Chemigation is another optional type of fertilization in which fertilizers or pesticides are applied with irrigation water. For this operation, the date of application of the fertilizer or pesticide must coincide with that of the irrigation, and the application must be properly coded as a chemigation method. Detailed instructions for specifying various management operations is given in the User's Manual (vol. II).

Testing, Verification, and Validation

Testing is commonly understood to be the evaluation of the ability of a model to reproduce the measured characteristics of the performance of an experimental prototype. Given the complexity and interactivity of the processes covered by the Opus model, it is important to understand not only that no data sets are available to allow truly comprehensive testing, but also that it is next to impossible to know or measure enough of what is happening in even a small agricultural field, compared with what the model can simulate. Even with a simple model of a relatively isolated process, the data needed for rigorous testing should include all the degrees of freedom of the model variables and input conditions. Seldom are they available. The technical literature abounds with models of all types that have been developed with appeal to generality, but are applied to rather restricted or idealized conditions.

The realistic appreciation of testing of a model such as Opus requires a common understanding of the meaning of "testing," its purposes, and its limitations. First, testing of a model should be done only in full understanding of the model's intended use(s). When the Opus model is used without calibration to reflect the relative effects of alternative management practices, it is improper to evaluate it on the basis of the accuracy of its uncalibrated reproduction of a given set of data, or to compare its results with the calibrated results of a different model.

There are two general types of testing in the language of models: verification and validation. Verification refers to the process by which it is ascertained that the model is performing as designed--that its response is mathematically equal to the equations on which it has been constructed. This is "debugging." For a large complex model such as Opus, debugging is a process of diminishing returns, and is rarely actually "completed" in an economic time frame. Many years have been spent in the verification of Opus code.

Validation involves comparison of the performance of the model to that of a prototype. This aspect is the most difficult, because it is usually limited by the paucity (in extent and intensity) of useful data.

An important point to remember in testing any model of a natural system is the masking effect of natural variability on the accuracy of reproduction of measured data. A perfect model of some process at a point on the field may be a very approximate model for the combined action of a field made up of an assembly of points, each having properties that differ slightly from those of its neighbor. With greater amounts of such spatial variability, the underlying point model may be overwhelmed by the variation, if an attempt is made to identify it by the measured performance of the field as a whole. This does not, of itself, negate the value of the physically valid (point)

model, because (a) the physical model is usually not so masked for every input case, and (b) the problem indicated is not with the model but with the complexity of the conditions. This example represents many phenomena such as leaching, infiltration, evapotranspiration, and surface erosion.

The above points are important to remember when evaluating the role of testing in the determination of the acceptability of a model. It is just as important to (a) understand the relative merits of the process components within their disciplines and also the testing that each has already undergone, and (b) appreciate the structure of the interactions that make up the basis of the model as a whole.

Tests of Component Processes

In looking at a model such as Opus, validation is most appropriately applied on a component-by-component basis. In this regard, one should be careful to fairly apply similar standards of acceptability to all components. It is not sensible to expect a high degree of accuracy in simulating the measured distribution of sediment-particle sizes, for example, when the whole basis for the runoff phenomena is a time and spatially lumped method, which commonly exhibits large variance in prediction of daily amounts. Interactive effects must also be kept in mind in validation efforts. For example, a discrepancy that may be observed between the simulated and measured runoffs, in applying the model, may be due to errors not in the traditional hydrologic components (such as infiltration and runoff routing) but in the simulation of the evapotranspiration that controls the initial conditions.

The components making up Opus each represent a considerable amount of research, including validation of their response to the appropriate input effects, and it is unnecessary to ask that such validation be reapplied for their use in the combined model. It is proper to look carefully at how the various components interact, in light of what we think we know about how the water cycle works on a small field. It is also proper to compare each component with any alternate models in each respective discipline (that work with the same level of input information), and to ask if that component can be improved. In many cases, increasing the expected accuracy involves an increase in sophistication, which in turn requires more detailed input information and longer computational effort. This tradeoff has been considered in all the components of Opus and should be kept in mind when model testing is considered.

Daily Weather Model

As indicated in chapter 3, the WGEN weather model used in Opus was extensively tested elsewhere (Richardson 1981). In addition, several simulation runs of 50 years with various combina-

tions of options were performed, and statistics were compiled to verify that the model was reproducing the specified statistics.

Evaporation from soil and plants is calculated by modifications of the method developed by Ritchie (1972). The modifications are minor and were suggested by Ritchie for EPIC (Williams et al. 1984). EPIC has been tested for row crops (Ritchie 1972, Ritchie et al. 1976) and for grassland conditions (Ritchie et al. 1976, Pochop et al. 1985). In addition, the Opus ET model was applied to sites across the United States where pan-evaporation data are available for investigating corrections that are applicable to account in the average for effects of wind and relative humidity (Opus User Manual, vol. II).

Rainfall/Runoff Models

Extensive tests of the performance of the daily hydrology model were presented in the documentation to CREAMS (Smith and Williams 1980). As expected, because the parameter (the curve number) that characterizes runoff represents lumped results, the performance of this method is often quite adequate for the longer term although not very good on a day-to-day basis.

The erosion method accompanying the Curve Number runoff method, the MUSLE model, was tested extensively elsewhere (Williams 1982). Like the Curve Number method, it should properly be judged on a longer term basis; in those applications it has shown quite reasonable results.

A simpler version of the breakpoint simulation of small-catchment hydrology was tested for use in CREAMS (Smith and Williams 1980). The model in Opus makes several conceptual improvements over the CREAMS model without sacrificing any of the basic methodology on which these test results are based. Further tests of the analytic/kinematic infiltration/runoff model were reported by Rovey et al. (1977) and Smith (1976, 1981a). The model for surface crusting effects used in Opus was partly developed on the results of tests reported by Chevalier (1984).

Soil Water Flow

Over the last 30 years or more, soil physicists such as White et al. (1979) and Gilham et al. (1979) have shown that Richards' equation properly describes the one-dimensional vertical movement of soil water, as long as the general conditions are appropriate. More rigorous treatment is required for some conditions, such as when the escape of air is severely restricted. Further testing of this equation for use in Opus should not be necessary. The most common variation of measured

data from theory is the existence of spatial variation in soil hydraulic properties, rather than the inadequacy of the theory or assumptions involved in Richards' equation. Studies of the effect of spatial variability (Bresler and Dagan 1983) indicate that model results that ignore spatial variability will show much less apparent dispersion in soil-water content than is found in spatially variable soil. This bias should not be a serious detriment, especially considering the expense of data collection and the computational complexity necessary to treat spatial variability in the numerical simulation. Results of some testing of the Separable Flux method of solution of Richards' equation are presented in chapter 4. Although the increase in allowable time step is a consequence of the increase in layer size used, less apparent bias is introduced than for more conventional or linearized solutions when layer sizes are increased.

Transport of Solutes

Almost all reported soil-water-transport data from laboratory experiments deal with saturated flow and include diffusion processes. Few data are available for unsaturated flow from intermittent flows such as those obtained in the field. A field data set that allows limited testing comes from work done in Watkinsville, GA (Smith et al. 1978). This EPA report on the study describes the catchment and management operations in detail. An example of Opus' simulation of these data is presented in the followng pages.

Opus Demonstration Example

A relatively extensive set of test data covering a 3-year period (referred to above) is provided by a study of a set of small-field-sized watersheds near Watkinsville, GA. This study was carried out by the Agricultural Research Service between 1973 and 1975, and forms the basis of a technical report published by the Environmental Protection Agency (Smith et al. 1978).

The unique value of these data is the scope of measurements made during this period, including rainfall; runoff; sediment production; soil-water profiles; pesticide and nutrient distributions in soils; and presentation of a complete schedule of tillage operations, chemical applications, and resulting crop yields for these fields. The experimental watershed chosen for this example is called P-3, and a topographic map for this field is shown in figure 42. The field was planted with soybeans each of the 3 years of the study, with a winter cover crop of barley or rye. At least one application of two pesticides and one application of fertilizers was used each

year. A drawback of this data set is the apparent lack of consistency in the source of raingage data for the period of the other measurements (Smith et al. 1978). Raingages were replaced or data were substituted due to mechanical failure during the experimental period. This substitution seems to be reflected in the simulation results shown below.

Description of Topography

Figure 43 shows the equivalent furrowed and unfurrowed topography used in Opus to represent this simple catchment. The estimated mean slope length along furrows and estimated length of concentrated flow path were preserved, along with total field area. The topographic map also provided a means to estimate the slope profile along the mean furrow flow path when furrows control the direction of runoff (which is most of the time) as well as when furrow control is absent.

The measurements of outlet runoff were made with an H-flume in the center of an artificial dike, which forms a pond. The geometry of the pond was taken from height of the flume and slope of the land at the outlet. The pond-outflow rating is the flume rating, taken from handbooks (USDA SEA 1979).

Description of Soil Horizon

The various soils mapped on this field are similar in characteristics, and data to hydraulically describe them were found from the EPA report (Smith et al. 1978) and an ARS soil survey (Holtan et al. 1968). When particular information was unavailable, the default options within Opus were used. No extensive fitting or optimization was attempted.

The EPA report described the watershed soils as being composed of Cecil sandy loam and sandy clay loam, and reported sand/silt/clay fractions for surface samples at seven locations over the catchment (Smith et al. 1978, table A3, p. 173). From this information, an estimated representative profile was constructed for use in Opus (shown in table 1). The upper and lower horizons are sandier than the middle two, which have noticeably higher clay contents. Thus, a slightly restrictive layer occurs at about 6 inches.

Management Actions

The schedule of tillage, planting, harvesting, pesticide application, and fertilizer application is reported in appendix B of the EPA study and is summarized here in table 2. The schedule was translated directly into data instructions in Opus, and a 3-year simulation was performed.

Simulation of Runoff

Table 3 summarizes the amounts of runoff and sediment produced by the major runoff-producing storms during the 3-year period for which data were taken. Like all experimental data, there are included some points of quite doubtful validity, such as the occurrence of almost 7 cm of rain without reported runoff, and the reported runoff of almost 6 cm from another 7-cm storm. Nevertheless, comparisons can be made of the comparative prediction of daily and breakpoint models within Opus.

Table 3 contains only those events with either a predicted or a measured amount of runoff. Many storms are omitted in which both values are 0. Thus the sample is truncated because it excludes correct predictions in this limiting if not trivial case. Often the prediction of no runoff from storms is not trivial but requires the ability to use the fact that the rain intensity was very low. Indeed, this table shows many cases in which the Curve Number method predicts runoff when there was none, and the breakpoint infiltration model correctly predicts none because of low-intensity rain.

A very crude statistical comparison of results can be performed using regression analysis on these event-runoff data. Table 4 presents some of the results obtained by this means. This table shows how differently each year's simulation performed and also compares the overall period results.

If one merely plots storm (or daily) runoff as a function of rainfall, it is clear that a formula such as the Curve Number, even considering initial soil conditions, cannot explain the variation in the relation. Indeed, the computed Curve Numbers for the storms on this catchment, based on reported runoff, ranged from 44 to 96. Another measure of this is the r^2 for comparison of predicted to measured runoff, using this runoff model. Keeping in mind that the Opus daily model uses an improved method to relate changes in runoff to soil wetness, r^2 between measured and CN-predicted runoff is nevertheless only 0.49. Comparative r^2 values for all years of breakpoint simulation are 0.61. Forcing the intercept to 0 decreased this r^2 to 0.54. On a yearly basis, the r^2 values go up to 0.77, 0.88, and 0.87 for the three successive years. Figure 44 shows the breakpoint-model prediction for total runoff as a function of total rainfall for this data set, compared with the reported data.

The breakpoint model simulates initial conditions and runoff hydrographs for all storms during a period when major disturbances affect the soil's capacity for intake. Opus had mixed success in comparison with reported measurements, and some of the simulations are shown in figures 45 through 53. As

expected, the simulation of runoff that was a very small percentage of total rainfall is the most difficult, and in general, the errors are largest in such cases. The differences between simulated and reported runoffs are believed to be largely due to either of two factors: quality of knowledge about the true state of the catchment, and quality of the rainfall-intensity data.

Figures 45 through 47 suggest some of the problems of the reported data: in these cases, apparent errors either in the reported runoff or in the reported rainfall. It is known from comments in the EPA report (Smith et al. 1978) that rainfall records were not continuously good, and often nearby gage data were borrowed to fill a record. Timing errors of a few minutes seem to explain the cases in figures 45 and 46. Many hydrographs were reported only with a few data points, such as in figure 45. Figure 46 suggests the loss of some of the recession data as well as timing inaccuracies. When the runoff increases several minutes after the beginning of a rainfall pulse, one can often argue that a delay has occurred in the system. This should be relatively consistent. However, when the runoff begins to decrease much earlier than the decrease in the rainfall rate, one cannot use the same argument. This seems to be the case in figure 47. Figure 48 shows an excellent simulation except for a somewhat clipped peak in the reported hydrograph, for which we do not speculate a cause. Figures 49 and 50 are common cases in which runoff comes after significant initial irregular rainfall that prewets the soil and is a severe test of the somewhat simplified soil physics in Opus. Nevertheless, the results are not severely in error because the runoff is only a small fraction of the rain input. More typical and successful simulations are shown in figures 51 and 52.

One or two events such as illustrated in figure 53 suggest that the storage properties for the catchment are larger than those used by the simulation. Either other processes are occurring or the surface hydraulic roughness is much larger. Overall, there appears to be no consistent bias, and the simulation is generally good. The small but significant differences between years in statistical quality of the simulation and also the apparent seasonal change in hydrologic response (some of which is accounted for by the crust model) suggest that the watershed is very much a changing creature and that the attempt to continuously simulate the hydrology remains a formidable challenge. In this respect, Opus is none too complex.

Production of Sediment

With some exceptions, the results in table 3 show that most of the time, relatively accurate simulation of runoff was accompanied by similar accuracy in simulation of sediment production.

The one major exception is the storms on May 28, 1973. Given the usual uncertainty and error in simulating a storm's sediment production, the relative success over such a range of storms is reassuring and adds to our confidence in the model's utility for transport-simulation applications.

Distribution of Soil Water

The EPA report (Smith et al. 1978) includes reports of soil water averaged for depth increments and sampled at irregular intervals from July 1972 to October 1974. The Opus model output includes the option to report soil-water contents by computational layer for a specified interval, and comparisons can be made for the dates of reported data.

In this Opus application, soil-input parameters were largely estimated by the default option described in chapter 2, and the only fitted parameter was the hydraulic conductivity of the surface horizon. In light of this, the predicted soil-water contents were an excellent fit to the reported data, as exemplified in figures 54 to 57. The only significant bias appears to be in the porosity for the third horizon, where simulated water contents are generally too high. Selecting a lower θ_s for that horizon could easily improve this simulation. Indeed, the use of Opus with a long sequence of observed water contents could be one way to infer the general shape of the moisture-release curves of each horizon. One uncertainty in the comparison is the actual time of soil sampling on days when a rainfall occurred. This is illustrated in figure 55, where soil-water distributions before and after a storm are shown. The relatively good fit at near-surface depths is also an indication of relatively good estimation of amounts and distributions of surface evaporation and root transpiration of water.

Movement of Pesticides

The same EPA report (Smith et al. 1978) presents sample concentrations, at various depths during the study period, of three pesticides applied at spring planting (see table 2). Opus was used to study our ability to simulate the measured concentration distributions, assuming representative quality of the sample reports. Both the equilibrium and kinetic absorption models were used, and a limited variation in kinetic rate and interactive depth parameters were tried.

The three pesticides were trifluralin, paraquat, and diphenamid. Paraquat is very highly adsorbed and moves only slightly with water. The other pesticides are more mobile and are a better test of the model's ability to mimic actual soil transport. Table 5 lists the important pesticide parameters used for the results shown in the following figures.

The EPA data (Smith et al. 1978) are apparently based on one or a few samples, although the sampling is not discussed. As expected, this results in considerable sample variation, as the data show. Pesticide concentrations in soil are reported for 1 or 2 years of the 3 years of hydrologic data, so a limited basis for comparison exists. This limitation, coupled with the year-to-year variation in measured data (such as apparent decay rates), diminishes the rigor of the tests.

In this test of Opus we did not specify detailed vertical distribution of pesticide initial concentrations. Thus the initial concentrations before first application (June 1973) are not precise because the simulation starts in April and some mixing occurs, but the total amounts are small in any case. The situation after application is much better, but some small limitations of the model are apparent. Opus (or any other model) is not able to accurately predict the nonuniform redistribution of pesticides at a particular spot in the field after a cultivation event. The mixing is not uniform either in space or with depth, as Opus assumes. Neither is Opus able to separately treat the surface degradation of pesticides, as distinguished from root-zone degradation as a whole. Thus Opus' results are handicapped in predicting very precisely the surface concentrations, which are crucial to predicting runoff concentrations. Moreover, although Opus can predict the concentration of mobile material in the surface (10 mm) due to soil evaporation, it appears that Opus is not able to accurately predict the higher surface values because of the extreme gradients near the surface. Opus simulates the total amount in the top 10 mm, but probably much more occurs in the top millimeter than in the tenth millimeter. Thus, Opus is expected to underpredict some amounts carried off in sediment.

Figure 58 compares simulated and reported concentration profiles of diphenamid at 14, 25, and 87 days after application. The kinetic adsorption model was used. The largest error is related to the initial overestimate of pesticide in the upper 100 mm. The loss with time over this season is well simulated. Of course, not all measured data were simulated well. Figure 59 shows an anomalous period of 10 days in which the measured amount of diphenamid at the surface fell far below that simulated, reversing a previous steady trend. Other anomalies are indicated in table 6, which compares amounts of pesticides in runoff (both dissolved and attached to sediment) to reported amounts, for the sampled storms during the period of measurement. An expected sampling variability is involved in the reported data here, because only a few samples were taken during the runoff and because concentrations will be time variable. In almost all cases, a lower value of runoff pesticide is associated with a lower value of sediment-associated pesticide. But diphenamid on July 27, 1974, shows much higher sediment pesticide with lower runoff pesticides.

Also, on June 11, 1975, the reported soil concentrations are much lower than those simulated, but the reported sediment concentrations of diphenamid are high. Nevertheless, the results are generally good in simulating the general amounts of pesticides in the runoff and sediment several months after application. In most cases, simulation of the amount of paraquat in sediment was as good as the prediction of sediment mass.

In general, the kinetic model simulated the persistence of pesticides at the surface better than did the equilibrium adsorption model. The difference is typified by figure 60. The difference was not large, which may indicate that these two mobile pesticides are rapidly desorbed and adsorbed.

The equilibrium and kinetic adsorption models give very similar results for paraquat because this pesticide is so highly bound to the soil. In this example the kinetic model is usually more accurate in predicting the amount of pesticide on sediment. Measured data for dissolved amounts of the two more mobile pesticides give mixed results in comparisons of the equilibrium and kinetic models. Neither model is consistently superior in simulation.

Figure 61 shows samples of Opus' simulation of paraquat distribution in the surface soil during 1973 and 1974 in comparison to reported measurements. The results from June 21, 1974, illustrate the apparent persistence of paraquat at the surface compared to the simulated persistence. A small error in simulating the actual mixing efficiency for such a persistent, immobile pesticide can make all the difference in the simulated amount at the surface. The manipulation of mixing efficiencies could easily match the measured amount, but this is not the point of our testing here.

A notable difference was observed between the rate of decay of diphenamid during the growing season and the rate that occurred over winter. This change could not be simulated by Opus, even taking into account the response to water contents and temperature as presented in chapter 6. The difference at the beginning of the growing season in the second year was notable in relative terms but negligible compared to the amount applied. Furthermore, a striking difference was seen in the rate of decay for the growing season of 1973 and the rate for 1974, which remains outside the scope of Opus to simulate. This is because the difference cannot be explained in terms of the processes on which Opus' simulation is based. Although this may result in a bias in the simulated amount of pesticide after several months, the error is quite small compared to the amount applied.

Most storms showed steady consistency for bias in surface amounts and bias in runoff amounts. This consistency somewhat validates the lumped estimation of the interaction of surface water and soil water during storms. As the results indicate, although sampling at larger depths may have been limited, no data indicated that the convective transport model in Opus did not reasonably simulate the transport of pesticides with moving water in this soil.

Summary

Conclusions that are general to the performance of Opus cannot be drawn from one test example, but some observations may be made. Because Opus cannot simulate the spatial distribution of soil properties and because the actual daily temperature or radiation data for this period were not available, expectations about the accuracy of simulation of any storm event should be limited. The crop was simulated rather well in terms of reported yield. Predicted runoff correlated rather well with measured values, most hydrographs were well simulated, and predicted soil moisture matched the reported measurements quite well. The general movement of pesticides with soil water and with surface water and sediment was reasonably well simulated. The accuracy was limited as much by our ability to model the complex pesticide-degradation processes and by sampling uncertainty, as by the model of the movement mechanisms.

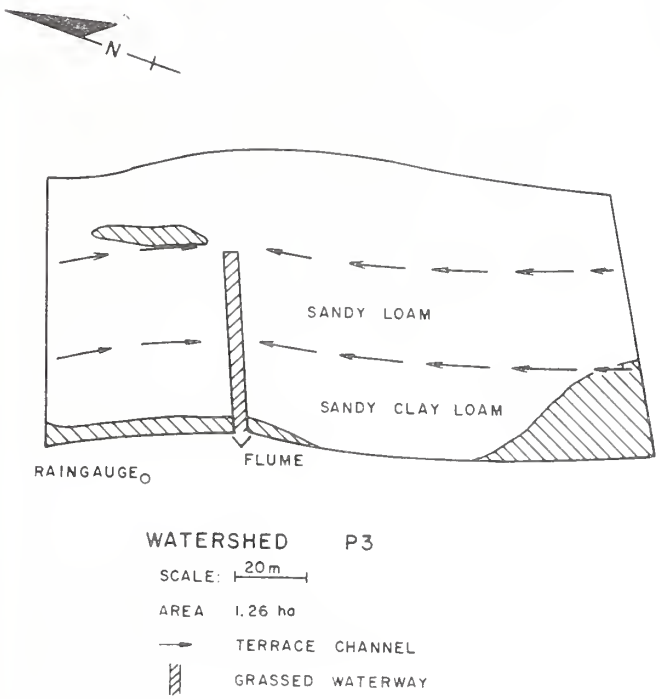

Figure 42.
Plan of watershed P-3 in Watkinsville, GA, one of the set of watersheds reported in the EPA study of pesticide transport (Smith et al. 1978).

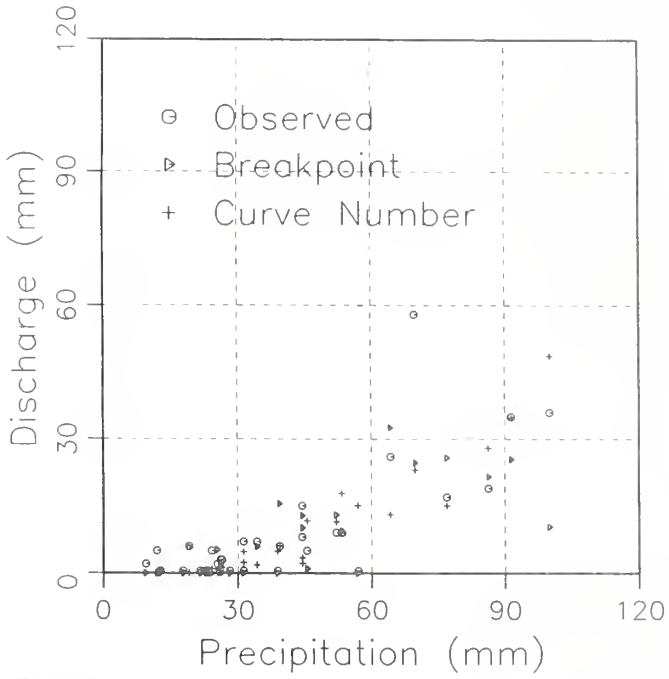

Figure 44.
Comparison of Opus simulation of runoff with reported data for watershed P-3. Only days with runoff are shown, covering the 3-year period of simulation.

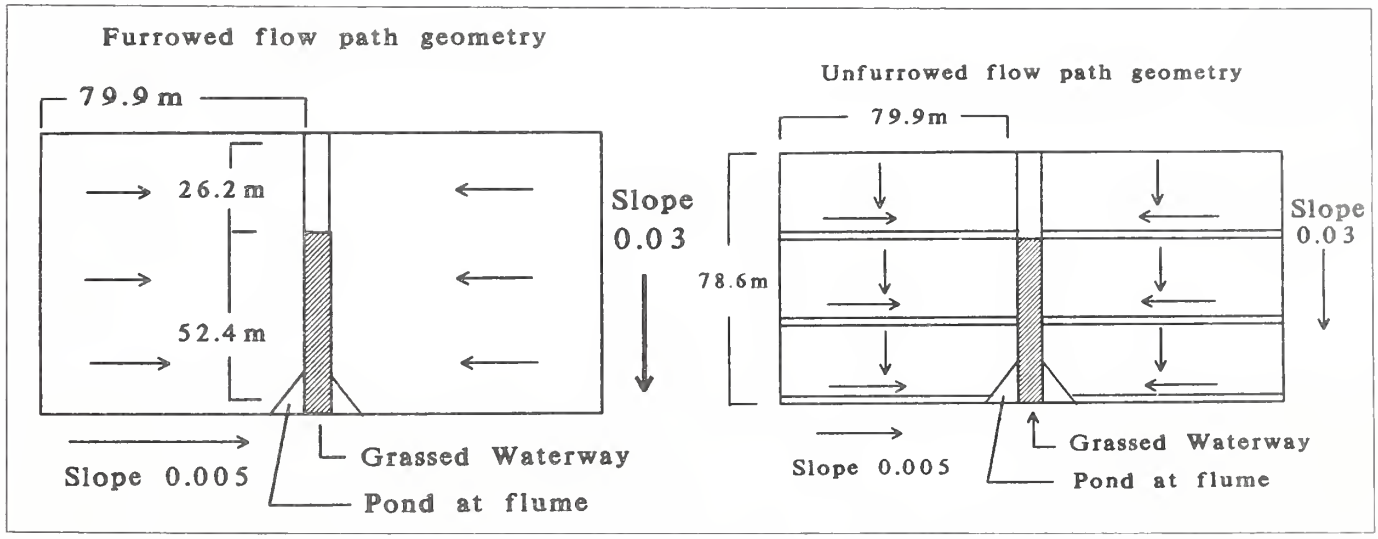

Figure 43.
Geometric representations of watershed P-3 used by Opus for test example.

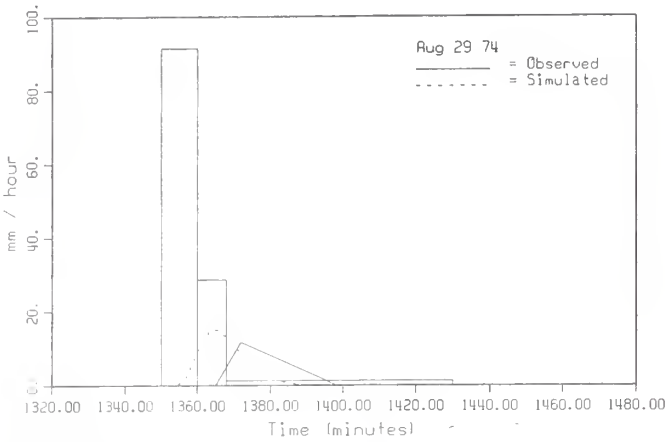

Figure 45.
Opus simulation of runoff event on August 29, 1974. From the rainfall pattern, a timing error is indicated, but the few recorded data points do not adequately define the hydrograph. Square blocks in this and subsequent graphs are recorded rainfall pulses.

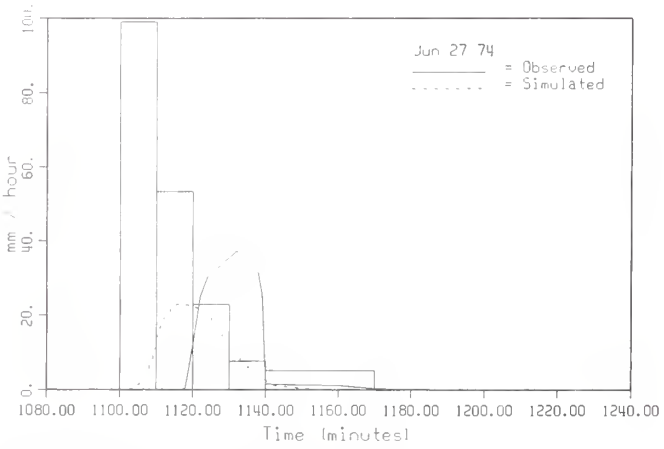

Figure 46.
Opus simulation of runoff from P-3 on June 27, 1974. A timing error is suggested, but the simulation is reasonable with this caveat. Graph of recorded data also points to an error on the recession; the rapid drop at time 1140 is otherwise inexplicable.

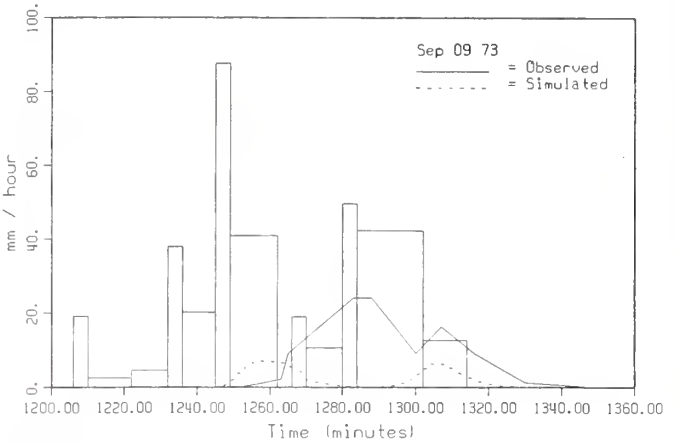

Figure 47.
Comparison of Opus simulation with reported data for the event of September 9, 1973. A problem in the data is indicated by the lack of correspondence between timing of rainfall and runoff increase (time 1260-1270 and 1300). Such data problems confound validation of any model.

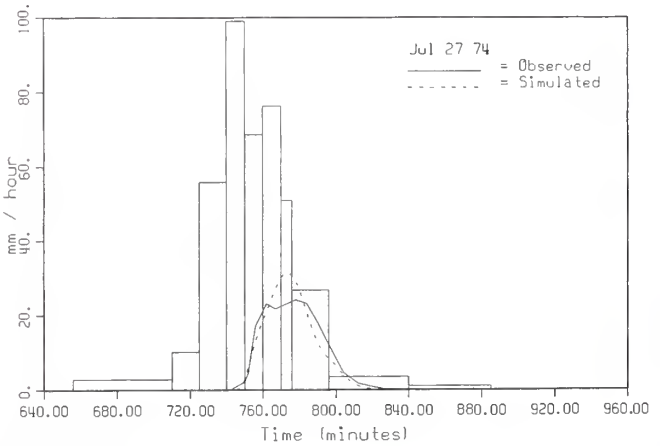

Figure 48.
Simulation and reported runoff on July 27, 1974. This case is curious in regard to reported data: the flattening of the hydrograph when rainfall is still high is suspect. Otherwise the fit is excellent.

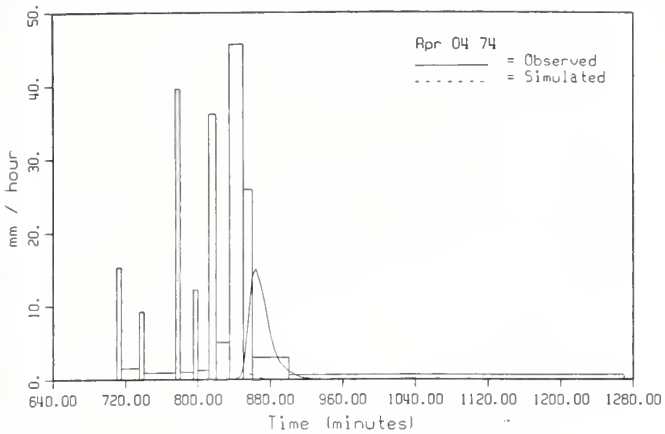

Figure 49.
A good example of the case where runoff is a tiny fraction of the rain, coming at the end of a long period of soil wetting. This is the most sensitive test of runoff simulation. Opus underestimates the reported amount, but this kind of error is not surprising.

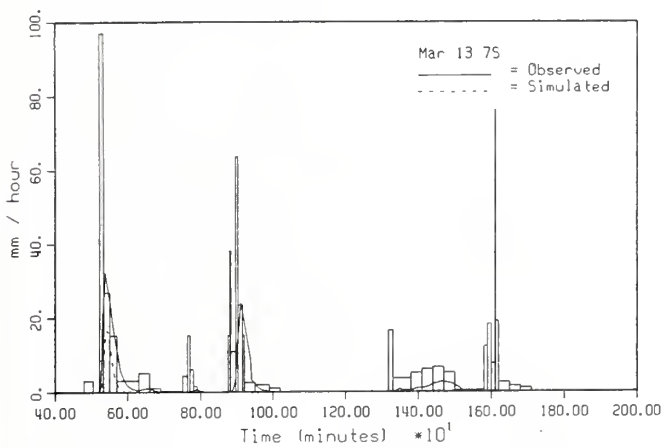

Figure 50.
Simulation of the storm of March 13, 1975, exemplifying sensitivity of prediction of soil redistribution during storm hiatuses. Here Opus methodology apparently does not accurately simulate sustained wetness of the surface, and fails to match the second (and following) small runoff.

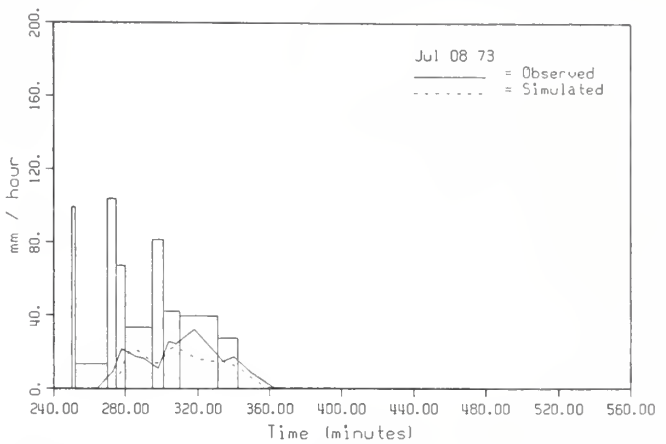

Figure 51.
Simulation of runoff event of July 8, 1973.

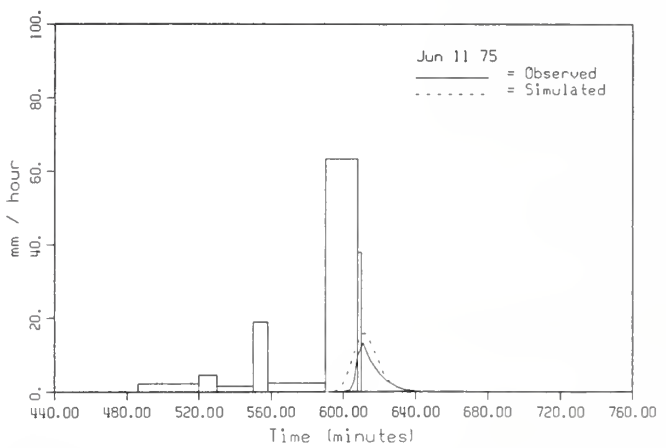

Figure 52.
Simulation of the storm runoff of July 11, 1975. Here again, runoff comes just at the end of the rainfall burst, emphasizing any simulation error. Opus' result is very close to reported values.

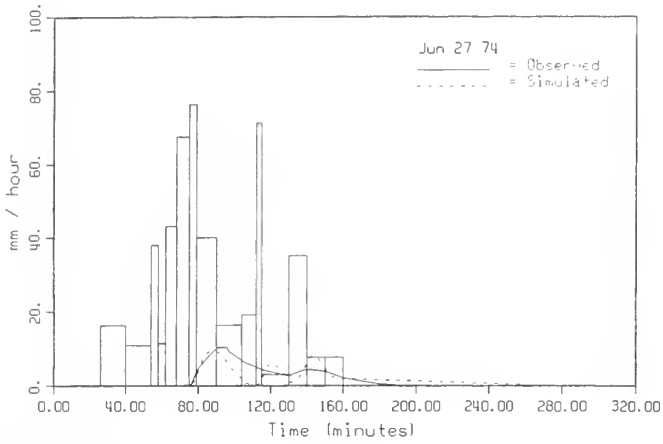

Figure 53.
Simulation of the first event of June 27, 1974. This simulation indicates much more damping or hydraulic roughness in the actual system than that simulated by Opus. This is the only such case in this test.

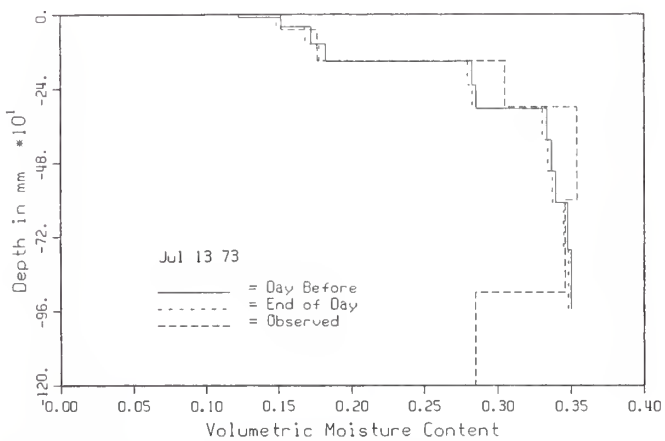

Figure 54.
Comparison of measured and simulated soil-water distribution for July 13, 1973. Comparison of day-before and end-of-day simulations indicates little movement during the day. Opus simulations extended to 96-cm depth, and maximum root zone was assumed to be about 60 cm.

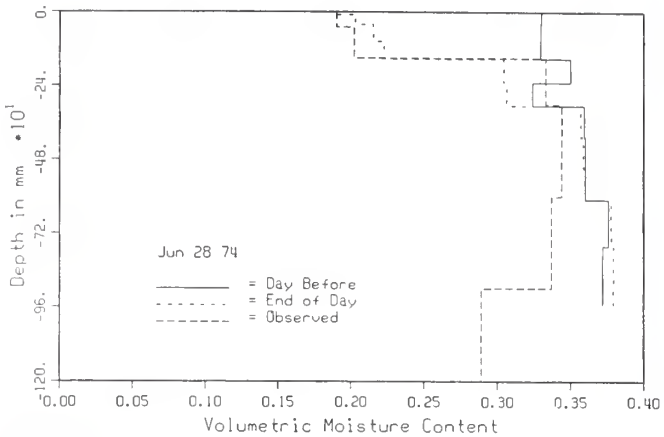

Figure 55.
Measured and simulated water contents for June 28, 1974. Day-before values indicate active surface drying during this day. Some bias in simulated values at intermediate depths is also indicated.

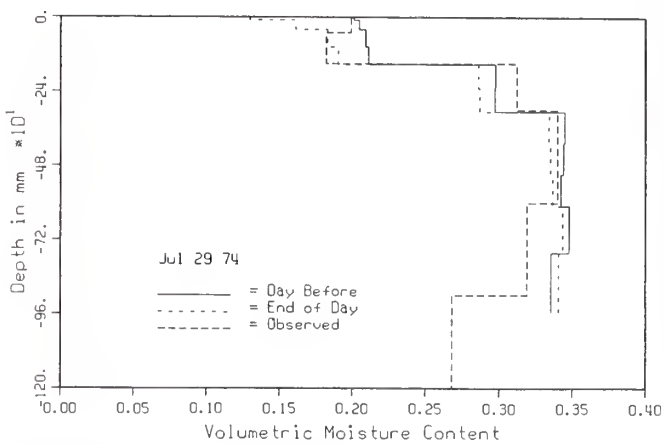

Figure 56.
Measured and simulated water contents for July 29, 1974. This is further into the growing season, and water contents are somewhat reduced in intermediate depths.

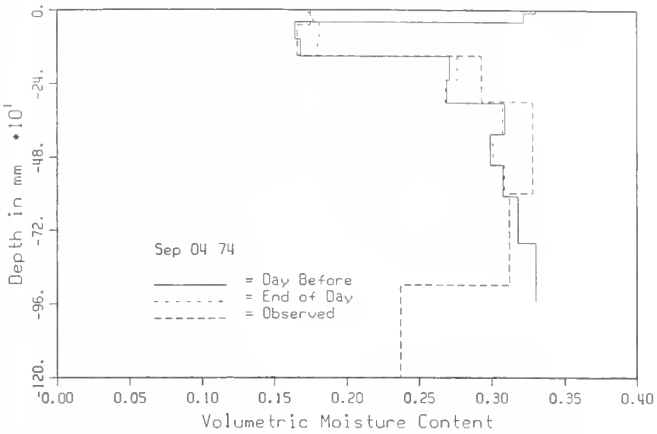

Figure 57.
Measured and simulated water content distributions for September 4, 1974. This is near end of growing season. Root zone is deeper and water content is somewhat reduced down to 70 cm, with active drying during the day at the surface.

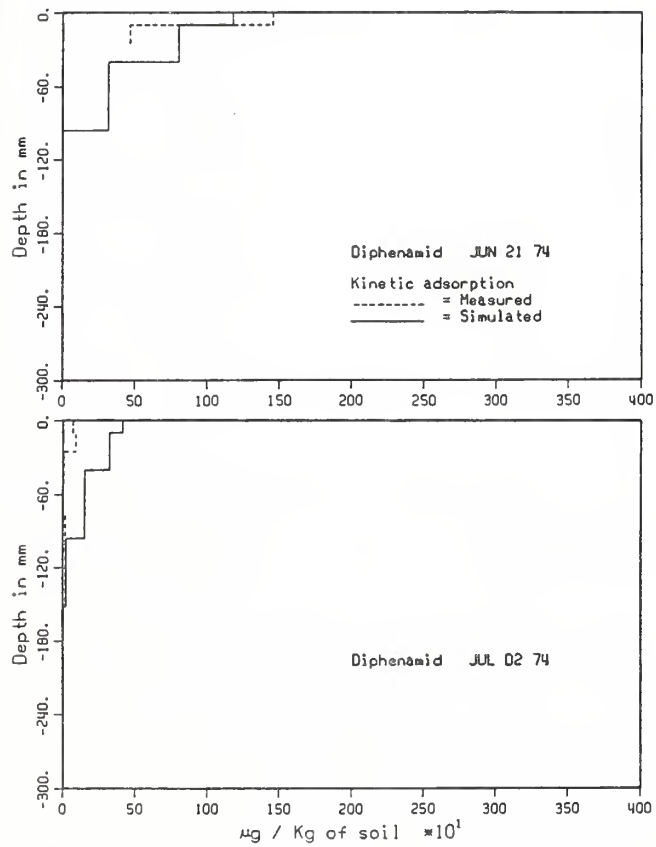

Figure 59.
Simulated and reported diphenamid concentrations over an 11-day interval in 1974.

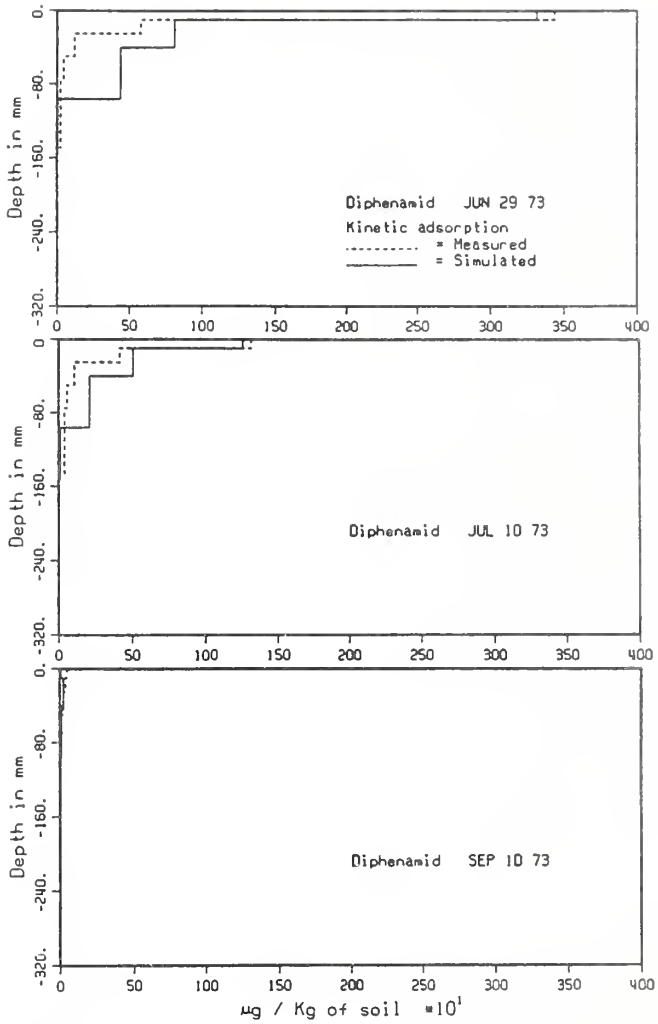

Figure 58.
Simulated and reported distributions of diphenamid concentrations at three sampling times during the 1973 growing season.

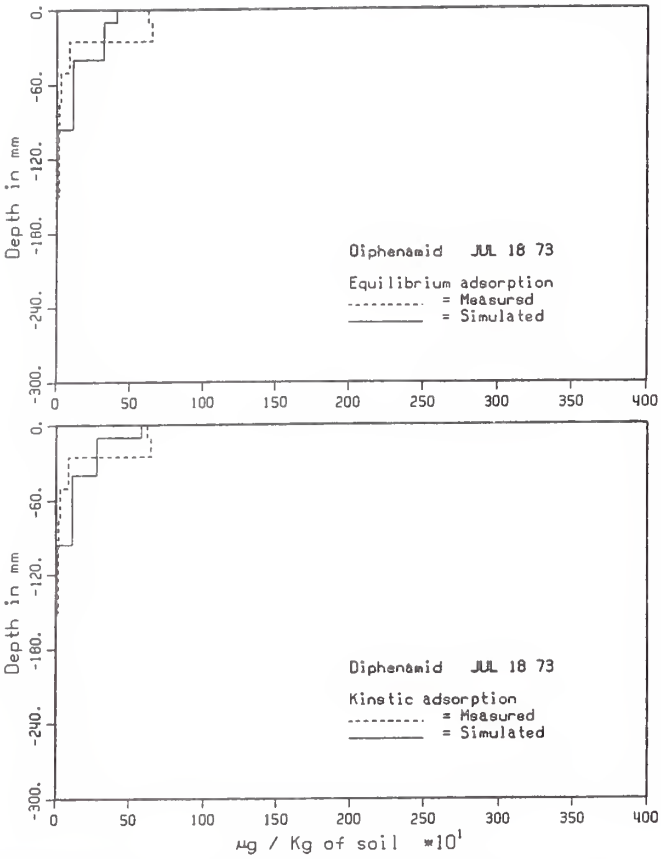

Figure 60.
Comparison of simulation differences for kinetic and equilibrium adsorption models on a typical day in 1973. Relatively rapid transfer rates were used in the kinematic model.

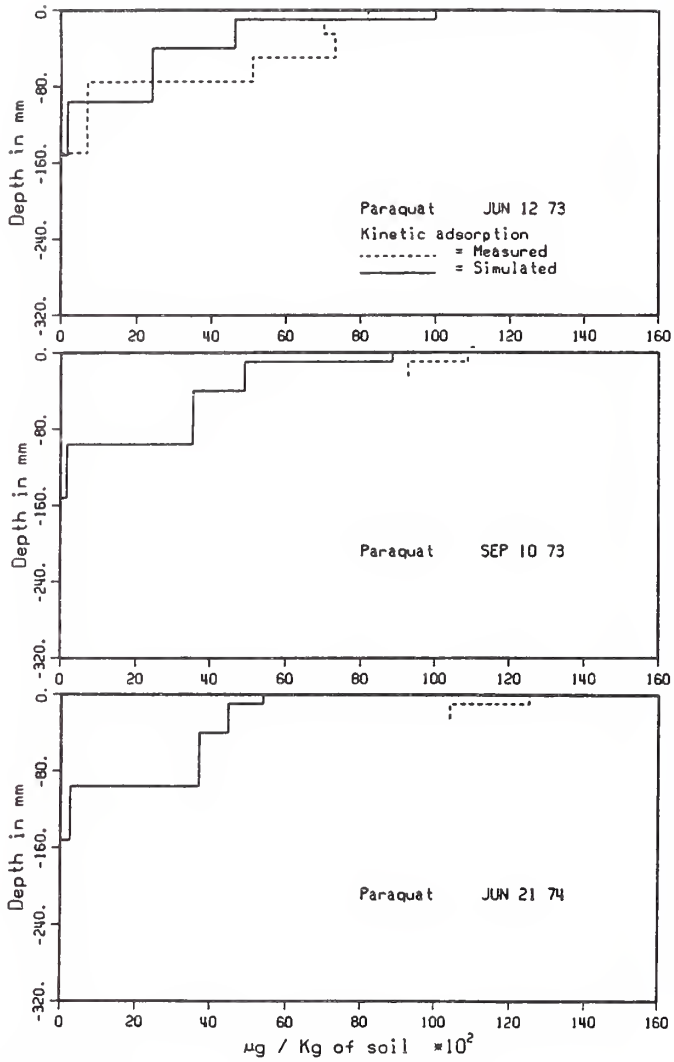

Figure 61.
Three examples of simulated and reported distributions of soil concentration of paraquat during the 1973 and 1974 growing seasons. Paraquat is strongly adsorbed and is thus relatively immobile.

Table 1.
Soil profile used for watershed P-3

Depth (mm)	Sand (%)	Silt (%)	Clay (%)	Saturated conductivity (mm/min)	θ_s	θ_r
0-152	64	19	17	0.212	0.32	0.08
152-305	49	14	37	0.169	0.35	0.20
305-610	46	16	38	0.132	0.40	0.24
610-1520	51	27	22	0.306	0.40	0.21

Table 2.
Management operations for watershed Watkinsville P-3, 1973-75

Management operation	Date	Depth (mm)	Efficiency (mixing)	Material/Plant	Amount applied (kg/ha)
Fertilizer	5/22/73			Ammonium nitrate-N	21
				Superphosphate-P	19
Disk harrow	5/5/73	102	0.5		
Fertilizer	6/4/73			Ammonium nitrate-N	25
				Superphosphate-P	22
Rolling Cultivator	6/4/73	51	0.7		
Pesticides	6/15/73	0		Trifluralin	1.12
		0		Paraquat	1.53
		0		Diphenamid	3.36
Planting	6/15/73	76	0.7	Soybeans	
	10/5/73	0	0.1	Winter rye	
Harvest	11/7/73			Soybeans	
Planting	1/14/74	51	0.1	Winter rye	
Harvest	5/1/74			Winter rye	
Fertilizer	5/22/74			Ammonium nitrate-N	17
				Superphosphate-P	15
Disk harrow	5/22/74	102	0.5		
Rolling Cultivator	5/28/74	51	0.7		
Pesticides	5/30/74	0		Trifluralin	1.12
		0		Paraquat	1.53
		0		Diphenamid	3.36
Planting	5/30/74	76	0.7	Soybeans	
Rolling Cultivator	6/13/74	51	0.7		
Rolling Cultivator	7/5/74	51	0.7		
Harvest	10/18/74			Soybeans	
Disk harrow	10/22/74	102	0.5		
Planting	10/22/74	51	0.3	Barley	
Harvest	4/15/75			Barley	
Fertilizer	5/8/75			Superphosphate-P	15
Disk harrow	5/13/75	102	0.5		
Pesticide	5/28/75	0		Trifluralin	1.12
		0		Paraquat	1.53
		0		Diphenamid	3.36
Planting	5/28/75	76	0.7	Soybeans	
Sweep	6/16/75	51	0.7		
	7/9/75	51	0.7		

Table 3.
Summary of amounts of runoff and sediment for Watkinsville watershed P-3, May 1973 to September 1975

Date (mm/dd/yy)	Storm rainfall (cm)	Measured runoff (cm)	Simulated breakpoint (cm)	Runoff CN (cm)	Measured sediment (kg)	Simulated sediment (kg)
5/23/73	2.21	0	0	0	10	0
5/28/73	4.83	1.6	1.5	1.77	1122	60
5/28/73	4.32	1.9	1.1	1.58	1618	30
6/6/73	3.94	0.6	1.4	0.44	405	410
6/7/73	2.21	0	0.05	0.09	0	20
6/9/73	1.19	0.5	0	0	728	0
7/8/73	6.43	2.6	2.4	1.21	1184	560
7/14/73	1.9	0.6	0.6	0	210	150
7/17/73	0.94	0.2	0	0	66	0
9/9/73	4.45	1.5	1.2	0.23	58	180
9/13/73	4.12	0.7	0.6	0.18	25	120
12/5/73	3.86	0	0.6	0.37	0	120
12/20/73	2.11	0.3	0.2	0.16	39	80
12/26/73	2.08	0	0	0.05	0	0
12/31/73	5.33	0.9	0.9	1.78	78	250
1/20/74	2.34	0	0	0.05	0	0
2/16/74	1.85	0	0	0.05	0	0
3/21/74	1.55	0	0	0	0	0
3/29/74	1.75	0	0	0.01	0	0
4/4/74	3.55	0.26	0.03	0.36	*0	50
4/13/74	2.54	0.2	0.5	0.09	42	170
5/23/74	6.88	0	0.75	1.63	0	30
6/27/74	5.33	0.8	0.9	1.59	196	240
6/27/74	3.3	1.1	1.2	0.99	557	450
7/24/74	1.17	0	0	0	0	0
7/27/74	7.7	1.7	2.5	1.53	537	490
8/16/74	4.45	0.8	1	0.32	227	250
8/29/74	2.03	0.2	0.5	0	42	150
9/1/74	1.27	0.05	0.04	0	16	20
11/30/74	3.56	0	0	0.24	0	0
12/15/74	3.12	0	0	0.20	0	0
12/19/74	2.16	0	0	0.05	0	0
1/10/75	2.59	0.05	0.01	0.08	22	10
1/12/75	3.12	0.7	0	0.44	75	0
2/16/75	2.62	0.1	0	0.41	3.5	0
2/18/75	4.54	0.5	1	1.03	47	20
2/24/75	2.41	0.5	0.001	0.08	97	10
3/13/75	10.01	3.6	1	3.23	258	250
3/14/75	2.54	0	0	0.28	0	0
3/15/75	3.73	0	0.45	0.82	0	1450
3/24/75	2.64	0.3	0.01	0.12	24	10
3/30/75	1.52	0	0	0	0	6
4/2/75	6.99	5.8	2.5	2.32	305	650
4/14/75	2.29	0	0	0.02	0	0
5/3/75	3.94	0	0.1	0.42	0	70
5/7/75	2.79	0	0.03	0.1	0	20
5/14/75	1.9	0	0	0	0	0
5/31/75	3.56	0	0.3	0.06	0	200
6/11/75	2.67	0.3	0.7	0.63	73	220
6/11/75	2.54	0.6	0.6	0.59	168	160
9/6/75	1.79	0	0	0	0	0
9/12/75	1.85	0	0.13	0	0	30
9/17/75	3.4	0	0.5	0.12	0	60
9/22/75	1.55	0	0.04	0	0	20
9/23/75	4.88	0.1	0	1.25	3.5	0

Table 4.
Regression analysis of simulated runoff

Model	Sample	Sim. = a+b*Meas. a (Intercept)	b (Slope)	R^2	Sim. = b*Meas. b Slope	R^2
Curve number	1973	0.064	0.605	0.49	0.646	0.49
	1974	0.198	0.799	0.43	0.964	0.37
	1975	0.256	0.488	0.69	0.554	0.6
	All	0.215	0.521	0.57	0.609	0.49
Break-point	1973	0.106	0.785	0.77	0.854	0.76
	1974	0.055	1.269	0.88	1.32	0.88
	1975	0.12	0.367	0.87	0.398	0.72
	All	0.195	0.503	0.61	0.582	0.54

Note: Sim. = simulated value,
Meas. = measured value.

Table 5.
Parameters for pesticides used at watershed P-3, Watkinsville, GA

Pesticide	Basic half-life (days)	K_{oc} (1) (liter/kg)	Solubility (mg/liter)	f_z (2)	Kinetic (3) rate factor, (liter/min)
Diphenamid	6.9	400	260	0.03	0.009
Paraquat	462.0	1.6E7	5.0E5	0.03	0.009
Trifluralin	17.3	600	1	0.03	0.009

(1) Carbon-dependent adsorption ratio. See ch. 4.
(2) Surface-water extraction ratio. See ch. 6.
(3) ν, defined for equation [36].

Table 6.
Summary of pesticides in runoff and sediment for major storms

Date	Pesticide	In runoff (g/ha): Reported	Kinetic	Equilib.	On sediment (g/ha): Reported	Kinetic	Equilib.
July 8/73	Diphenamid	16	3.4	5.1	0.75	0.93	0.15
	Paraquat	0	0.025	0.025	67	28	28
	Trifluralin	2.2	1.5	2.3	0.11	0.43	0.098
July 14/73	Diphenamid	2.5	1.5	2.7	0.094	0.067	0.1
	Paraquat	0	0.0043	0.0043	11	6.5	6.5
	Trifluralin	0.28	0.76	1.4	0.015	0.049	0.079
June 27/74	Diphenamid	3.4	1.5	2.8	0.23	0.17	0.11
	Paraquat	0	0.009	0.009	31	13.2	13.2
	Trifluralin	-	0.66	1.52	-	0.09	0.085
July 27/74	Diphenamid	0.0017	0.051	0.11	0.088	0.0027	0.00045
	Paraquat	0	0.009	0.0091	18	1.4	1.4
	Trifluralin	-	0.08	0.22	-	0.0044	0.0013
May 31/75	Diphenamid	-	4.0	9.9	-	2.0	1.7
	Paraquat	-	0.0016	0.0016	-	11	11
	Trifluralin	-	0.9	2.2	-	0.53	0.55
June 11/75	Diphenamid	1.1	3.2	7.2	0.062	0.5	0.46
	Paraquat	0	0.0061	0.0061	4.5	15.2	15.2
	Trifluralin	-	1.2	2.8	-	0.22	0.26

(-) indicates data not measured or reported.

LITERATURE CITED

Alonso, C.V. 1978. Selecting a formula to estimate sediment transport capacity in nonvegetated channels. Agricultural Research Service, An unpublished internal task progress report.

Alonso, C.V., W.H. Niebling, and G.R. Foster. 1981. Estimating sediment transport capacity in watershed modeling. Transactions of the American Society of Agricultural Engineers 24:1211-1220, 1226.

Bassett, D.M., W.D. Anderson, and C.H. Werkoven. 1970. Dry matter production and nutrient uptake in irrigated cotton (Gossypium hirsutum). Agronomy Journal 62:299-303.

Bennett, J.P. 1974. Concepts of mathematical modeling of sediment yield. Water Resources Research 10:485-592.

Boatwright, G.O., and H.J. Haas. 1961. Development and composition of spring wheat as influenced by nitrogen and phosphorus fertilization. Agronomy Journal 53:33-36.

Bouwer, H., and J. van Schilfgaarde. 1963. Simplified method of predicting fall of water table in drained land. Transactions of the American Society of Agricultural Engineers 6:288-291, 296.

Brakensiek, D.L., W.J. Rawls, and G.R. Stephenson. 1984. Modifying SCS hydrologic soil groups and curve numbers for rangeland soils. Paper No. PNR-84-203, Annual Meeting, Pacific Northwest Region, American Society of Agricultural Engineers, September 26-28.

Bresler, E., and G. Dagan. 1983. Unsaturated flow in spatially variable fields: 2. Application of water flow models to various fields. Water Resources Research 19:421-428.

Brooks, R.H., and A.T. Corey. 1964. Hydraulic properties of porous media. Colorado State University (Fort Collins, CO) Hydrology Paper 3, 27 pp.

Chevalier, B.E. 1984. The hydraulic effects of surface layer development on an unprotected soil due to rainfall energy. M.S. Thesis, 110 pp. Department of Civil Engineering, Colorado State University, Fort Collins, CO.

De Vries, D.A. 1966. Thermal properties of soils, chapter 7. In W.R. van Wijk, ed., Physics of Plant Environment, pp. 210-230. North-Holland Publishing Co., Amsterdam.

Engelund, F., and E. Hansen. 1967. A monograph on sediment transport in alluvial streams. 62 pp. Teknisk Vorlag, Copenhagen.

Foster, G.R. 1982. Modeling the erosion process, chapter 8. In C.T. Haan et al., eds., Hydrologic Modeling of Small Watersheds, pp 297-388. American Society of Agricultural Engineers. Monograph No. 5, St. Joseph, MI.

Foster, G.R., C.B. Johnson, and W.C. Moldenhauer. 1982. Hydraulics of failure of unanchored cornstalk and wheat straw mulches for erosion control. Transactions of the American Society of Agricultural Engineers 25:940-947.

Foster, G.R., L.J. Lane, and J.D. Nowlin. 1980a. A model to estimate sediment yield from field-sized areas: Selection of parameter values, chapter 2. In CREAMS, A Field Scale Model for Chemicals, Runoff, and Erosion From Agricultural Management Systems, Volume II: User Manual, pp. 193-281. U.S. Department of Agriculture, Conservation Research Report No. 26.

Foster, G.R., L.J. Lane, J.D. Nowlin, et al. 1980b. A model to estimate sediment yield from field-sized areas: Development of model, chapter 3. In CREAMS, A Field Scale Model for Chemicals, Runoff, and Erosion From Agricultural Management Systems, Volume I: Model Documentation, pp. 36-640. U.S. Department of Agriculture, Conservation Research Report No. 26.

Foster, G.R., R.E. Smith, W.G. Knisel, and T.E. Hakonsen. 1983. Modeling the effectiveness of on-site sediment control. Paper No. 83-2092, presented at summer 1983 meeting, American Society of Agricultural Engineers, Bozeman, MT, 15 pp.

Foster, G.R., R.A. Young, and W.H. Niebling. 1985. Sediment composition for nonpoint source pollution analysis. Transactions of the American Society of Agricultural Engineers 28:133-139, 146.

Gilham, R.W., A. Klute, and D.F. Heerman. 1979. Measurement and numerical simulation of hysteretic flow in a heterogeneous porous medium. Soil Science Society of America Journal 43:1061-1067.

Hanaway, J.J. 1962. Corn growth and composition in relation to soil fertility: II. Uptake of N, P, and K in different plant parts in relation to stage growth. Agronomy Journal 54:217-222.

Hanaway, J.J., and C.R. Weber. 1971. Accumulation of N, P, and K by soybean (Glycine max (L.) Merrill) plants. Agronomy Journal 63:406-408.

Havercamp, R., and M. Vauclin. 1979. A note on estimating finite difference interblock hydraulic conductivity values for transient unsaturated flow problems. Water Resources Research 15:181-187.

Havis, R.N. 1986. Solute transport from soil to overland flow. Ph.D. Dissertation, 131 pp. Department of Civil Engineering, Colorado State University, Fort Collins, CO.

Holtan, H.N., C.B. England, G.P. Lawless, and G.A. Schumaker. 1968. Moisture-tension data for selected soils on experimental watersheds. U.S. Department of Agriculture, Agricultural Research Service, ARS 41-144, 609 pp.

Linsley, R.K, M.A. Kohler, and J.H. Paulus. 1958. Runoff relations, chapter 8. In Hydrology for Engineers. 340 pp. McGraw-Hill, New York.

Melillo, J.M., R.J. Naiman, J.D. Aber, and A.E. Linkins. 1984. Factors controlling mass loss and nitrogen dynamics of plant litter decaying in northern streams. Science 35:341-356.

Montgomery, R.J. 1980. A data-based evaluation of the SCS curve number method for runoff prediction. M.S. Thesis, 106 pp. Colorado State University, Fort Collins, CO.

Morris, E.M., and D.A. Woolhiser. 1980. Unsteady one-dimensional flow over a plane: Partial equilibrium and recession hydrographs. Water Resources Research 16:355-360.

Parlange, J.-Y., and R.E. Smith. 1976. Ponding time for variable rainfall rates. Canadian Journal of Soil Science 56:121-123.

Parton, W.J., A.R. Mosier, and D.S. Schimel. 1988a. Rates and pathways of nitrous oxide production in a shortgrass steppe. Biogeochemistry 6:45-58.

Parton, W.J., D.S. Schimel, C.D. Cole, and D.S. Ojima. 1987. Analysis of factors controlling soil organic matter levels in great plains grasslands. Soil Science Society of America Journal 51:1173-1179.

Parton, W.J., J.W.B. Stewart, and C.V. Cole. 1988b. Dynamics of C, N, P and S in grassland soils: A model. Biogeochemistry 5:109-131.

Pinck, L.A., F.E. Allison, and M.S. Sherman. 1950. Maintenance of soil organic matter: II. Losses of carbon and nitrogen from young and mature plant material during decomposition in soil. Soil Science 69:391-401.

Pochop, L.O., F.M. Smith, and R.E. Smith. 1985. Evapotranspiration estimates of the Pawnee grasslands. In Proceedings of National Symposium of Advances in Evapotranspiration. American Society of Agricultural Engineers, December 16-17, Chicago.

Rawls, W.J., D.L. Brakensiek, and K.E. Saxton. 1982. Estimation of soil water properties. Transactions of the American Society of Agricultural Engineers 25:1316-1320, 1328.

Rawls, W.J., D.L. Brakensiek, and B. Soni. 1983. Agricultural management effects on soil water processes. Part I: Soil water retention and Green and Ampt infiltration parameters. Transactions of the American Society of Agricultural Engineers 26:1747-1752.

Richardson, C.S. 1981. Stochastic simulation of daily precipitation, temperature, and solar radiation. Water Resources Research 17:182-190.

Richardson, C.W., and D.A. Wright. 1984. WGEN: A model for generating daily weather variables. U.S. Department of Agriculture, Agricultural Research Service, ARS-8, 83 pp.

Ritchie, J.T. 1972. A model for predicting evaporation from a row crop with incomplete cover. Water Resources Research 8:1204-1213.

Ritchie, J.T., E.D. Rhoades, and C.W. Richardson. 1976. Calculating evaporation from native grassland watersheds. Transactions of the American Society of Agricultural Engineers 19:1098-1103.

Rovey, E.W., D.A. Woolhiser, and R.E. Smith. 1977. A distributed kinematic model of upland watersheds. Colorado State University (Fort Collins, CO) Hydrology Paper 93, 52 pp.

Schrieber, J.D. 1990. Estimating soluble phosphorus from green crops and their residues in agricultural runoff. In D.G. DeCoursey, ed., Small Watershed Model (SWAM) for Water, Sediment, and Chemical Movement: Supporting Documentation, pp. 77-95. U.S. Department of Agriculture, Agricultural Research Service, ARS-80.

Smith, C.N., R.A. Leonard, G.W. Langdale, and G.W. Bailey. 1978. Transport of chemicals from small upland Piedman watersheds. Environmental Protection Agency Research Report EPA-600/3-78-056, Environmental Research Laboratory, Athens, GA, 363 pp.

Smith, R.E. 1970. Mathematical simulation of infiltrating watersheds. Colorado State University (Fort Collins, CO) Hydrology Paper 47, 44 pp.

Smith, R.E. 1976. Field test of a distributed watershed erosion/sedimentation model. In Soil Erosion: Prediction and Control, pp. 201-209. Soil Conservation Society of America, Ankeny, IA.

Smith, R.E. 1981a. A kinematic model for surface mine sediment yield. Transactions of the American Society of Agricultural Engineers 24:1508-1514.

Smith, R.E. 1981b. Rational models of infiltration hydrodynamics. In V.P. Singh, ed., Modeling Components of the Hydrologic Cycle, pp. 107-126. Water Resources Publications, Littleton, CO.

Smith, R.E. 1983a. Flux infiltration theory for use in watershed hydrology. In Advances in Infiltration: Proceedings of the National Conference on Advances in Infiltration, Publication No. 11-83, pp. 313-323. American Society of Agricultural Engineers, St. Joseph, MI.

Smith, R.E. 1983b. Approximate soil water movement by kinematic characteristics. Soil Science Society of America Journal 47:3-8.

Smith, R.E. 1990. Analysis of infiltration into a two-layer soil profile. Soil Science Society of America Journal 54:1219-1227.

Smith, R.E., and V.A. Ferreira. 1989. Comparative evaluation of unsaturated flow methods in selected USDA simulation models. In H.J. Morel-Seytoux, ed., Unsaturated Flow in Hydrologic Modeling Theory and Practice, pp. 391-412. North Atlantic Treaty Organization, ASI Series, C, vol. 275, Dordrecht, The Netherlands.

Smith, R.E., and J-Y. Parlange. 1978. A parameter-efficient hydrologic infiltration model. Water Resources Research 14:533-538.

Smith, R.E., and J.R. Williams. 1980. Simulation of the surface water hydrology, chapter 2. In CREAMS, A Field Scale Model for Chemicals, Runoff, and Erosion From Agricultural Management Systems, Volume I, pp. 13-35. U.S. Department of Agriculture, Conservation Research Report No. 26.

Sorensen, L.H. 1981. Carbon-nitrogen relationships during the humification of cellulose in soils containing different amounts of clay. Soil Biology and Biochemistry 13:313-321.

U.S. Department of Agriculture. 1980. CREAMS: A field scale model for chemicals, runoff, and erosion from agricultural management systems. U.S. Department of Agriculture, Conservation Research Report No. 26, 640 pp.

U.S. Department of Agriculture, Science and Education Administration. 1979. Field manual for research in agricultural hydrology. U.S. Department of Agriculture, Agriculture Handbook No. 224, 550 pp.

U.S. Department of Agriculture, Soil Conservation Service. 1972. Estimation of direct runoff from storm rainfall, chapter 10. In National Engineering Handbook, pp. 10.1-10.24.

Van Genuchten, M. Th. 1980. A closed form equation for predicting the hydraulic conductivity of unsaturated soils. Soil Science Society of America Journal 44:892-898.

Walker, A. 1974. A simulation model for prediction of herbicide persistence. Journal of Environmental Quality 3:396-401.

White, I., D.E. Smiles, and K.M. Perroux. 1979. Absorption of water by soil: The constant flux boundary condition. Soil Science Society of America Journal 43:659-664.

Williams, J.R. 1975. Sediment yield prediction with universal equation using runoff energy factor. U.S. Department of Agriculture, Agricultural Research Service, ARS-S-40, pp. 244-252.

Williams, J.R. 1982. Testing the modified universal soil loss equation. In Proceedings of the Workshop on Estimating Erosion and Sediment Yield on Rangelands (Tucson, AZ, March 1981), pp. 157-165. U.S. Department of Agriculture, Agricultural Research Service, Agricultural Reviews and Manuals ARM-W-26.

Williams, J.R., and H.D. Berndt. 1977. Sediment yield prediction based on watershed hydrology. Transactions of the American Society of Agricultural Engineers 20:1100-1104.

Williams, J.R., C.A. Jones, and P.T. Dyke. 1984. A modeling approach to determining the relationship between erosion and soil productivity. Transactions of the American Society of Agricultural Engineers 27:129-144.

Wischmeier, W.H., and D.D. Smith. 1978. Predicting rainfall erosion losses: A guide to conservation planning. U.S. Department of Agriculture, Agriculture Handbook No. 537, 58 pp.

Woolhiser, D.A., R.E. Smith, and D.C. Goodrich. 1990. KINEROS, A kinematic runoff and erosion model: Documentation and user manual. U.S. Department of Agriculture, Agricultural Research Service ARS-77, 130 pp.